Università degli Studi di Ferrara

DOTTORATO DI RICERCA IN SISTEMI BIOLOGICI: STRUTTURA, FUNZIONE, EVOLUZIONE

COORDINATORE PROF. ENRICO GRAZI

PHOTOSYNTHETIC ACTIVITY AND THYLAKOID BIOCHEMISTRY IN PLASTIDS OF *Arum italicum* MILLER

DOTTORANDA
DOTT.SSA LAURA PANTALEONI

TUTORE
PROF.SSA SIMONETTA PANCALDI

CO -TUTORE
PROF.SSA EVA-MARI ARO

XX° CICLO

ANNI 2005 - 2007

CONTENT

1. INTRODUCTION

1.1. THE PLASTIDS

Plastids are semi-autonomous organelles found in practically all plant and algal cells.
The members of the plastid family play central roles in photosynthesis, amino acid and lipid synthesis, starch and oil storage, fruit and flower coloration, gravity sensing, stomatal functioning, and environment perception.

1.1.1. Evolution of Plastids (Overview)

The idea that chloroplasts are the result of a symbiosis between a photosynthetic organism and a non-photosynthetic host was originally suggested by Andreas Schimper more than 100 year ago, and than developed by Constantin Mereschkowsky in the early 20th century (for a recent translation of Mereschkowsky's work see: Martin *et al.* 1999). According to this hypothesis, plastids are reduced forms of cyanobacteria, acting as "little green slaves" within the cell (Martin *et al.* 1999). In the 1960s and 1970s, further support to this hypothesis came from demonstration that plastids contain DNA (Ris *et al.* 1962), up to the sequencing of chloroplast nucleotide. Analyses of plastid genome result in a circular map, of size ranging between 120 and 160 Kbp in higher plants. Plastids are highly polyploidy: proplastids contain 20 copies of the genome while chloroplasts contain around 100 copies (Sugiura, 1992).
Analyses performed on fossils of red algae-like organisms suggest that multicellular eukaryotes with plastids existed 1.2 billion years ago, and most probably there is evidence of those organisms already around 1.5 billion years ago.
Plastid may derive from two types of symbiotic events: *primary endosymbiosis*, which is established directly between cyanobacteria and the host cell, and *secondary* and *tertiary endosymbiosis*, which are established between an eukaryotic alga already equipped with plastids and a second eukaryotic host (Moreira *et al.* 2001). In 1962, Gibbs provided the first undeniable evidence that plastids may also originate from secondary endosymbiosis, reporting the presence in Cryptomonads of a highly reduced eukaryotic nucleus, known as *nucleomorph*, in addition to the main nucleus (Moreira *et al.* 2001; Nozaki, 2005).
Most authors accept as primary plastids only the organelles of three eukaryotic lineages: green plants (green algae and plants), red algae and glaucophytes. One of the most debated

questions is whether multiple endosymbioses have happened (a polyphyletic origin) or whether a single one was sufficient (a monophyletic origin). Higher plant chloroplast DNA is highly conserved, supporting the conclusion that a single endosymbiotic event has given rise to all the existing chloroplasts (Timmis *et al.* 2004). Nevertheless, the three plastid lineages display important differences which raise doubts about the hypothesis of a unique origin, suggesting rather a series of independent primary endosymbiosis events. Moreover, a relatively large number of secondary endosymbioses has been suggested (Moreira *et al.* 2001).

Over the few past decades, the endosymbiotic theory has been widely accepted, however a precise understanding of the origin of eukaryotic plastids is still unclear, considering (i) the scarcity of knowledge about the features of cyanobacteria over a billion years ago (Larkum *et al.* 2007), (ii) the fact that plastids have diverged enormously from their cyanobacterial ancestors during their intracellular evolution (Rodriguez-Ezpeleta *et al.* 2006) and (iii) that the representatives of intermediate stages are lacking (Rodriguez-Ezpeleta *et al.* 2006). In addition, other organisms have recently been suggested as containing primary endosymbionts on their way to becoming permanent organelles, and which are not closely related to plastids (For a recent review see: Larkum *et al.* 2007). In spite of this, the evolutional and functional differences between endosymbiont and organelles have been strongly articulated in the 1980s and more recently argued by Theissen and co-workers (2006). The features that distinguish a genuine plastid from an endosymbiont include not only indefinite stable maintenance but also the transfer of DNA from the organelle to the nucleus with the concomitant development of the protein import machinery (Theissen *et al.* 2006).

In contrast to the straightforward assumption that plastids arose via an endosymbiontic event in which a protoeukaryotic cell engulfed and retained a photosynthetic bacterium, several steps are required for a cyanobacterium to be transformed into an eukaryotic organelle. First of all, following the phagotrophic ingestion of a cyanobacteria, the eukaryote develops the ability to retain and use its pray for short period of time before digestion. After that, several steps should be achieved to consider the endosymbiont as factually correct plastid: (i) the host and symbiont cell division becomes synchronised, (ii) genes are transferred from the symbiont to the host, and (iii) a protein import system develops, to translocate proteins encoded by the nucleus into the plastid (Fig. 1).

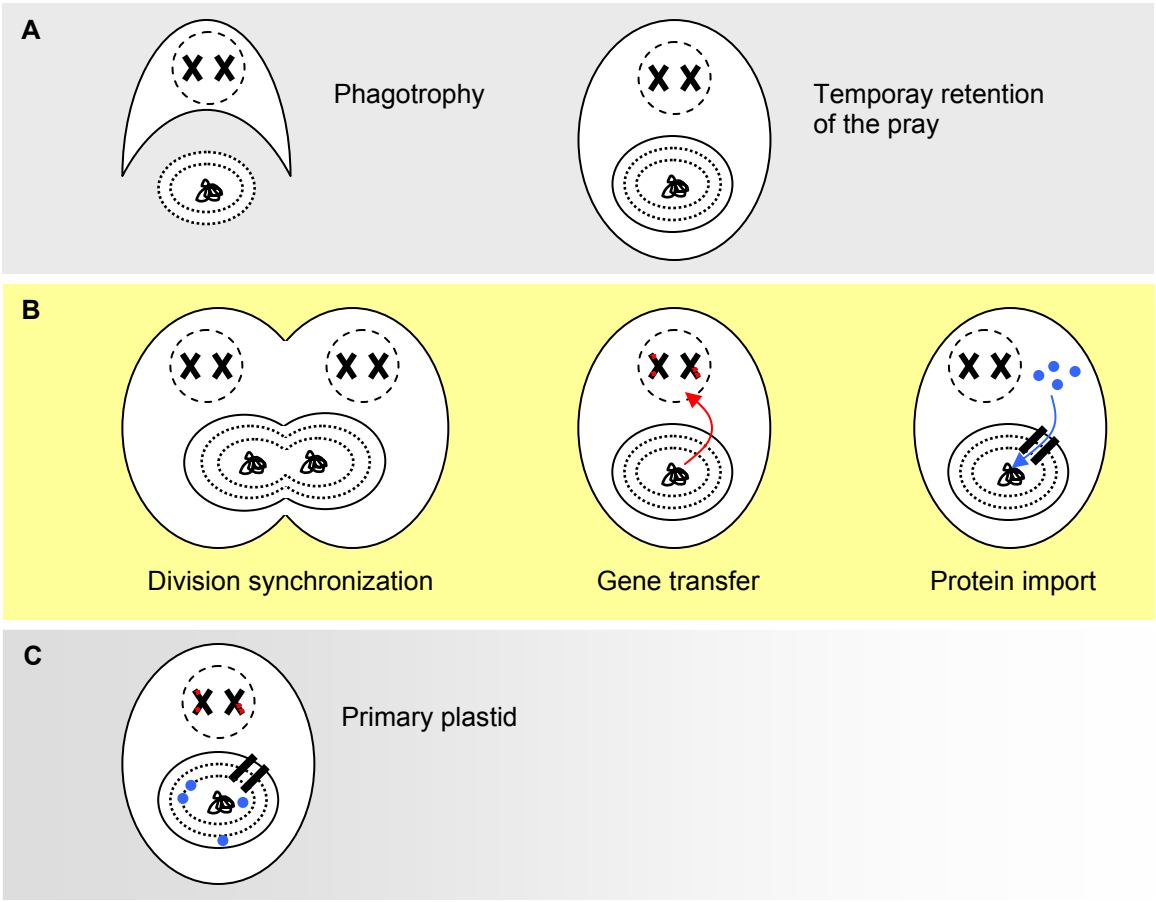

Fig. 1: Main steps required for the transformation of a cyanobacterium into a plastid. A) first interactions between pray and host, B) after the pray has lost one of the membranes, its division syncronise with that of the host, while gene transfer occurs from pray to host and a protein import system is developed, C) the pray is now considered a primary plastid. (Modified form Rodriguez-Ezpeleta and Philippe, 2006)

It is not known whether these steps occurred in a particular order or in parallel, but, once they were completed, the symbiont became a primary plastid (Rodriguez-Ezpeleta *et al.* 2006). Resuming, in order to build up the new process that the enodsymbiontic relationship required, plastids accepted several contributions form their original hosts (Lopez-Juez *et al.* 2005) and gained various regulatory mechanisms. It is noteworthy that chloroplasts acquired roles as a part of the biology of the organisms also by differentiating into a variety of interconvertible plastid forms, according to the cell type. This phenomenon characterises the land plants.

In fact, in addition to chloroplasts, plants have evolved non-photosynthetic plastid types that are essential components of cells. All the plastid derivatives, that now we call "other plastid types", carry out other essential or specialised functions in cells that are no longer photosynthetically active, or are merely transmitted more easily and more economically in young, embryonic or undifferentiated cells (Lopez-Juez *et al.* 2005). Recent studies indicate that the biogenesis of various plastid types relies on distinct but homologous Toc-Tic import

pathways that have specialised in the import of specific classes of substrates (Kessler *et al.* 2006).

Finally, it appears that plastids have never been lost in Plantae, even when photosynthesis was lost in parasitic species. Presumably they are dependent on the lipid biosynthesis pathway of the plastid (Wise *et al.* 2004; Cavalier-Smith, 1999).

1.1.2. The Plastid Family

The French phycologist Pierre Dangeard (1862-1947) was the first to express the relatedness of members of the plastid family and classified them as a part of the overall "plastidiome" (for a recent review see: Wise *et al.* 2004). In fact, accompanying the development of the plant cell in different tissues, plastids also develop and differentiate in clearly distinct types: chloroplasts in green tissues, amyloplasts in roots and storage tissues, chromoplasts in fruits, flowers and some roots, etc. (Marano *et al.* 1993). The extent of the integration of plastid into the biology of the cell is evident in the diversity of plastid structures and functions and in the roles played by plastids in the whole plant development and phenotype (Lopez-Juez *et al.* 2005). The integration of plastids into the biology of the plant cell makes necessary for the organelle to show a high degree of "plasticity" and responds to the signals that control the host cell type (Lopez-Juez *et al.* 2005)

Seeds, meristematic tissues and several other tissues contain *proplastids*, the smallest and least complicated members of the plastid family, and the ontological precursor to all other plastid types. In 1893 A. Sergeevitch Famintzin, one of the founders of Russian plant physiology, demonstrated that chloroplasts persist as small, shrivelled structures in seeds, and that those in the seedlings develop from them, further establishing the uninterrupted continuity of plastids (Wise *et al.* 2004). In 1927 C. Zirkle called the colourless precursors: "primordial" and then "proplastids" (for a recent review see: Staehelin, 2003). Proplastids are generally small and undifferentiated, with a poorly defined internal membrane system consisting of only few tubules.

If the plant tissue is exposed to light during development, the proplastid will enlarge, turn green and develop into mature, photosynthetically competent *chloroplast*. On the other hand, if development of the meristematic or embryonic tissues is allowed to proceed in the dark, plastid development proceeds to and is arrested at the *etioplast* stage. The etioplast interior is dominated by a paracrystalline tubular structure called the proplamellar body.

Leucoplasts are colorless (i.e. non-pigmented) plastids, of which three types are generally recognized: amyloplast, elaioplast and proteinoplast. Proplastids in root tissues typically develop into starch-containing *amyloplasts*, which are distinguished by the presence of one to many large starch grains and a minimal/absent internal membrane system. Some amyloplasts function entirely in starch storage whereas other amyloplasts, found primarily in the root cap, are said to be "sedimentable" and are intimately involved in gravity perception (statolithes). Amyloplasts are also found in other plant tissues and organs, like pith, tubers, rhizomes, endosperm, cotyledons. *Elaioplasts* play roles in oil storage and metabolism, and are centrally involved in pollen grain maturation. *Proteinoplasts* may be sites of protein storage, for instance in sieve tubes, but their significance is questionable.
Brightly coloured *chromoplast*s contain a high level of carotenoids and provide the colour to many flowers, fruits and vegetables. Finally, *gerontoplasts* represent a degrading, but still functional, stage in the plastid life cycle found in senescent tissues (Wise *et al.* 2004).

"While it is easy to envision the evolution of chloroplast from a cyanobacterium, it is much more difficult to understand the evolutionary processes that created the multiple forms of plastids. There is no indication that the structures found in proplastids, chromoplast or leucoplasts have been part of the genetic plan that the endosymbiont transferred to the host cell. It must be assumed that this development took place after the endosymbiotic event and was imposed on the plastid by the host cell" (Vothknecht *et al.* 2001)

1.1.3. Conversion Between Different Forms

Interconversion between different plastid forms requires deep changes in ultrastructure, including the biogenesis, reorganization or regression of internal membranes (Vothknecht *et al.* 2001), and acquisition of new functions, hence involving changes in gene expression, degradation and synthesis of different proteins and changes in metabolic pathways. These processes have been studied with particular focus on two plastid types of major crop and biotechnological importance: the starch-storing amyloplast and the carotenoid-storing chromoplast (Lopez-Juez, 2007). Nevertheless, knowledge of the regulatory networks underlying the conversion between different plastid types is surprisingly limited (Lopez-Juez *et al.* 2005). It appears that both cell and organelle genome are involved in the control of plastids development (Vothknecht *et al.* 2001), responding to endogenous hormonal control

and environmental signals. There are also evidences that plastid-derived signals are perhaps involved in a feedback loop (Lopez-Juez, 2007).

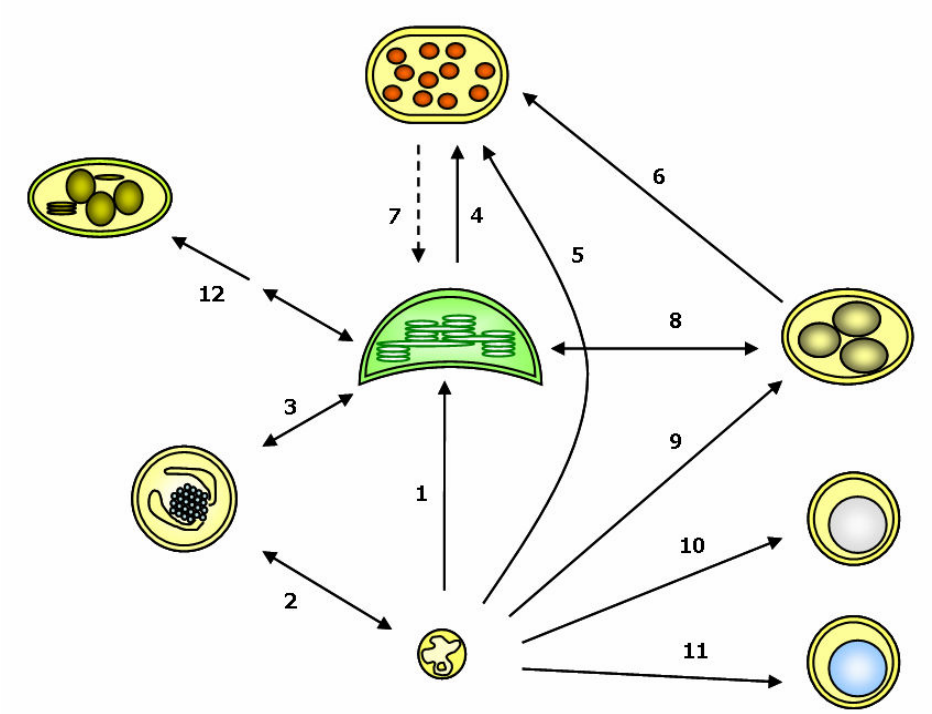

Chloroplast development		
1	Proplastid - Chloroplast	Meristematic tissues during development
2	Proplastid – Etioplast	Meristematic tissues developing in darkness
3	Etioplast – Chloroplast	Etiolated tissues exposed to light
Chromoplast differentiation and dedifferentiation		
4	Chloroplast – Chromoplast	Fruit ripening, petal development
5	Proplastid – Chromoplast	Squash fruits
6	Amyloplast – Chromoplast	Tobacco, carrot roots, squash fruits
7	Chromoplast – Chloroplast	Citrus fruits (*in vitro*)
Amyloplast differentiation		
8	Chloroplast – Amyloplast	*In vitro* coltures
9	Proplastid – Amyloplast	Roots
Other leucoplast differentiation		
10	Proplastid – Elaioplast	Tapetum cells
11	Proplastid – Proteoplast	Sieve tubes
Chloroplast senescence		
12	Chloroplast – Gerontoplast	Senescent tissues
13	Gerontoplast – Chloroplast	Regreened leaves

Fig. 2: Conversion between different plastid forms. Examples are given in the table.

Amyloplast differentiation

The relationship between amyloplast differentiation and phytohormones has been investigated by several authors, leading to the conclusion that auxin and cytokinin exert opposite effects on amyloplast development. More precisely, depletion of auxines and exposure to cytokinin accelerate the starch accumulation by regulating the expression of the nuclear genes required for starch biosynthesis (Miyazawa *et al.* 1999; Miyazawa *et al.* 2002). Moreover, it has been shown that the development of amyloplast parallels a decrease in plastid genome transcription (Sakai *et al.* 1999). Conversely, a high level of transcription of the plastid genome is induced by light, causing the transition from amyloplast to chloroplast (Ljubicic *et al.* 1998). Besides the level of transcription, amyloplast and chloroplast differ also in the protein import mechanism. Some authors suggest that amyloplast could be interpreted as a plastid that has become a semi-passive recipient of specific nuclear-encoded proteins (Lopez-Juez *et al.* 2005). Although the central transfer mechanisms appear to be the same, there are enough differences to allow a different import of precursor proteins into one type of plastid *versus* the other (Wan *et al.* 1996).

Chromoplast differentiation

One of the most widely studied plastid transitions is the differentiation of chromoplasts from fully developed chloroplasts in green fruits or petals. This process is the result of a complex interaction among developmental, hormonal and light signalling systems (Giovannoni, 2001). Positive and negative modulations by phytohormones have been demonstrated for both chromoplast biogenesis and carotenoid synthesis. The development of chromoplast is accompanied by the dismantling of the photosynthetic machinery. Several authors have reported falls in expression of photosynthetic nuclear genes (Piechulla *et al.* 1987) reflecting a lower amount of those photosynthetic proteins in plastid membranes (Faurobert *et al.* 2007), while the transcriptional activity of the plastid genome is reported to remain virtually unchanged (Marano *et al.* 1992). On the other hand, expression of carotenoid biogenesis genes and overexpression of proteins related to stress response and fruit senescence are observed (Giovannoni, 2004; Faurobert *et al.* 2007). Once again it appears that in this transition plastids act as acceptors of proteins encoded by nuclear genes (Lopez-Juez *et al.* 2005).

In many cases, chromoplasts originate from other non photosynthetic plastids. Chromoplasts can develop directly from undifferentiated proplastids, as in squash (*Cucurbita* sp.) plants (see: Marano *et al.* 1993 and references therein) or from other colourless plastids. Fruits where the greening has been impaired (by growth in darkness or by the presence of greening-

mutations) are still able to develop fully functional chromoplasts, showing that the transition from chloroplast is not needed. Moreover, direct conversion of amyloplast to chromoplast has been observed in carrot roots and squash fruits (Marano *et al.* 1993) and Horner and co-workers (2007) have described various stages of amylo-chromoplasts in ornamental tobacco floral nectaries.

Finally, chromoplast redifferentiation into chloroplasts has been observed in several organisms (*Citrus synensis*, *Cucurbita pepo* and *Citrus sinensis*), exposed to particular conditions of nutrition and illumination. These evidences show that the chromoplast remains an active organelle and not merely a degenerated or senescent form of chloroplast.

In spite of many years of observations, our knowledge about the development of different type of plastids, other than chloroplasts, is still limited (Lopez-Juez, 2007). The relative contribution of nucleus and plastid genomes to plastid differentiation and dedifferentiation is still unclear, but, according to many authors, it appears that the majority of the proteins required for plastid development and function are encoded in the nucleus. However, very little is known so far about the regulation of plastid import in relation to plastid development (Vothknecht *et al.* 2001) and very little work has been carried out to understand the mechanisms and the possible signalling pathways presumably underlying the plastid differentiation processes (Lopez-Juez, 2007). Even though some particular type of differentiations, as the chloroplast to chromoplast transition in *Capsicum* sp. and in *Lycopersicon esculentum*, have been documented many times, some systems may have unique aspects that warrant further study (Horner *et al.* 2007).

1.2. PLASTID STRUCTURE

1.2.1. Structure of the Chloroplast

Chloroplasts in higher plants present three major structural regions (Fig. 3): (i) a highly organized internal membrane network formed by flat compressed vesicles, the *thylakoids*, (ii) an amorphous background rich in soluble proteins and ribosomes, the *stroma*, and (iii) a pair of outer membranes, the chloroplast *envelope* (Block *et al.* 2007).

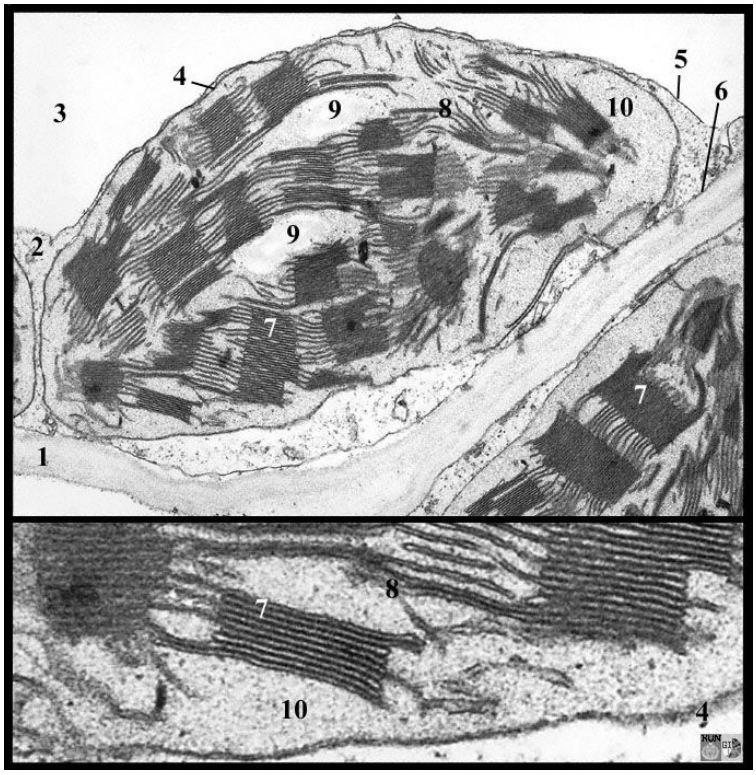

Fig. 3: Ultrastructure of a chloroplast of tobacco (*Nicotiana tabacum*). 1) cell wall, 2) cytoplasm, 3) vacuole, 4) chloroplast envelope (2 membranes), 5) tonoplast, 6) plasma membrane, 7) grana, 8) stroma thylakoids, 9) starch grains, 10) stroma. (From http://www.vcbio.science.ru.nl/en/image-gallery/show/PL0337/ - Radboud University, Nijmeng, Netherlands)

The Envelope

The two limiting envelope membranes are actually the only permanent membrane structure of the different type of plastids (Block *et al.* 2007). Analyses of whole envelope membranes from spinach chloroplasts, cauliflower proplastid, pea etioplasts, etc.., lead to the conclusion that the glycerolipid pattern of envelope membranes from all plastid types are almost identical (Block *et al.* 2007; Douce *et al.* 1990). However, it is still unclear whether and how the envelope participates to the integration of the various types of plastids in all plant tissues. In fact, at all stages of these transformations, the two limiting envelope membranes remain

apparently unchanged, despite the fact that envelope protein profiles undergo considerable transformation during development. (Block *et al.* 2007). An emerging concept suggests that multiple types of import complexes could be present within the same cell, each having a unique affinity for different plastid precursor proteins, depending upon the mix of Toc-Tic isoforms it contains (Block *et al.* 2007, Gutensohn *et al.* 2006). It should be considered that the envelope membranes control the uptake of raw material for all synthesis occurring in the plastids and regulate the export to the cytosol of the newly synthesised molecules. The same is true for all types of plastids. Envelope membranes, at the border between plastids and the cytosol, may therefore be a key structure for the integration of plastid metabolism within the cell (Block *et al.* 2007).

The Thylakoids (Models)

In higher plants and green algae two types of thylakoids are distinguished, granum (stacked) and stroma (unstacked) thylakoids. This phenomenon is thought to be a morphological reflection of the uneven distribution of the major photosynthetic complexes within the constituent membranes.

Since Menke's observation of thylakoids in electron micrographs of chloroplast cross sections (Menke, 1966), several models have been proposed to describe the structure and interconnections of granum-stroma assemblies in the thylakoid membranes of higher-plant chloroplasts (Brangeon *et al.* 1979; Arvidsson *et al.* 1999). The original model for the spatial arrangement of grana and stroma thylakoids was elaborated by Menke (1966). According to this model, every single granum thylakoid is continued in sheets that intersect several grana (Fig. 4a). This model is now considered obsolete and oversimplified, but it was subsequently elaborated and developed. The helical arrangement of stromal thylakoids around grana was proposed by Paolillo (1970) and subsequently modified by Brangeon and Mustardy (1979). This model suggests an essentially bipartite structure, consisting of a cylindrical granum body, made of discs piled one on top of the other, around which the stroma lamellae are wound as right-handed helices. The granum discs connect to each others through the stroma lamella helices that make multiple contacts with successive layers through slits located at the rim of the granum cylinder (Fig. 4b). Also a large lateral heterogeneity has been documented in the distribution of the macromolecular thylakoid protein complexes: photosystem (PS) II and the associated main chlorophyll *a*/*b* light-harvesting complex (LHC) II are found predominantly in the stacked region, while PSI and LHCI are located mainly in the unstacked region of the membrane, together with the ATPase complex. To illustrate the segregation of

the two PSs into granum and stroma lamellar domains, the so-called folded-membrane model was proposed by Andersson and co-workers (1980). More recently, it was extended by Arvidsson and co-workers (1999) to explain how the thylakoid network may be constructed by the folding of a single continuous membrane and to account for the complete or almost complete unstacking of grana layers seen in isolated thylakoids subjected to low ionic strength conditions. In this model, grana are formed by symmetrical invaginations of stroma thylakoid pairs into piles of three discs. This arrangement gives rise to a regular folded structure, which is stabilized solely by surface interactions between appressed grana membranes and, hence, can be readily dismantled (Fig. 4c).

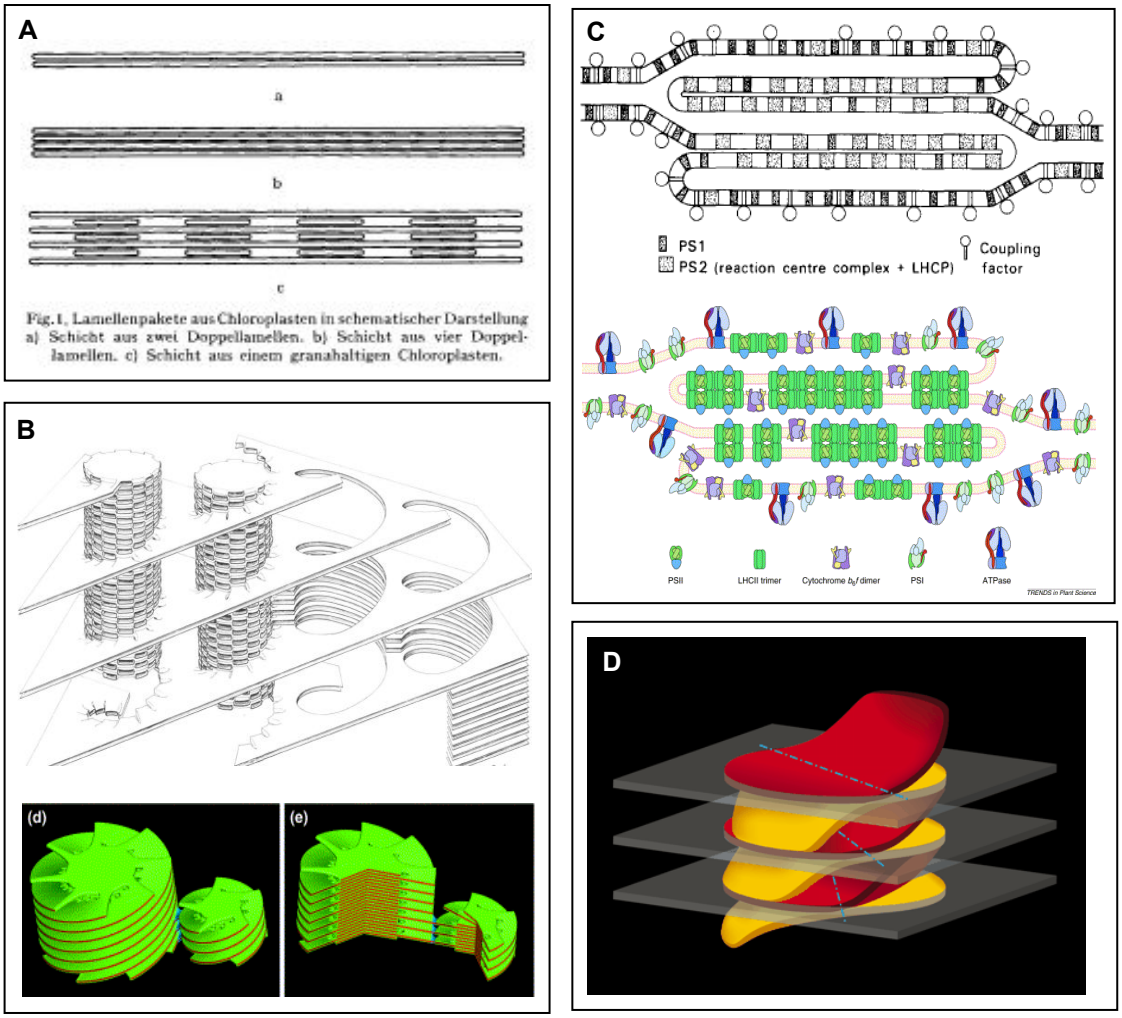

Fig. 4: Models of thylakoid organisation. A) original model from Menke (1960) , B) helical arrangement of stromal thylakoids around grana, above from Paolillo (1970) and below from Mustardy *et al*. (2003), C) folded-membrane model, above from Andersson (1980) and belowe from Arvidsson (1999), D) new model, proposed by Shimoni *et al*. (2005).

Recently, a new model has been proposed by Shimoni and co-workers (2005). Those authors examined thylakoid membranes of cryo-immobilized, freeze-substituted lettuce leaves with

electron tomography and proposed that adjacent layers in the granum are not connected to each other through the stroma lamellae. Thylakoid membranes are suggested to be interconnected directly through their edges, which bend toward and fuse with neighbouring layers within the granum body. These units are rotated relative to each other around the axis of the granum cylinder (Fig. 4d).

The ontogeny and evolution of this type of granum-stroma thylakoid assembly and its ancestor is not well understood. An evolutionary hypothesis has been proposed by Mullineaux (2005). In a paper published in 2005, the author argues that land-plants adapting to low-light environments developed grana as a novel way to increase the size of the LHCII in order to achieve an efficient photosynthesis in shade.

1.2.2. Structure of Chromoplasts

Ultrastructural studies of chromoplasts have revealed different kinds of carotenoid-accumulating structures, leading to the subclassification of chromoplasts into: (i) globular, (ii) fibrillar-tubular, (iii) crystalline, and (iv) membranous (Vishnevetsky *et al.* 1999; Camara *et al.* 1995; Thomson *et al.* 1980), even if the classification results sometimes in difficulties because of the overlap of different morphological characteristics in the same organelle (Paolillo *et al.* 2004; Bonora *et al.* 2000). Moreover, little is known about the reasons for these various morphological types.

Globular chromoplasts that contain large lens-shaped or spheroidal plastoglobules are the most common type and are considered to be the oldest and more primitive in evolutionary terms (Vishnevetsky *et al.* 1999). Many organisms present this type of chromoplasts, including tomato (*Lycopersicon esculentum*) and mango (*Mangifera indica*) (Simkin *et al.* 2007; Vasquez-Caicedo *et al.* 2006; Fig. 5a). Because the ultrastructure and carotenoid-protein interactions in *fibrillar* and *tubular* chromoplasts are very similar, they are often considered as a single group by many authors (Vishnevetsky *et al.* 1999; Thomson *et al.* 1980). Fibrils are characterized by a high homogeneity of apolar compounds, most of which are esterified xantophylls. Two models have been suggested to describe these associations of proteins and carotenoids: both of them propose that carotenoids accumulate in the centre of the fibrils, which are surrounded by a single layer of proteins and lipids (Vishnevetsky *et al.* 1999) or by a layer of polar lipids which in turn are surrounded by an outer layer of proteins (Deruere *et al.* 1994). Several insights suggest that the fibril formation does not rely on material released form degraded thylakoid membranes (Deruere *et al.* 1994) and that the 30-

35 kDa proteins, collectively named as carotenoid-associated proteins, are nuclear encoded and their accumulation parallels carotenoid accumulation and chromoplast fibril formation during flower mophogenesis and fruit ripening (Vishnevetsky *et al.* 1999; Deruere *et al.* 1994). These structures have been well characterized in the chromoplast of bell pepper (*Capsicum annum*) fruits, where carotenoids accumulate in clearly distinct plastid substructures (Fig. 5b from Deruere *et al.* 1994).

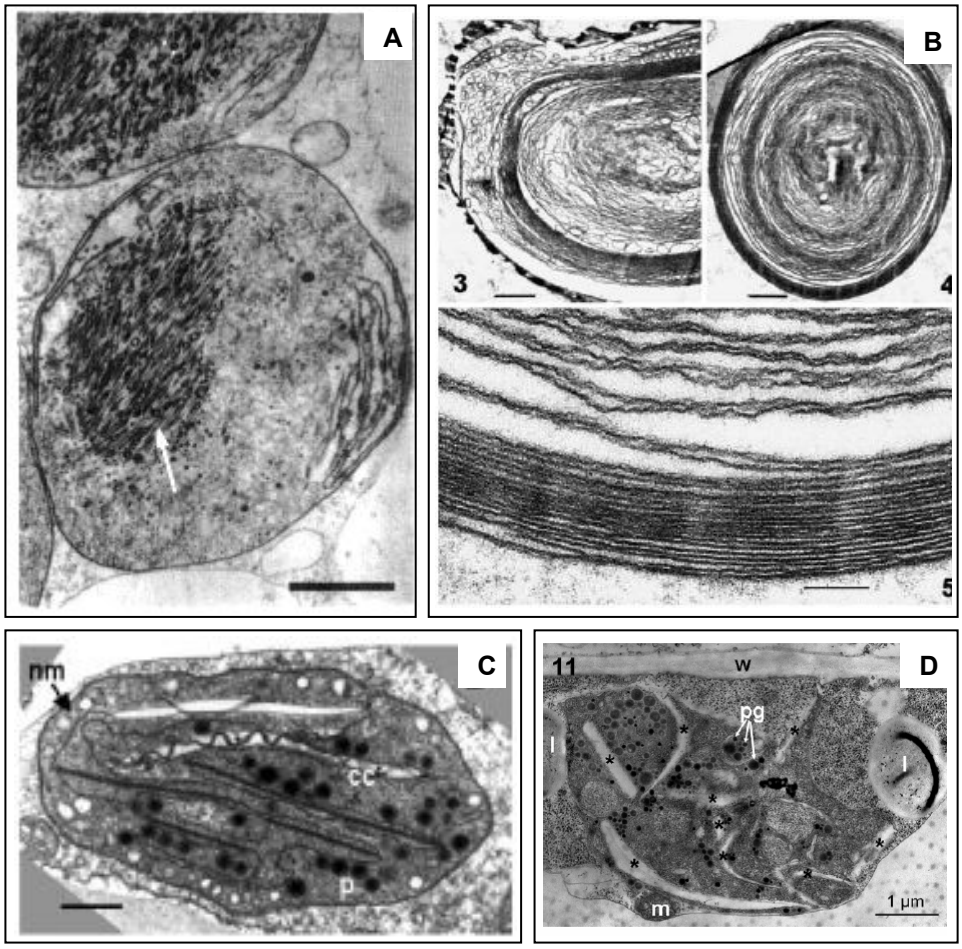

Fig. 5: Examples of chromoplast types. A) Fibrillar chromoplast form *Capsicum annum* (Deruere *et al*. 1994). B) Membranous chromoplasts from *Brassica oleracea* (Paolillo *et al.* 2004). C) Globular chromoplast from *Lycopersicon esculentum* (Simkin *et al*. 2007). D) Crystalline chromoplast from *Daucus carota* (Vasquez-Caicedo *et al*. 2006).

Crystalline chromoplasts are characterized by crystals composed primarily of β-carotene or lycopene sequestered into membrane structures. As the crystals increase in size, they can distort the shape of the chromoplast. A well-known example of this is the chromoplast of the carrot (*Daucus carota*) root which contains long, often needle-shaped, carotene crystals (Vasquez-Caicedo *et al.* 2006 and references therein, Fig. 5c). *Membranous* chromoplasts are characterized by multiple layers of membranes which contain carotenoid pigments. A good illustration of this kind of plastids is the chromoplast of *Or* mutants of cauliflower (*Brassica*

oleracea), which present various stacked membranes rolled and folded into three-dimensional objects in a relatively dense stroma (Fig. 5d, from Paolillo *et al.* 2004).

1.3. PHOTOSYNTHESIS

The production of oxygen and the assimilation of carbon dioxide into organic matter determine, to a large extent, the composition of our atmosphere and provide all life forms with essential organic compound:

$$6CO_2 + 6H_2O \rightarrow C_6H_{12}O_6 + 6O_2$$

The photosynthetic process requires the coordination of two phases: the so-called light reactions, which produce O_2, ATP and NADPH, and the carbon fixation reactions or Calvin Cycle, which reduces CO_2 to carbohydrate and consumes the ATP and NADPH produced in the light reactions (Nelson *et al.* 2004).

The light reactions occur on the thylakoid membranes, which physically separate two different compartments, the thylakoid lumen and the stroma. Four main protein complexes are embedded in the thylakoid membrane: PSII, cytochrome (Cyt) b_6f, PSI and ATPase. These complexes generate a proton gradient across the membrane and are capable of light-dependent water oxidation (water splitting), $NADP^+$ reduction and ATP formation. Photosynthetic organisms developed structures that contain a large number of accessory pigment molecules that harvest light energy and funnel the energy to the reaction centre complexes. In fact, in oxygenic photosynthesis two reaction centres operate in series: the PSII, which oxidizes water to O_2 in the lumen, while releasing protons into the lumen, and the PSI, which reduces $NADP^+$ to NADPH at the stromal side of the thylakoid membrane by the action of ferredoxin (Fd) and the flavoprotein ferredoxin-$NADP^+$ oxido-reductase (FNR). The two PSs, each surrounded by its own LHC, are linked by an electron transport chain involving the Cyt b_6f, which receives electrons from PSII and delivers them to PSI. Cyt b6f also transports additional protons from the stroma to the lumen. Finally, the ATP synthase produces ATP by exploiting the back diffusion of protons from the lumen to the stroma (Fig. 6).

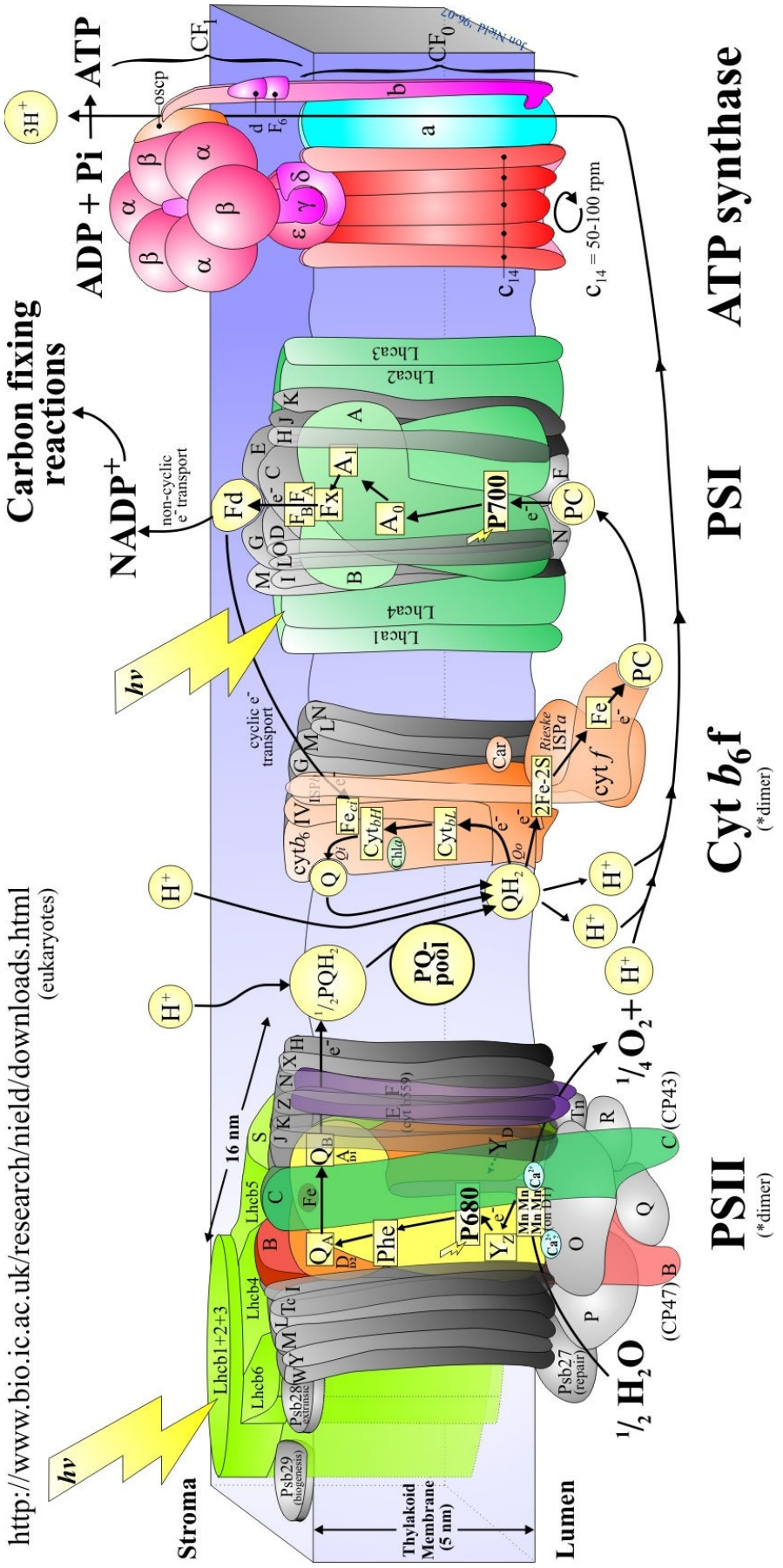

Fig. 6: Diagrammatic representation of the complexes embedded in the thylakoid membrane and involved in the light reactions of photosynthesis. The electron flow is also shown.

During the dark reactions, the reduction of CO_2 to carbohydrate is coupled to the consumption of the NADPH and ATP synthesized by the light reactions. The Calvin cycle takes place in the stroma, and fixes CO_2 on a molecule of ribulose-1,5-bisphosphate to form two molecules of 3-phosphoglycerate, which are reduced and converted to carbohydrates. At the end of the cycle a net gain of sugar is achieved, and the ribulose-1,5-bisphosphate is regenerated.
After the invention of SDS–PAGE (Laemmli, 1970) the biochemical composition of the macromolecular protein complexes present in the thylakoid membrane began to be elucidated and were revealed to be composed of an astonishing number of subunits (Fig. 6) whose detailed functions still partially remain to be elucidated.

1.3.1. Photosystem II: a Water–Plastoquinone Oxidoreductase

The PSII reaction centre (RC) is composed of two homologous ca. 32-kDa proteins known as D1 and D2, each consisting of 5 transmembrane helices. Two intrinsic light-harvesting Chlorophyll (Chl) *a*-containing proteins (CP), named CP43 and CP47, are closely associated with the D1 and D2 proteins. These proteins consist of 6 transmembrane helices and bind 14 and 16 Chl *a* molecules, respectively. There is also a number of other low-molecular-mass subunits usually having a single transmembrane helix, which are rather featureless except for the PsbE and PsbF proteins that provide histidine ligands for the high-potential haeme of Cyt b559. Finally, the PSII RC core complex has several extrinsic proteins attached to its lumenal surface, where they form a protein shield over the catalytic site of water splitting. The PSII RC core complex is surrounded by peripheral LHC systems, containing Chl *a* and *b*. These are trimers of the light-harvesting proteins Lhcb1, Lhcb2 and Lhcb3, although each trimer can contain different stoichiometries of these proteins. Energy transfer from LHCII to CP43/CP47 or D1/D2 is mediated by the minor light-harvesting proteins Lhcb6 (CP24), Lhcb5 (CP26) and Lhcb4 (CP29). The number of trimers that are associated with PSII varies with irradiance level. In fact, one response to variation in light intensity involves the rapid (within minutes) redistribution of absorbed energy between PSII and PSI, with the so-called state I-II transition (Kanervo *et al.* 2005). When excess light is captured by PSII, a subpopulation of LHCII trimers dissociates from PSII and associates with PSI. This response is correlated with the activity of a kinase that phosphorylates LHCII proteins, increasing its affinity for PSI. However, long term light adaptation can also occur and involves changes in the antenna size of PSII: LHCII is particularly abundant in plants adapted to shade conditions, thus promoting light capture (Nelson *et al.* 2006; Danielsson *et al.* 2006).

The chemical reactions involved in electron transfer during photosynthesis start with the excitation of a Chl by light and the reduction of the first electron acceptor. After absorption of the first photon, the reaction centre Chl, known as P680 (680 nm is the peak of the lowest-energy absorption band of P680), translocates an electron through a pheophytin (Pheo) molecule to the tightly bound quinine Q_A, and then to the mobile quinone Q_B. The oxidized $P680^+$, which has the highest redox potential observed in a biological system (> 1 V), oxidizes a nearby tyrosine (Y_Z) residue of the D1 protein. Y_Z then extracts an electron from a cluster of four manganese ions, which binds two substrate water molecules and has a calcium ion, a chloride ion and a bicarbonate ion as necessary cofactors. After another photochemical cycle, the doubly reduced Q_B (Q_B^{2-}) takes up two protons from the stroma to form PQ_BH_2 and is released into the lipid bilayer to be replaced by an oxidized quinone from the membrane quinone pool. This pool consists of oxidized (PQ) and reduced (PQH_2) plastoquinones. After two more photochemical cycles, the manganese cluster is provided with a total of four oxidizing equivalents, which are used to oxidize two water molecules to produce O_2. The manganese cluster is then reset to its initially reduced state, which is designated S_0 in the so-called five S-states reaction (S_0–S_4) (Nelson *et al.* 2004).

1.3.2. Cytochrome-*b_6f* Complex: a Plastoquinone–Plastocyanin Oxidoreductase

Each monomer of the dimeric Cyt b_6f complex contains eight polypeptide subunits. This complex consists of four large subunits (17–32 kDa): the membrane bound c-type Cyt f (PetA), Cyt b_6 (PetB), the ISP (PetC), and the subunit IV (PetD); and four low-molecular-weight (3–4 kDa) hydrophobic subunits: PetG, PetL, PetM and PetN, which form a "picket fence" type structure around the core of the large subunits. This leads to a dimer that has a molecular weight of about 217 kDa (Nelson *et al.* 2004).

In the chloroplast cytochrome-b_6f complex, the two-electron oxidation of a reduced quinone (PQH_2) bound to the lumenal Qo site results in the release of two protons to the aqueous lumen. One electron is transferred from the reduced quinone to plastocyanin through a high-potential chain: this consists of the Rieske iron–sulphur protein and the Cyt f. Conversely, the second electron is translocated across the membrane through two haem groups of Cyt b_6, to reduce a quinone that is bound at the stromal Qi site. Following a second reduction event at the Qi site, two protons are taken up from the stroma at this site and the reduced quinone is released into the lipid bilayer, where it joins the reduced quinone pool. Therefore, a proton-

motive force is formed across the membrane due to both the water splitting activity of PSII and the recycling of quinones at the Cyt b_6f (Nelson *et al.* 2004).

1.3.3. Photosystem I: a Plastocyanin–Ferredoxin Oxidoreductase

PSI of higher plants is composed of two moieties: the reaction centre and the peripheral LHCI. Fifteen core subunits (PsaA to PsaL, PsaN to PsaP) of PSI are known so far, and LHCI consists of up to six Lhca proteins (Lhca1–6).

The PsaA–PsaB heterodimer forms the reaction centre of PSI. It binds the P700 special Chl pair, where the light-driven charge separation occurs, and it also includes the primary electron acceptors A0 (Chl *a*), A1 (phylloquinone) and FX (a Fe_4S_4 cluster). In addition, this heterodimer coordinates about 80 Chls that function as an intrinsic light-harvesting antenna. Two further Fe_4S_4 clusters (FA and FB) are the terminal components of the electron-transfer chain and bound to PsaC. The other protein subunits carry out other functions: PsaF and PsaN are important for the interaction with the lumenal electron donor plastocyanin; PsaD and PsaE provide the docking site for soluble ferredoxin on the stromal side of the thylakoid membrane; PsaF is crucial for binding of the Lhca1/Lhca4-dimer. The LHCI is composed of a modular arrangement of four light-harvesting Chl-containing proteins (Lhca1–Lhca4). The monomer Lhca1 binds tightly to the reaction centre, whereas the other Lhca monomers are bound to the reaction centre through relatively weak interactions. (Nelson *et al.* 2006; Scheller *et al.* 2001, Melkozernov *et al.* 2005)

As for PSII, also PSI functions as a light-dependent oxido-reductase to transport electrons from a donor (plastocyanin) to a final acceptor, which is ultimately $NADP^+$. When the excitation energy arrives to the primary electron donor P700, the excited state of these special Chls can be converted into a charge separated state, resulting in oxidized $P700^+$ and a reduced Chl molecule acting as the primary electron acceptor, named A_0. The charge separation is stabilized by fast electron transfer from this first acceptor to secondary acceptors, one of which is a phylloquinone molecule. Through a chain of electron transporters these electrons are driven to the soluble, stroma localised ferredoxin, which provides in its turn electrons for the reduction of $NADP^+$ (Nelson *et al.* 2004).

1.3.4. F-ATPase: a Proton-Motive Force-Driven ATP Synthase

ATP synthase (F-ATPase) is ubiquitously found on energy-transducing membranes, such as chloroplast thylakoid membranes, mitochondrial inner membranes and bacterial plasma membranes. The general structural features of the chloroplast ATPase are highly conserved, and its structure and functional mechanism are similar to those of bacterial and mitochondrial ATPases. The enzyme is a multisubunit complex with distinct stromal and transmembrane regions that are known as CF1 and CF0, respectively. It is a molecular motor that is driven by the proton-motive force generated by the complexes of the photosynthetic electron transport chain. In chloroplasts, CF0 contains four subunits, named a, b, c and d, with probable stoichiometry of 1:1:14:1. The 14 c subunits form a ring-like structure that is equivalent to the c-ring of other F-ATPases. The CF1 contains five subunits: α, β, γ, δ, and ε (Nelson *et al.* 2004).

Proton flux from lumen to stroma through CF0 is coupled to ATP synthesis at sites in the β-subunits of CF1. The whole CF0–CF1 complex is thought to function as a rotary proton-driven motor, in which the stationary subunits are a, b, d, δ, α and β, and the rotary subunits are c, γ and ε. Therefore, a complete cycle of the rotor yields three ATP molecules, requiring 14/3 = 4.6 protons for the formation of each ATP molecule (Nelson *et al.* 2004).

The relationships among the various complexes of the thylakoid membranes are ultimately responsible for the three-dimensional arrangement of the thylakoid membranes. The most interesting feature of these membranes is the construction of stacked domains in the grana. Chow et al. (2005) recently reviewed the electrochemical forces driving the formation/maintenance of grana stacks, whose importance can be deduced from the fact that, although they are not essential for photosynthesis, they are ubiquitous in higher plants. Therefore, they argue that grana may have been selected during evolution for the functional advantages that they confer to higher plants. In the Authors' review, they list eight possible functional consequences of the differentiation of granal stacks: (1) enhancement of light capture through a vastly increased area-to-volume ratio and connectivity of several PSIIs with large functional antenna size, (2) the ability to control the lateral separation of PSI from PSII and, therefore, the balanced distribution of excitation energy between two PSs working in series, (3) the reversible fine-tuning of energy distribution between the PSs by state I-II transitions, (4) the ability to regulate light-harvesting via controlled thermal dissipation of excess excitation energy, detected as non-photochemical quenching, (5) dynamic flexibility in

the light reactions mediated by a granal structure in response to regulation by a trans-thylakoid pH gradient, (6) delaying the premature degradation of D1 and D2 reaction-centre protein(s) in PSII by harbouring photoinactived PSIIs in appressed granal domains, (7) enhancement of the rate of non-cyclic synthesis of adenosine triphosphate (ATP) as well as the regulation of non-cyclic vs. cyclic ATP synthesis, and (8) the potential increase of photosynthetic capacity for a given composition of chloroplast constituents in full sunlight, concomitantly with enhancement of photochemical efficiency in canopy shade.

Based on a wide literature coverage, the assumption that chloroplast ultrastructure and function are intimately intertwined remains a well-grounded concept (Chow *et al.* 2005).

1.3.5. Photosynthesis in Fruits

Green leaves are regarded as the main sources of photosynthate production in plants, however, other tissue can also be photosynthetically active. Stem tissues, roots, and reproductive organs can contribute to the overall carbon gain of plants. Net photosynthesis by reproductive structures has been observed in many species in sterile and fertile parts of the inflorescence, such as bracts, stalks, sepals, petals, anthers, pistils, and also in fruits. As to the fruits, it is possible to distinguish between green-ripe fruits, such as cucumber, kiwi, pea, pepper, green apple varieties, etc., and green-young-fruits, which vary in colour upon ripening, such as currant, orange, lemon, grape, etc. The main function of colouration in ripe fruits is considered to be the attraction of dispersers. In fact, the role of fruits remains mainly linked to seed development and dispersal. However, green fruits typically perform an effective CO_2 internal recycling using the respiratory CO_2 released or, in some cases, can even get a net carbon gain. Carbon fixation in fruits has typically been measured using gas exchange or ^{14}C-uptake techniques. When calculated on a Chl basis, the CO_2 fixation of fruits usually results quite comparable with that of the leaf. In many species, fruit photosynthesis can provide a significant proportion of the carbon requirement of reproduction and may positively contribute to the whole plant carbon budget. Consequently, the photosynthetic capability is proposed as the main ecological advantage of green fruits (Aschan *et al.* 2003).

Nevertheless, estimation of the photosynthetic contribution of green fruits to their own carbon requirement varies and depends on the environmental conditions, the species considered and the type of fruit developed, for instance whether it is fleshy or not. A part of this complexity arises from the double role of green fruits, as a sink and as a source, with changing importance during ontogeny. (For a recent review, see: Aschan *et al.* 2003)

1.4. Arum italicum

Arum italicum Miller is common in south and west Europe and belongs to a large family of perennial herbs: the Araceae (Liliopsida, Arecidae, Arales). Containing significant amounts of calcium oxalate crystals, oxalic acid and oxalates, in addition to volatile and/or easily destroyed irritating substances, *Arum* plants are toxic. However, dried or fresh parts are used for food and in folk medicine in Turkey (Saglik *et al.* 2002).

Fig. 7: Draw of *Arum italicum*, showing the petiolated leaves, the spadix wrapped in the spathe, the infructescence.

A. italicum plants are characterised by underground tubers and by basal and petiolated leaves (Fig. 7). The leaves are hastate, with lateral lobes divergent and often with conspicuous whitish veins (Flora Europaea, Cambridge University Press). This species forms two types of leaves: the "winter leaves" appear in autumn or early winter, reach the fully vegetative stage in February-March and are then substituted by the "spring leaves", that abscise at the end of flowering (Pancaldi *et al.* 1998). Flowers are unisexual, arranged in a compact spike, called spadix. The spadix consists of two main parts: a cylindroid fertile portion and a clavate sterile portion, which is prolonged beyond the flower-bearing zone in a fleshy, coloured appendix. In the fertile portion with both male and female zones, there are two zones of sterile flowers, called bristles. The female flowers are located near the basis of the spadix and the male flowers above them, meanwhile sterile flowers are present both between male and female and

above the male (Barabe *et al.* 2003). The flowers are partially enfolded by a large petaloid bract, the spathe, which is withering before the fruits are ripe. *A. italicum* attracts olfactory dung-breeding flies through deceit. These insects are principally represented by Diptera, all belonging to saprophyte families. The insects are attracted by the volatilization of odoriferous compounds, and trapped inside the spathe. (Albre *et al.* 2003). The fruits are berries, developing from late spring to early summer. Each berry can contain 2-4 seeds and the seed number per berry is likely to be determined by resource or pollen limitation and not by seed-packaging costs. Nevertheless, this causes variation in seed size, in fact, seeds in upper berries are more numerous and smaller than seeds in lower berries (Mendez *et al.* 2001).

In the plant of *A. italicum*, several green tissues can be observed. In fact, the whole leaf, including the lamina and the long petiole, is photosynthetically active. Moreover, *A. italicum* develops berries which are green in a stage characterised by the presence of chloroplasts with ultrastuctural features similar to the lamina chloroplasts. Our knowledge about the plastid system in different tissues of *A. italicum* is based upon studies that have investigated the mature winter leaves (Pancaldi *et al.* 1998) and the berries during maturation and ripening (Bonora *et al.* 2000).

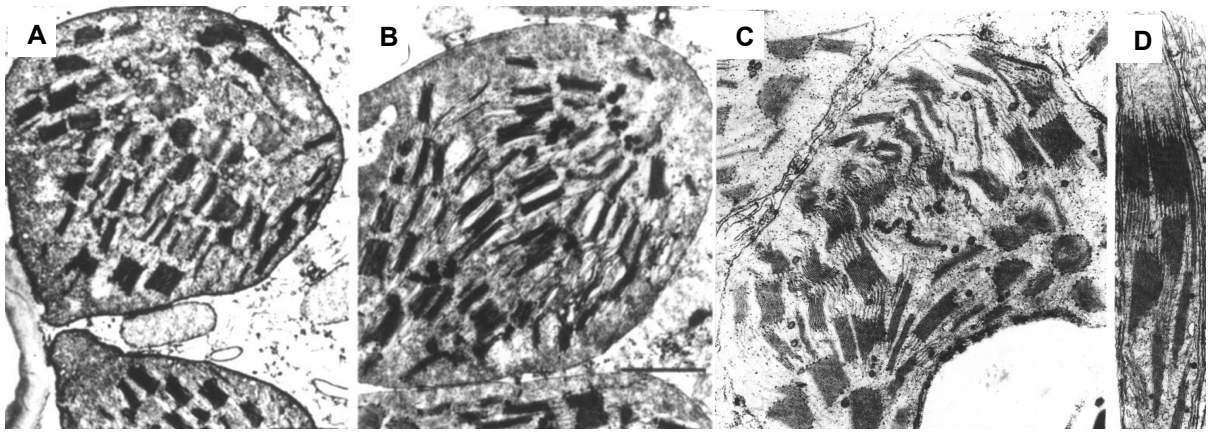

Fig. 8: Chloroplasts of *Arum italicum* leaf. A) palisade tissue, B) spongy tissue, C) outer petiole, D) inner petiole. (Modified from Pancaldi *et al.* 1998).

In particular, intra-tissue properties of chloroplasts in laminae and petioles of mature winter leaves have been characterised by means of ultrustructure observations of the plastids and carotenoid analyses (Pancaldi *et al.* 1998). The mesophyll of the lamina is divided into palisade and spongy tissues. When observed using transmission microscopy, both tissues contain chloroplasts with a well-organised lamellar system, with normally differentiated grana and stroma thylakoids. No differences are observed either in the appressed/non-appressed

membrane ratio or in the degree of stacking. In the petiole, two different parts are distinguished: an outer parenchyma and an inner aerenchyma. All chloroplasts of the outer region show structural aspects which are analogous to the chloroplasts in the lamina, while those of the inner aerenchyma have the characteristics of extreme shade adaptation. In fact, they show a high stacking degree of granal thylakoids (Fig. 8). The inner part of the petiole also presents a low Chl *a*/*b* ratio and anomalies in pigment composition, suggesting on the whole a low presence of reaction centres and abundant LHCs.

The development of berries has been studied with particular regard to plastid ultrastucture and carotenoid biosynthesis (Bonora *et al.* 2000). The berries of *A. italicum* develop in two phases. The first one is *maturation* and starts with large carpel modifications and ends when the maximum organ expansion has been reached. The colour of the berries changes from ivory to ivory-green till deep green, reflecting the differentiation of the amyloplasts, present in the ivory berry, to chloroplasts, characterizing the deep green berry. The second phase is *ripening* and is mainly characterised by modifications in the chemical composition of the organ. Moreover, the chloroplasts present in the green berry develop into chromoplast at the end of the ripening period (Fig. 9).

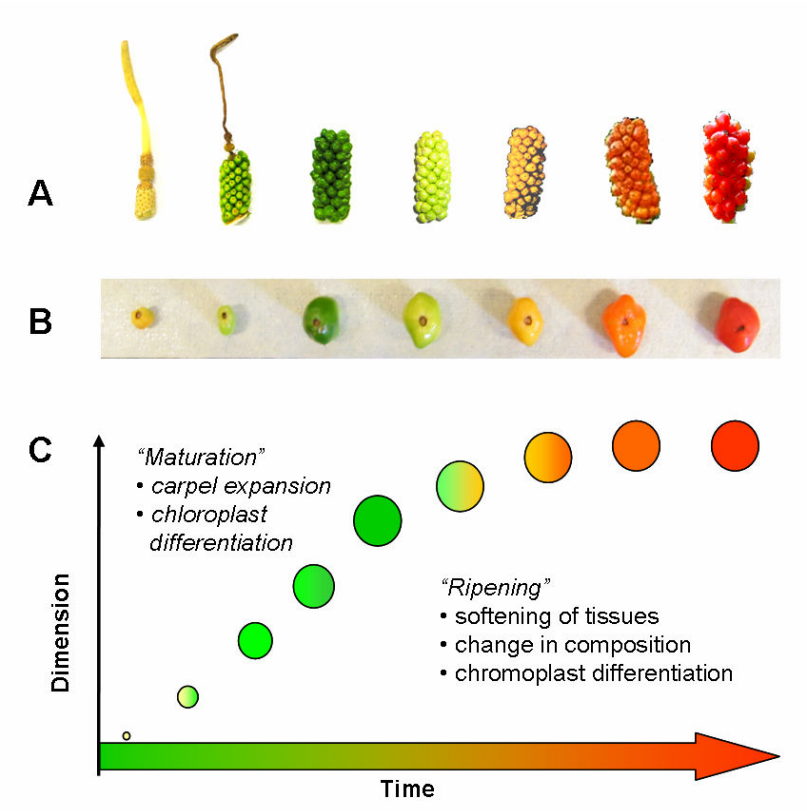

Fig. 9: Ontogeny of *Arum italicum* berries. A) series of developing infructescence and B) berries, showing the ivory, ivory-green, green, green-yellow, yellow, orange and red stages. C) dimension-time diagram of fruit development, showing the maturation and ripening phases.

The ivory berry represents the first stage of development of *A. italicum* berries. The plastids are amyloplast, with a round-shape and a conspicuous starch grain. The internal membrane system is hardly developed. Only few, long and usually concentrically ordered thylakoids are present. In ivory-green berry, transition forms from amyloplast to chloroplast are always observed. In the organelle, the stroma region is still partially occupied by starch grains, but a quite abundant membrane system is already differentiated into stromal and granal thylakoids. At the end of the maturation phase, the green berry contains fully developed chloroplasts. The well developed thylakoid membrane system appears ultrastructurally similar to that of the lamina chloroplasts. However, 5-10% of the green berry chloroplasts already show the first signs of transition into chromoplasts (Fig.10).

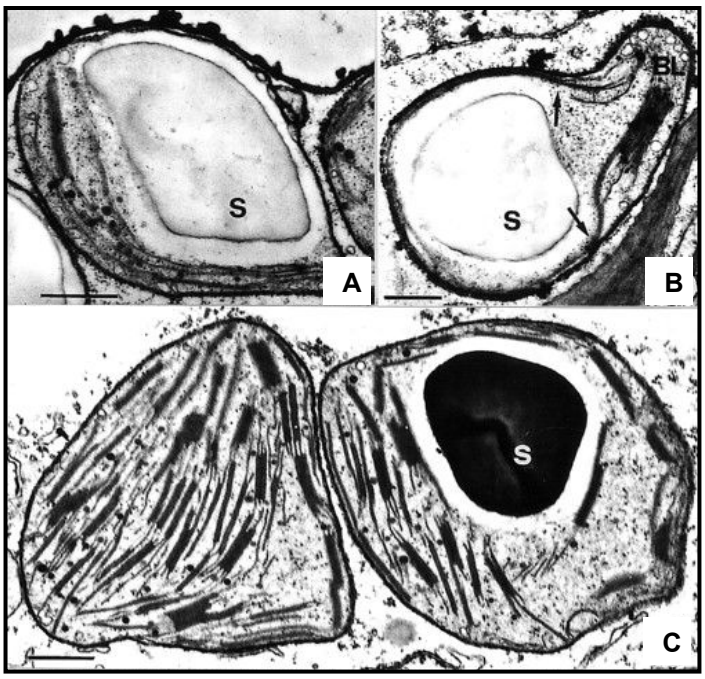

Fig. 10: Plastids of *Arum italicum* berry during maturation. A) amyloplast in ivory berry; B) amyloplast to chloroplast transition in ivory-green berry; C) chloroplasts in mature green berry. S = starch. (Modified from: Bonora *et al.* 2000).

During the ripening, chloroplasts are converted to chromoplasts. In yellow berry the chloroplast membranes are almost completely degraded, while thylakoid remnants are seen to lose their lumina. Simultaneously with the degradation of the thylakoids, carotenoid-bearing structures develop. In orange and red berries the development of chromoplasts is finally complete. Elliptical carotenoid crystalloids are abundant in the stroma and the membranous structures characterising the pre-ripe yellow stage have almost completely disappeared. However, some wavy membranes are also present in these chromoplasts, mainly localized under the envelope (Fig. 11). The variations in plastid structure accompanying the maturation

and ripening of the berry are parallel to wide changes in the carotenoid pattern, also including unique characteristics, as extensively analysed by Bonora and co-workers (2000).

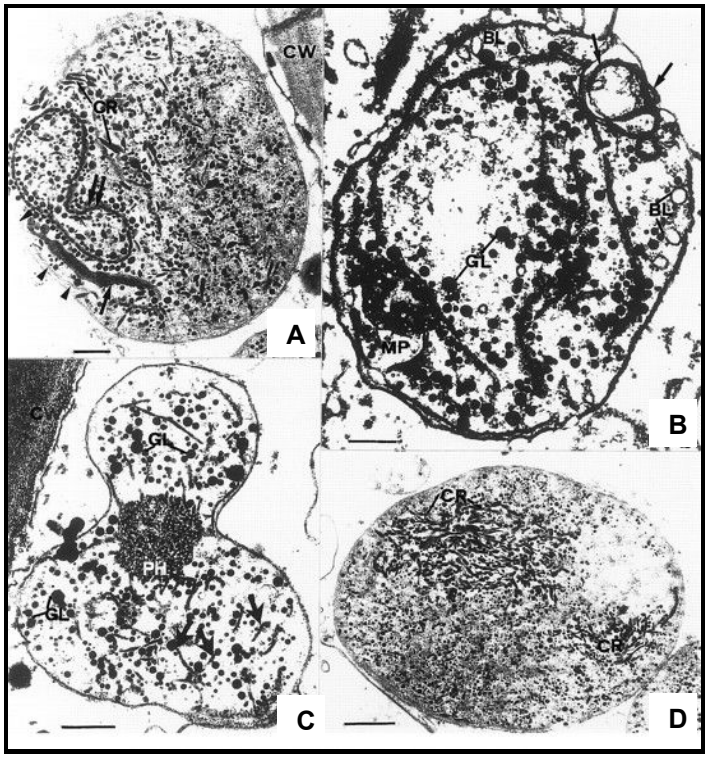

Fig. 11: Plastids of *Arum italicum* berry during ripening. A, B and C) several aspects of chromoplasts from yellow berry, D) fully-developed chromoplast in red-orange ripe berry. (Modified from: Bonora *et al*. 2000).

2. MATERIALS AND METHODS

2.1. PLANT MATERIAL

Plants of *Arum italicum* Miller (Araceae), grown in their natural environment in the area of the Po plains around Ferrara (Italy) were harvested during three vegetative seasons (2005-2007) and used for the studies presented in this thesis. The leaves were harvested in February and the berries were harvested from the beginning of April to the end of June. The berries were collected at the following seven stages of development:

1. immature *ivory* berries
2. immature *ivory-green* berries
3. mature dark *green* berries
4. partially ripe *green-yellow* berries
5. partially ripe *yellow* berries
6. ripe *orange* berries
7. fully ripe *red* berries

All analyses were carried out on at least three replicates collected from different plants.
The palisade and the spongy tissues of the leaf lamina were separated by gentle mechanical abrasion, using sandpaper. The outer and the inner parts of the petiole were separated using a blade. Since in each berry the distal cap (with respect to the insertion on the infructescence axis) was the zone most advanced in ontogenesis, all the analyses were performed only on this region of the pericarp, isolated using a scalpel.

2.2. LIGHT AND FLUORESCENCE MICROSCOPY

For light and fluorescence examinations, a Zeiss model Axiophot photomicroscope, equipped with conventional or reflected fluorescence condenser, was employed. For chlorophyll autofluorescence observations, the light source was a mercury pressure vapour lamp, HBO 100W, with excitation at 436 nm (Filter set: BP 436/10 and LP 470) (Ferroni *et al.* 2007).
Images were obtained with a Canon Powershot S40 digital camera (4 megapixel) mounted on the ocular lens through a Leica DC150 system.

2.3. CO_2 GAS EXCHANGE

Dark respiration and net photosynthesis were measured using an LCA-4 type (ADC Co. Ltd., Hoddesdon,U.K.) open system infrared gas analyzer, at ambient CO_2 concentration (420 ± 10 μL L^{-1}). Gas exchange was measured in unexcised leaves and in excised berries.

The dark respiration measurements were carried out on plant material after stabilisation in darkness for at least 1 min. Net photosynthesis measurements were carried out on the same material exposed to bright sun light. Irradiance was 1500 ± 200 μmol photons m^{-2} s^{-1}, as determined by the PAR sensor incorporated in the ACD leaf chamber. Each determination lasted for 4-5 min.

Gas exchange was determined both on a surface unit area and on a Chl unit basis.

2.4. PIGMENT EXTRACTION AND ANALYSIS

Pigments were extracted from small leaf or berry pieces by incubating in 80% aqueous acetone (v/v) for at least 24 h in complete darkness at -20°C. The extracts were clarified by centrifugation and analysed with a Pharmacia model Ultrospec 2000 UV-Vis spectrophotometer (1 nm resolution). For Chl and carotenoid determinations, the absorbtions were recorded at 663 nm (Chl *a*), 646 nm (Chl *b*), and 470 nm (carotenoids), and pigments concentrations were determined with the equations reported in (Wellburn, 1994).

2.5. THYLAKOID ISOLATION

Thylakoid membranes were isolated according to (Rokka *et al.* 2005). The plant material, frozen in liquid nitrogen and mixed with quartz sand, was homogenized in 50 mM Tricine-NaOH, pH 7.8, 330 mM sorbitol, 5 mM $MgCl_2$, 2 mM Na_2EDTA, 5mM ascorbate, 0.05% bovine serum albumin, and 10 mM NaF. The quartz sand was removed by centrifugation at 2000rpm, 5 min, at 4°C. The supernatant was collected and thylakoids where washed in 50 mM Tricine-NaOH, pH 7.8, 5 mM sorbitol, 5 mM $MgCl_2$, 2 mM Na_2EDTA, and 10 mM NaF and centrifuged again for 5 min, 18000g, at 4 °C. The thylakoid pellet was resuspended in 50 mM Tricine-NaOH, pH 7.8, with 100 mM sorbitol, 5 mM $MgCl_2$, 2 mM Na_2EDTA, 5mM ascorbate, 0.05% bovine serum albumin and 10 mM NaF, centrifuged for 5 min, 18000g, at 4 °C, and finally resuspended in the same buffer. The samples were rapidly frozen in liquid

nitrogen and stored at -80°C until further analyses. Manipulation of samples was peformed under a dim green safe-light.

Protein quantification was carried out using the RC DC Protein Assay kit (Biorad).

Chl was extracted with 80% (v/v) buffered acetone (2.5 mM HEPES-NaOH, pH 7.5) and quantified as described (Porra *et al.* 1989)

2.6. DENATURING ELECTROPHORESIS

Proteins were separated in SDS-PAGE (15% acrylamide, 6 M urea) according to (Laemmli, 1970) with minor modifications. In each well, 75 µg of proteins were loaded.

After electrophoresis, the proteins were visualized by silver staining, or were electroblotted onto a PVDF (Millipore, Watford, Herts., U.K.) membrane.

2.7. BLUE NATIVE ELECTROPHORESIS

BN/PAGE was performed as described by (Rokka *et al.* 2005) and co-workers (2005), with minor modifications as follows.

Thylakoids were resuspended in 10 volumes washing buffer (25mM BisTris-HCl, pH7.0 and 330 mM sorbitol), centrifuged at 18000g at 4°C for 5min and resuspended in medium A (25mM BisTris/HCl, pH7.0, 20%, w/v, glycerol and 0.25mg·ml^{-1} Pefabloc). An equal volume of 5% (w/v) dodecyl β-D-maltoside (Sigma), freshly prepared in medium A, was added. Thylakoids were then solubilized on ice for 10 min and centrifuged at 18000g at 4°C for 5min. The supernatant was supplemented with 1/10 volume of 100mM BisTris/HCl, pH7.0, 0.5M ε-amino-n-caproic acid, 30% (w/v) sucrose and 50mg·ml^{-1} Coomassie Brilliant Blue G250. Samples were loaded in a 5–12% gradient of acrylamide gel and electrophoresis was performed at 0°C for 3.5h by gradually increasing the voltage from 75 to 200V, using a Hoefer Mighty Small system (Amersham Biosciences).

After BN/PAGE, the lanes were cut and incubated for 30min at room temperature (21°C) in Laemmli sample buffer containing 5% (v/v) β-mercaptoethanol). Separation of the protein subunits of the complexes was perfomed with denaturing SDS/PAGE (15% polyacrylamide and 6M urea).

After electrophoresis, proteins were visualized by silver staining, or were electroblotted onto a polyvinylidene fluoride (PVDF) (Millipore, Watford, Herts., U.K.) membrane.

2.8. IMMUNOBLOT ANALYSIS

After electrophoresis, proteins were electroblotted to a PVDF membrane (Millipore). Western blotting with enhanced chemiluminescence detection was performed with standard techniques using a Phototope-Star Chemiluminescent Detection Kit (New England Biolabs) and protein-specific antibodies or an antibody raised against the entire PSI and LHCII complexes.

1. D2 protein (PSII)
2. D1 protein(D1 DE 1:5000)
3. CP47 (PSII)
4. LHCII proteins
5. Lhcb1 (LHCII)
6. Lhca4 (LHCI)
7. Cyt *f* (Cyt b_6f)
8. PSI A/B

Protein amount was quantified with FluorChem Image Analyser (Alpha Innotech Corporation, San Leandro, CA, U.S.A.).

2.9. LIQUID CHROMATOGRAPHY – ESI (ELECTROSPRAY) MS/MS

In-gel trypsin digestion and sample preparation for mass spectrometry (MS) analysis were performed manually, as described by Shevchenko and coworkers (1996). Tandem mass spectrometry was performed on API QSTAR (Applied Biosystems, Foster City, USA) equipped with Nano ESI source (Protana, Toronto, Canada) and connected in-line with the nano HPLC system and the autosampler (Ultimate, Switchos and Famos) (LC Packings, Amsterdam, Netherlands). Eluted and dried protein digests were dissolved in 10 µl of 2 % formic acid, centrifuged for 10 min at 12000 x g, and transferred into an autosampler vial. Aliquots (8 µl) of samples were loaded onto a C18 PepMap, 5 µm, 1 mm x 300 µm I.D. nano-precolumn (LC Packing, Amsterdam, Netherlands), desalted for 4 min (20 µl/min) and subjected to reverse-phase chromatography on a C18 PepMap, 3 µm, 15 cm x 75 µm I.D. nanoscale LC column (LC Packing, Amsterdam, Netherlands). The gradient of 2-70 % acetonitrile in 0.1 % formic acid was applied for 45 min with the flow rate of 0.2 µl/min. The acquisition of MS/MS data was performed on-line using fully automated IDA feature of the Analyst QS software (Applied Biosystems, Foster City, USA). The acquisition parameters were 1 sec for TOF MS survey scans and 2-3 sec for the product ion scans of two most

intensive doubly or triply charged peptides. The major trypsin peptides were excluded from MS/MS acquisition. Analyses of MS/MS data and *de novo* sequencing were performed with the Analyst QS software followed by the BLAST search for the homologous sequences in the NCBI database.

2.10. 77 K FLUORIMETRY

Seventy-seven-Kelvin (77 K) fluorescence emission spectra of thylakoid membranes were recorded with a diode array spectrophotometer (S2000; Ocean Optics) equipped with a reflectance probe as previously described (Keranen *et al.* 1999). Fluorescence excitation was obtained with light below 500 nm, defined using LS500S and LS700S filters (Corion, Holliston, MA) placed in front of a slide projector, and the emission was recorded between 600 and 800 nm.

2.11. MICROSPECTROFLUORIMETRY

For analyses, hand-made tissue sections were mounted onto polylysine microslides (Menzel-Gläser, Germany). Fluorescence emission spectra were recorded using a microspectrofluorimeter (RCS, Florence, Italy), associated with a photomicroscope Zeiss model Axiophot. All spectra were recorded *in vivo*, at room temperature, on small cell groups (2-4 cells) that were selected at the microscope under fluorescent light (1000x magnification). The excitation light at 436 nm was focused on small cell groups at a time using a 1.6 mm diaphragm. The emission light was collected by the objective lens and deviated to the detector system, which included a monochromator reticle (band pass 0.25 nm), endowed with a computer-assisted stepper-motor, and a photomultiplier tube, coupled with an analogue/digital converter for data transfer to the 'Autolab' software (RCS, Florence, Italy). The 'Autolab' software was also used to set the recording range (620–780 nm) and to optimize the photomultiplier response. Fluorescence levels, measured in arbitrary units of fluorescence directly established by the setting system, were visualized as emission spectra by the same program. For each sample at least five spectra were recorded.

Spectra elaboration was performed with the 'Origin 6.0' program (Microcal Software Inc.) (Pancaldi *et al.* 2002; Ferroni *et al.* 2007).

Each experimental spectrum was elaborated individually, after baseline correction. The resulting graph was smoothed with the "FFT (Fast Fourier Transform) filter" smoothing function. The degree of FFT filtering was controlled by specifying the number of points to be considered; routinely, two smoothing cycles with 10 points were made. Total fluorescence yield was calculated by integration, as area below the spectrum. For subsequent elaboration, a fourth derivative analysis of spectra was performed to obtain the first information on spectral components, taking into account the limitations of the method, as extensively analysed by (Boddi *et al.* 1997). The same spectra were fitted by Gaussian bands essentially following the procedure proposed by (Siffel *et al.* 1999), which is based on fixed parameters and is suitable for comparison of amplitudes. However, some modifications were introduced. For each spectrum, the same maxima and bandwidths were initially kept fixed and the amplitudes changed to obtain a first approximate reconstructed spectrum. Subsequently, the iterative fitting algorithm incorporated in Origin software was run to obtain a more precise correlation with the original spectrum. All spectra were fitted with nine Gaussian bands in the range of Chl emission (650-750 nm), whose maxima were obtained through a comparative analysis of the fourth derivatives of different spectra. Fluorescence yield of emission bands correspond to the areas subtended under the corresponding Gaussian curve.

Fluorescence emission bands were interpreted according to previous works (Pancaldi *et al.* 2002; Ferroni *et al.* 2004; Baldisserotto *et al.* 2004; Baldisserotto *et al.* 2005a; Baldisserotto *et al.* 2005b; Baldisserotto *et al.* 2007; Ferroni *et al.* 2007). The attribution of the bands is reported in Table 1.

For each spectrum, fluorescence emission ratios (RCII/CP43-47 and PSII/LHCII) were calculated and for each sample the average ratios were obtained.

Tab. 1: Attribution of fluorescence emission bands.

λ (nm)	Attribution	References
665-675	Uncoupled chlorophyll	(Santabarbara *et al.* 2001)
676-680	RCII	(Ignatov *et al.* 1994; Ignatov *et al.* 1998)
683-697	CP43-47	(Alfonso *et al.* 1994; Groot *et al.* 1999)
699-715	LHCII	(Vassiliev *et al.* 1995)
720-750	PSI and LHCI	(Krause *et al.* 1991)

2.12. STATISTICAL ANALYSES

Where differences are described as significant, a *t* test was performed using the algorithm incorporated into the Origin 6.0 programme (Microcal Software Inc.) and yielded a value below 5% ($P < 0.05$).

3. RESULTS

3.1. PHOTOSYNTHETIC CHARACTERISATION OF THE WINTER LEAF

The winter leaf of *Arum italicum* is formed by an expanded lamina carried by an elongated petiole, which connects the leaf with the underground tuber. Both lamina and petiole are green (plants used for this research did not show extensive variegation) representing the photosynthetic tissues (Pancaldi *et al.* 1998). These tissues can be further classified as follows:

- the palisade tissue - the upper part of the leaf lamina
- the spongy tissue - in the leaf lamina below the palisade
- the outer part of the petiole
- the inner part of the petiole

These photosynthetic tissues were individually analysed for their biochemical properties after mechanical separation of the tissues. On the other hand, the CO_2 exchange is a physiological parameter at the organ level. For this reason, its measurement have been performed on the two parts of the leaf i.e. the lamina and the petiole, although it is know that different tissues might have different contributions to overall CO_2 fixation rates.

A convenient reference for analyses of the photosynthetic performance of different tissues is the palisade tissue in the lamina, which is known to be the most photosynthetically active tissue in plants.

3.1.1. Light and Fluorescence Microscopy Studies

When observed using light microscopy (Fig. 12 a), the cross section of the lamina showed a dorsiventral structure, with a mesophyll composed of palisade and spongy tissues, enclosed by an upper and a lower epidermis, both with stomata. The palisade tissue is in the upper part of the mesophyll and is composed of cylindrical cells, rich in chloroplasts. The palisade tissue of *Arum italicum* presents only one layer of palisade cells. The spongy tissues is localised below the palisade. It is characterised by cells with irregular shape, with large intercellular spaces, which confer the “spongy” appearance to this tissue. *A. italicum* leaves also present

abundant raphides. Raphides are bundles of narrow, elongated needle-shaped crystals of calcium oxalate, usually of similar orientation. In Araceae one of the two ends is abruptly pointed. There are varying numbers of crystals in each bundle. They are usually found in crystal idioblasts in parenchymatous tissues, although raphides occur also in specialized tissues, such as aerenchyma (Prychid *et al.* 1999). Fluorescence microscopy did not reveal substantial differences in the features of the chloroplast in the two mesophyll compartments (Fig. 12 b). However, chloroplasts of the palisade tissue emitted less bright fluorescence than those of the spongy parenchyma.

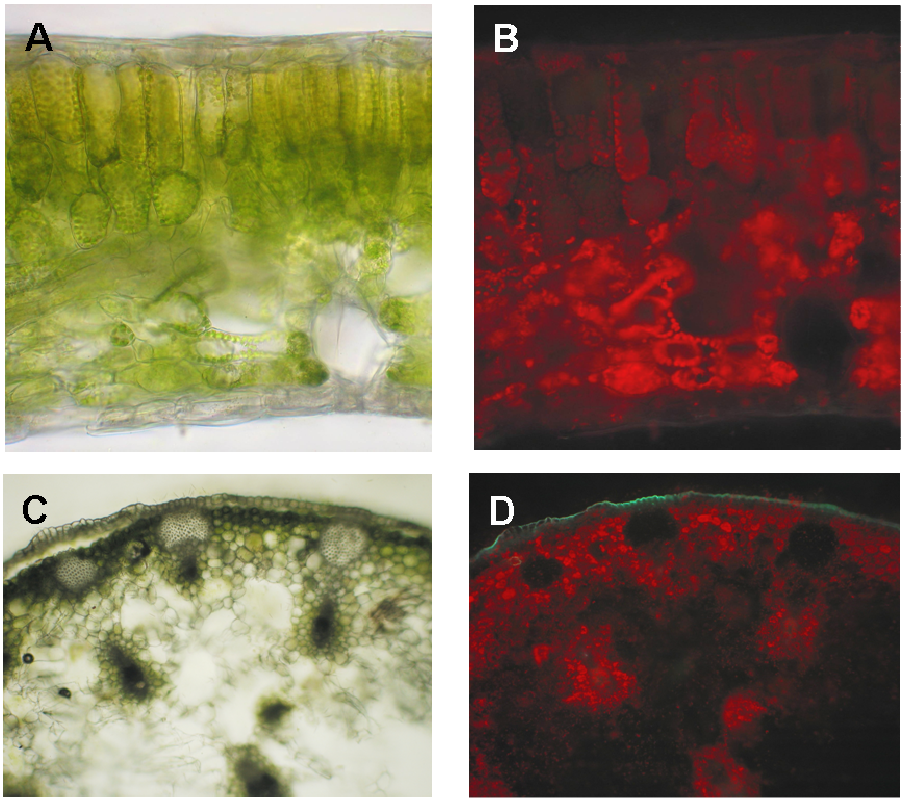

Fig. 12: Portions of a cross sections of the lamina (a-b) and petiole (c-d) of a dorsiventral leaf of *Arum italicum*. Light (a) and fluorescence (b) microscopy images of the lamina, showing the mesophyll enclosed between two epidermis; the mesophyll includes a palisade tissue in the upper part and a spongy tissue in the lower part. Light (c) and fluorescence (d) microscopy images of the petiole, red fluorescent chloroplasts are present in the innermost portion of the aerenchyma.

Light microscopy observations of the petiole (Fig. 12 c) showed, from outside to inside, a monolayered epidermis, lacking chloroplasts, and a compact subepidermal parenchyma made up of 4-5 cell layers, interrupted by collenchyma cords. The epidermis is interrupted by stomata. The inner part of the petiole is occupied by an extensive aerenchyma hosting numerous collateral vascular bundles, each surrounded by a parenchyma sheath. The aerenchyma tissue of the petiole allows the continuity of the lamina with the underground

tuber for gas exchange. Raphides are abundant also in the petiole. Fluorescence microscopy observation showed the presence of chloroplasts in the entire thickness of the petiole, including the inner aerenchyma (Fig. 12 d). The fluorescence intensity was apparently lower in the inner tissues than in the outer chlorenchyma.

3.1.2. Photosynthetic Pigments

Fig. 13 presents the result obtained from the analysis of the photosynthetic pigments of the four different tissues of *Arum italicum* leaves. The most evident aspect emerging from those analyses is the conspicuous difference in pigment concentration between the two parts of the leaf: the lamina and the petiole. This result is not surprising since it reflects the anatomical structure of the different tissues. In fact, the palisade and the spongy tissues contain many more chloroplasts than the outer and inner parts of the petiole. Moreover, a large portion of cells in the petiole are photosynthetically poorly or non active (many aerenchyma cells) (Fig. 12). For these reasons, the same unit of fresh-weight of lamina tissues would contain much more Chls than a fresh-weight unit of petiole tissues.

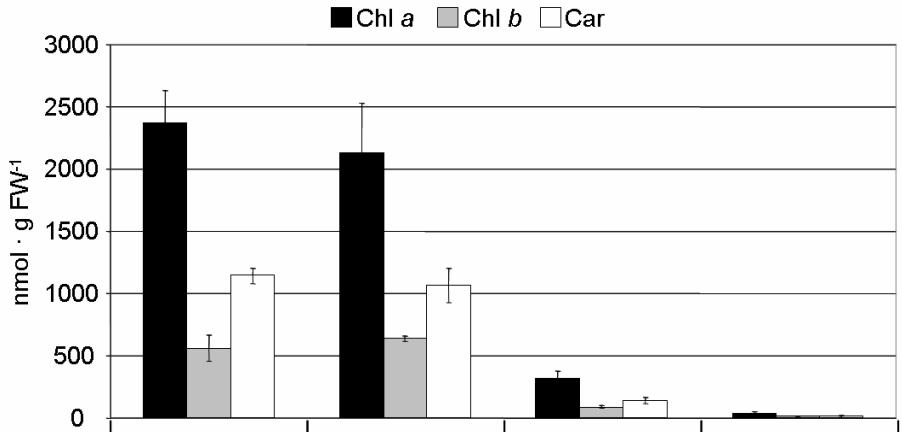

	Palisade	Spongy	Outer	Inner
Chl *a*/*b*	**4.28**	**3.32**	**3.56**	**3.40**
± SD	0.34	0.50	0.61	0.43
Chl (*a*+*b*) / Car	**2.56**	**2.59**	**2.94**	**3.60**
± SD	0.19	0.15	0.08	0.62

Fig. 13: Photosynthetic pigments and their molar ratios in the different tissues of mature winter leaf of *Arum italicum*. Data are means of three independent experiments (bars are S.D.).

No statistically significant differences were found between the palisade and the spongy tissues in any of the pigments tested, nevertheless there were significant differences between the Chl

a/*b* molar ratio. The latter is considered to be an index dependent on the available light, which is higher in sun-type tissues than is shade type ones. Fig. 13 shows that the Chl (*a*+*b*)/Car molar ratio of the inner part of the petiole was 3.60 ± 0.62, significantly higher than the values recorded for the other tissues.

3.1.3. Photosynthesis and Respiration Rates

Fig. 14 shows the CO_2 gas exchange rates of the lamina and the petiole, calculated per surface unit and on a Chl basis (Fig. 14 b). It is evident that the petiole is photosynthetically active, with an average net photosynthetic rate of 1.17 ± 0.14 μmol CO_2 m^{-2} s^{-1} (mean ± SD). Nevertheless, this value is markedly lower than that of the lamina. The lower photosynthetic activity of the petiole is only partially depending on the lower Chl content (Fig. 13). In fact, comparing the results presented in Fig. 14 a and b, it emerges that the petiole photosynthesis is lower even when calculated on a Chl basis. Conversely, no significant differences were observed in the respiration levels of the lamina and the petiole.

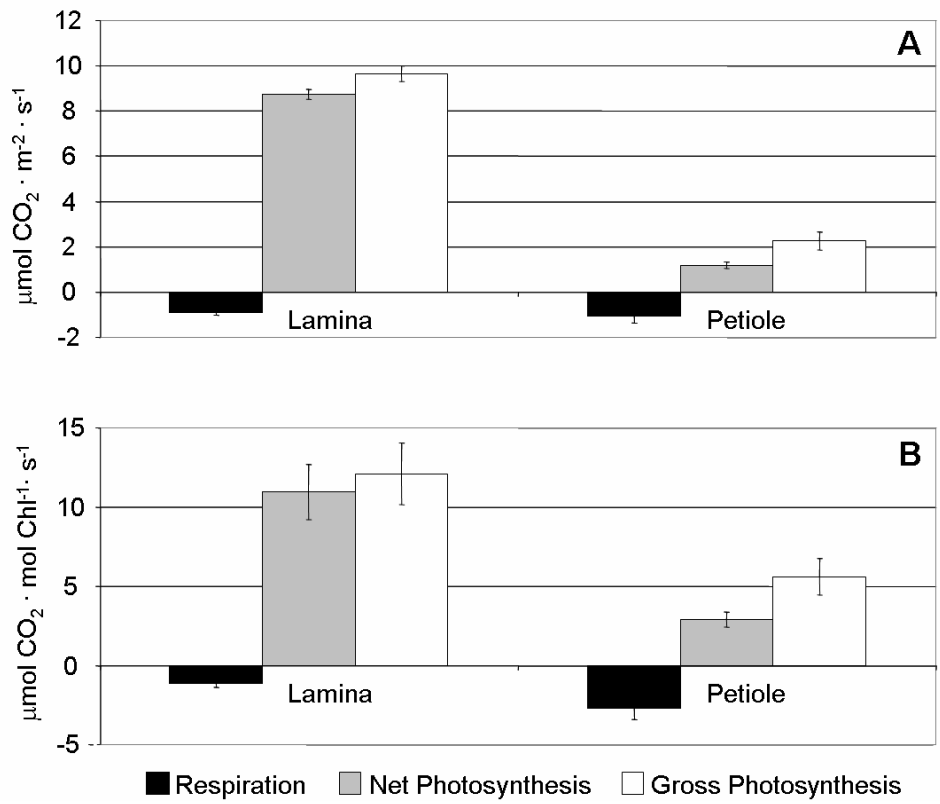

Fig. 14: CO_2 exchange in lamina and petiole of *Arum italicum* leaves, calculated per surface area (A) and on a Chl basis (B). Data are means of at least three independent experiments (bars are S.D.).

3.1.4. Thylakoid Protein Composition

Fig. 15 shows the silver-stained SDS-PAGE gel of *Arum italicum* thylakoids and immunoblot of thylakoid membrane proteins.

It was evident from the SDS-PAGE that there were differences in the protein patterns of the different tissues of *A. italicum* leaves. The observed differences seemed to be mainly due to different concentrations of the same proteins in different tissues. Some key proteins, belonging to different thylakoid complexes, were detected and quantified by immunoblot analysis (see Fig. 15 text for details).

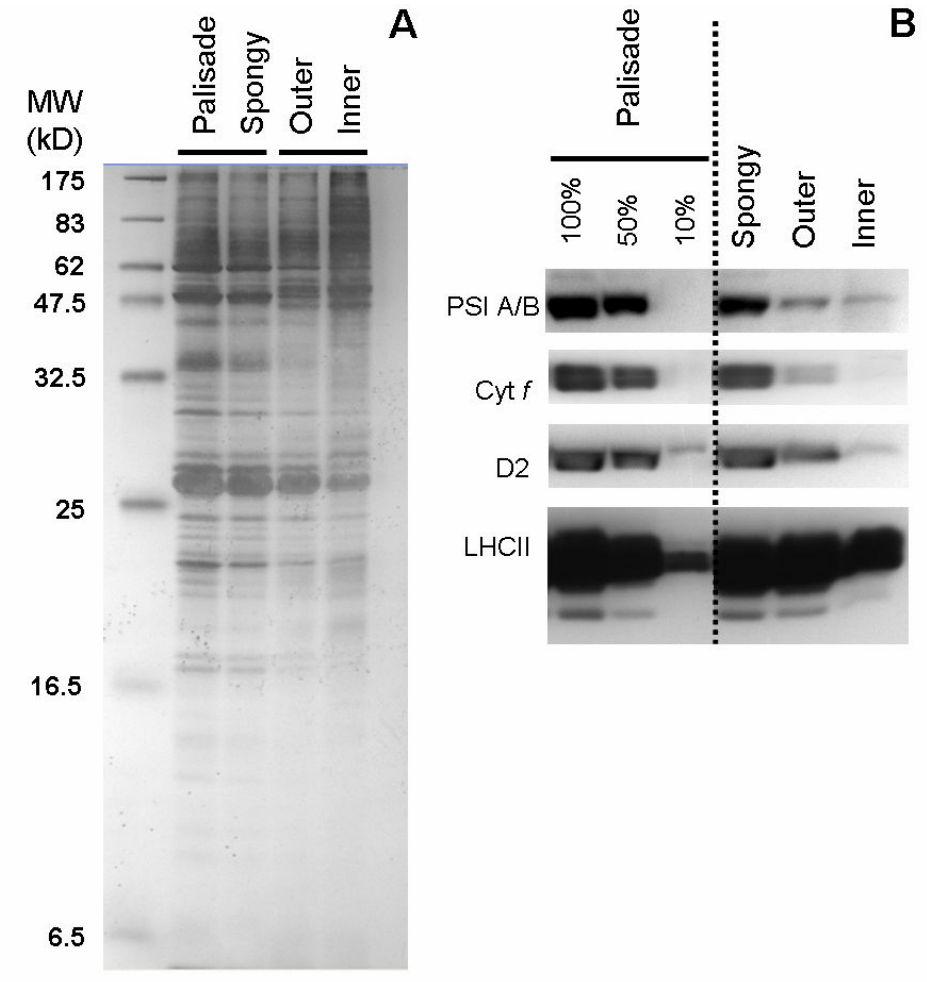

Fig. 15: Analyses of the thylakoid membrane proteins of different tissues of *Arum italicum* leaf. A) Silver stained SDS gel of the lamina (Palisade and Spongy) and the petiole tissues (Outer and Inner). On each lane, 75 μg of proteins were loaded. B) Immunoblot detection of thylakoid proteins in different tissues of the leaf. For semi-quantitative comparison, three different amounts of palisade sample were loaded. (Details on the antibodies are given in Materials and Methods).

The protein amounts, as revealed by immunoblotting, were very similar in the spongy and palisade tissues (Fig. 15 b). All the proteins analysed were present in both tissues, almost at the same concentration. Low amounts of PSI, Cyt *f* and D2 were present in the outer part of the petiole, corresponding to less than 50% of the same proteins in the palisade tissue. On the contrary, the LHCII proteins in the spongy mesophyll and the outer parts of the petiole were very similar as compared to the palisade tissue.

The inner tissue of the petiole differed most distinctively from the other tissues with respect to the thylakoid photosynthetic proteins. The PSI, Cyt *f* and D2 proteins were present at very low amounts (around 10% of the palisade), whereas the LHCII proteins were present in clearly higher amounts than in any other leaf or palisade tissues.

3.1.5. Thylakoid Protein Complexes

A BN-PAGE system was optimised for separation of the thylakoid membrane complexes of *Arum italicum* leaves. Membrane protein complexes from the four different tissues of Arum leaves were firstly separated by BN-PAGE, according to their size. Eleven distinct protein complexes could be resolved in BN gels of palisade and spongy tissues, whereas the same complexes were less visible or even absent in the outer and inner parts of the petiole, respectively (Fig. 16). Since the apparent molecular masses of the protein complexes in the first dimension BN-PAGE corresponded to the predicted molecular masses, each complex could be recognized based on its molecular mass. However, in order to more clearly identify the protein complexes and to resolve their composition, the proteins from the BN-gels were separated in the second dimension by denaturing gel electrophoresis (Fig. 17 and Fig. 18). Each stripe from the BN-PAGE, representing a different tissue of *A. italicum* leaf, was analyzed by SDS-PAGE in the second dimension, enabling the separation of different protein complexes into constituting subunits (Fig. 17 and Fig. 18). The subunits migrate in the denaturing gel according to their molecular mass, so that in the second dimension gel they are distributed along vertical lines, each line representing the subunit composition of the complex visible in the first dimension BN-gel. In this study, the identity of 10 thylakoid proteins was ascertained by immunoblotting. The position of the silver-stained spots, corresponding to the reaction centre proteins D1 and D2, the Chl *a*-biding proteins CP47 and CP43, and 6 proteins belonging to LHCII, are indicated for each fraction in Fig. 17and Fig. 18. Interestingly, different species give similar protein patterns even in the second dimension (Ciambella *et al.* 2005). This provided clues for the identification of other protein complexes present in *A.*

italicum samples, such as the PSI, different LHC complexes, the ATPsynthase and the Cyt b_6f complex.

On the lower part of the first dimension gel (Fig. 16), there was a dark-green band that corresponded to LHCII trimers not associated with PSII centers. This band was clearly visible in all four samples, even if a bit fainter in the inner part of the petiole. With the exception of LHCII trimers bands, the distribution of all the other complexes seemed to follow the same pattern, being clearly visible in the palisade and in spongy tissues, less evident in the outer petiole fraction but almost absent in the inner part of the petiole.

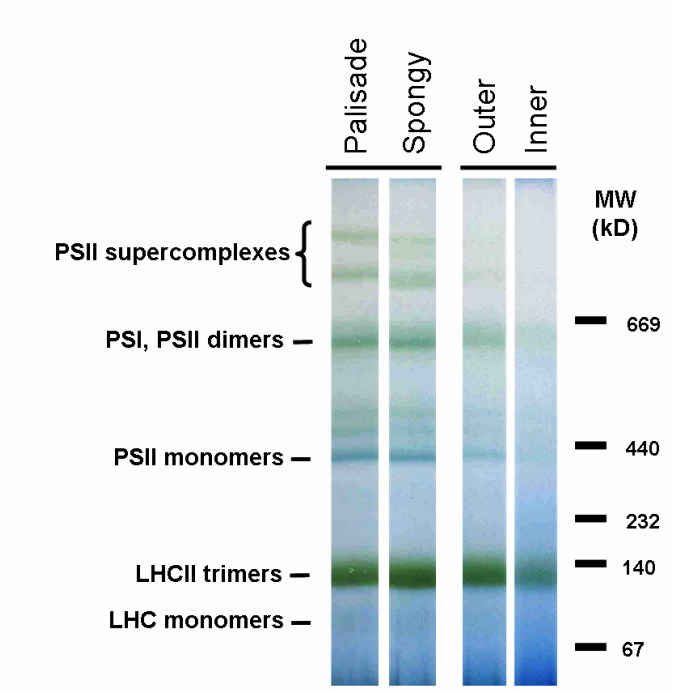

Fig. 16: Blue Native electrophoresis of thylakoid membranes from different parts of *Arum italicum* leaf: lamina tissues (Palisade and Spongy) and petiole parts (Outer and Inner). Each lane was loaded with 75μg of proteins.

Fig. 17 compares the 2-D protein maps obtained from the palisade and spongy tissues. In both cases, the first two lanes on the left contained PSII core proteins and some of the LHCII proteins, confirming that the bands with the highest molecular mass in the 1-D BN-gel represent supercomplexes of PSII. The third lane contained the PSI complex and the dimers of PSII core complexes, followed by strongly stained protein complexes with a high molecular mass, most probably corresponding to ATPsynthase. The next lane with decreasing molecur mass contained the monomeric core of PSII, which almost comigrated with the Cyt b_6/f complex, and the next lane contained the PSII core complex lacking the CP43 subunit. LHCII proteins were finally recognised on the right side of the gel, forming trimers or being present

in a monomeric state. The two tissues analysed exhibited protein patterns extremely similar with each other.

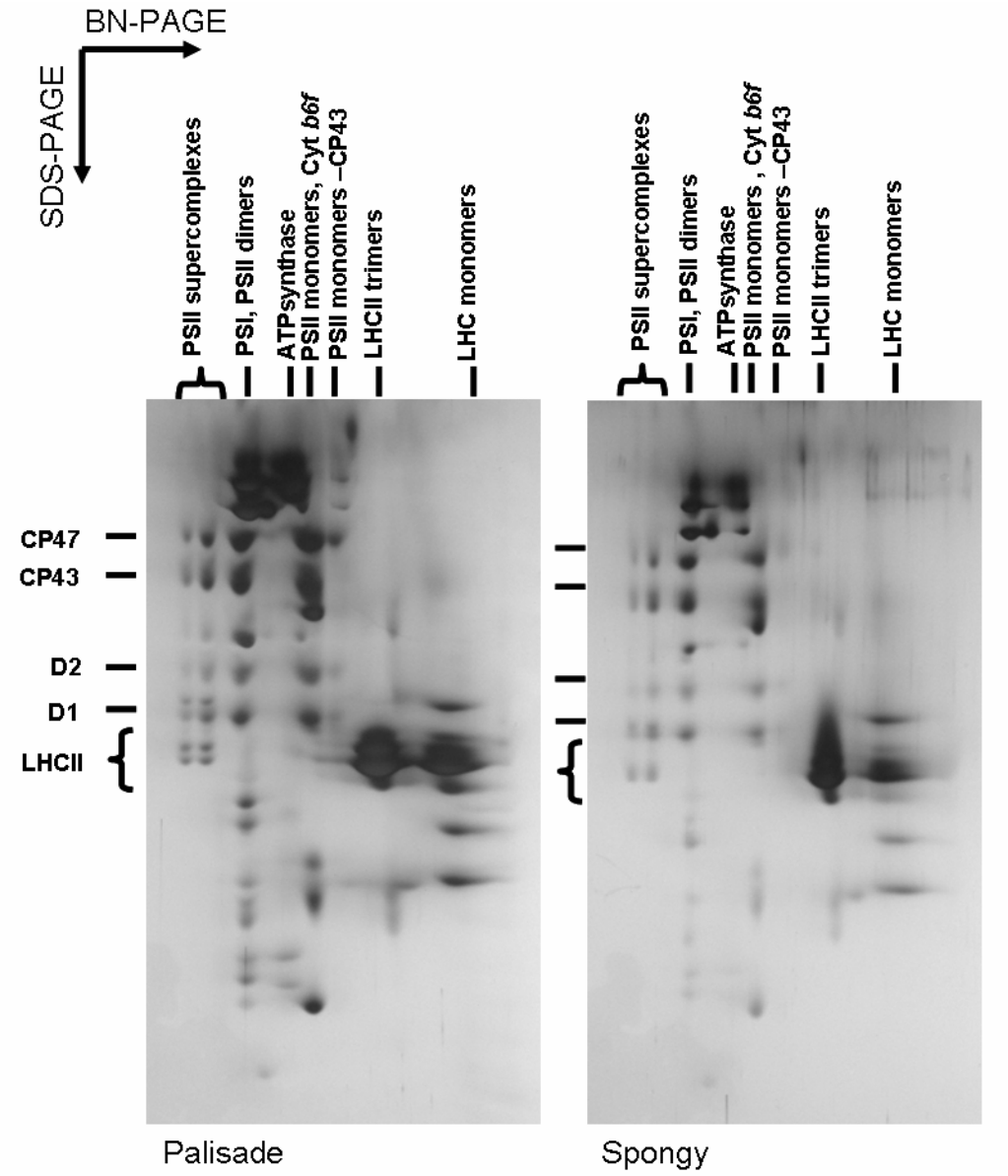

Fig. 17: Second dimension BN-SDS-PAGE of the lamina tissues of *Arum italicum* leaf: Palisade (left) and Spongy (right). The positions of silver-stained spots corresponding to the D1, D2, CP47, and CP43 subunits of PSII and the LHCII proteins are indicated.

In Fig.18 are reported the 2-D protein maps of the outer and inner parts of the petiole. The outer part of the petiole presented a protein pattern which resembled the one of the palisade and spongy tissues. However, in the palisade and spongy tissues, the PSII complexes were mainly resolved as dimers and monomers, and also as monomers lacking the CP43 subunit or as supercomplexes associated with LHCII proteins (Fig. 17). On the contrary, in the outer part of the petiole, the PSII supercomplexes were clearly less abundant, whereas free LHCII

trimers and monomers were present in higher abundance. In the inner part of the petiole, the PSII proteins were present in traces and assembled into core monomers and dimers, but, different from the other tissues, the PSII supercomplexes were not detected. The most abundant proteins identified were the LHCII proteins, organised both in trimers and monomers.

Finally, it was interesting to observe that in the petiole, and in particular in the inner tissue, other protein complexes were evident, characterised by a molecular mass a bit lower than that of the LHCII trimers and being composed of at least three different proteins.

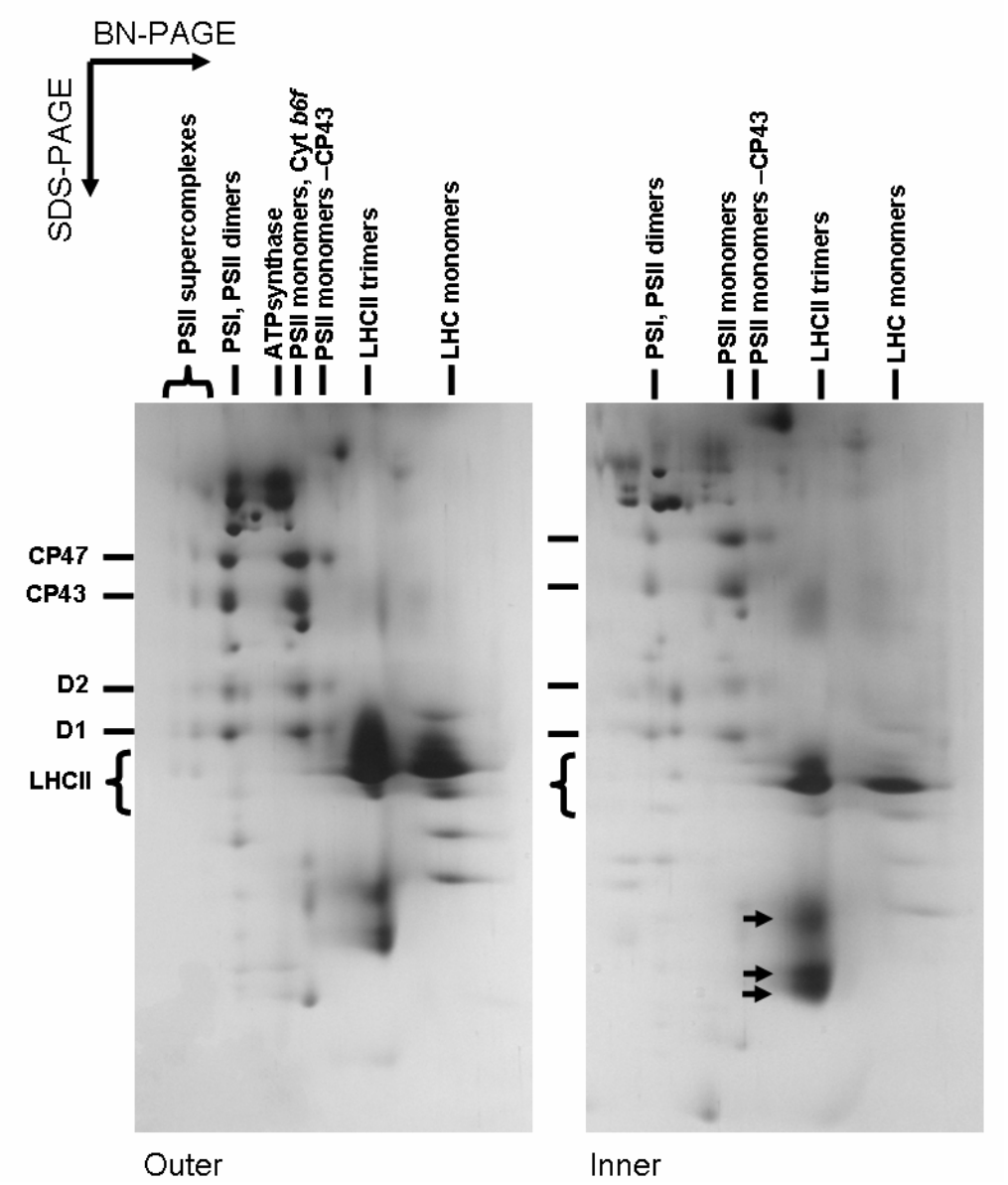

Fig. 18: Second dimension BN-SDS-PAGE of the petiole parts of *Arum italicum* leaf: Outer (left) and Inner (right). The positions of the silver-stained spots corresponding to the D1, D2, CP47, and CP43 subunits of PSII and the LHCII proteins are indicated. Arrows: unknown proteins.

3.1.6. 77 K Fluorescence Emission Spectra

The 77 K fluorescence emission spectra of thylakoids isolated from different tissues of *Arum italicum* are reported in Fig. 19 after normalisation at the maximum emission of PSII (684-685 nm).

In each sample the 77 K fluorescence emission spectra were characterised by two dominant peaks, corresponding to the emissions of PSII and PSI (684-685 nm and 730-733 nm). In 77 K spectra, the PSI emission is usually higher than that of PSII. This was not observed in Arum tissues. In fact, leaves were collected in the field and exposed to low-light conditions in the laboratory, which favoured the PSII excitation. State transition were not allowed because of the presence of NaF in all the buffers employed during thylakoid isolation.

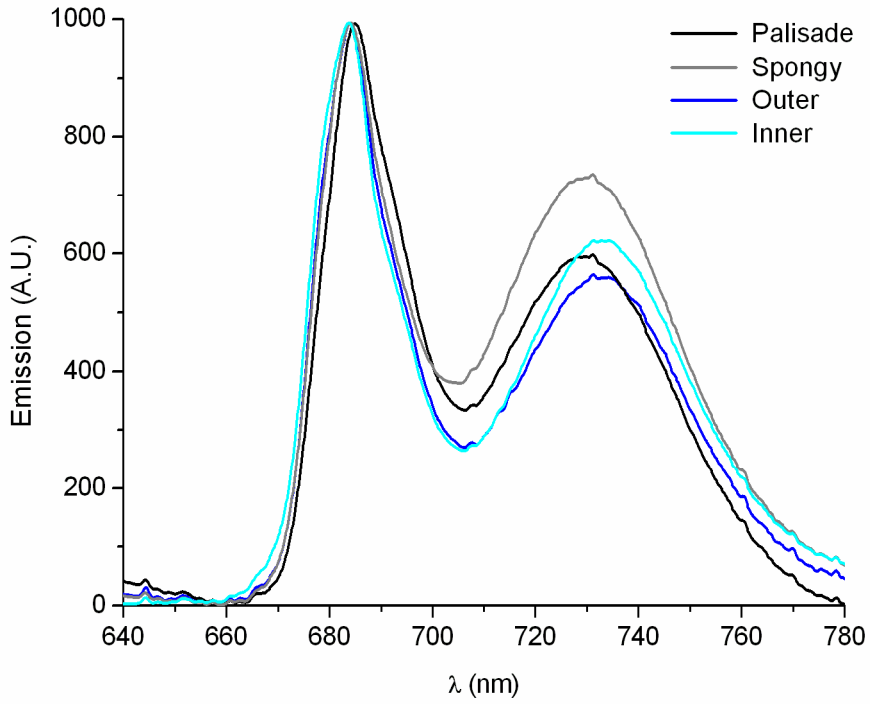

Fig. 19: 77 K fluorescence emission spectra from different thylakoid samples of the leaf of *Arum italicum*. Spectra are normalised to the maximum emission at 684-685 nm.

Interesting differences were observed in the positions of the PSI and PSII peaks between the lamina and the petiole thylakoids. Considering the palisade as a reference, the PSI peak of the petiole tissues was red-shifted of about 3 nm (from 730 nm to 733 nm), while the PSII emission peak was slightly blue shifted. The blue shift in PSII emission characterised also the spongy tissue.

In order to dissect more precisely the differences in emission with respect to the palisade tissue, the difference spectra were calculated from normalised emission spectra (Fig. 20). All the samples showed higher emission around 678 nm and lower emission at 690-692 nm. The smallest differences were observed for the spongy tissue and the biggest for the inner part of the petiole. Moreover, the petiole showed less emission around 720 nm, different from the spongy tissue, which emitted more than the palisade tissue in the region around 733 nm.

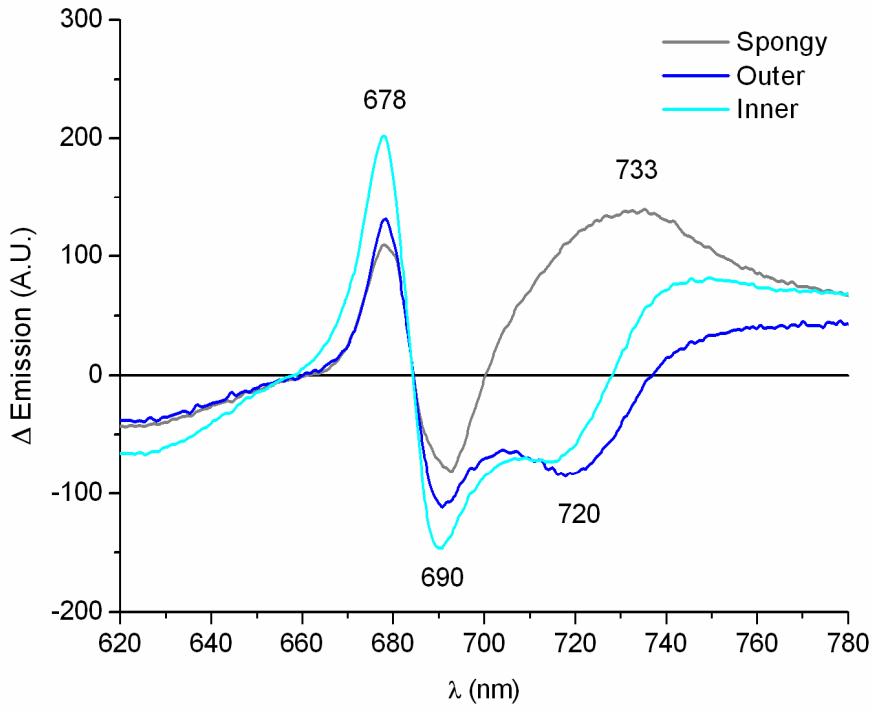

Fig. 20: Difference spectra calculated from the normalised 77 K fluorescence emission spectra reported in Fig. 19. Each line corresponds to "tissue-palisade".

3.1.7. Microspectrofluorimetric Analyses

The fluorescence emission spectra were recorded *in vivo* from small cell groups of different tissues of *Arum italicum* leaves and were used to calculate the emission intensity reported in Fig. 21, considering the palisade emission level as 100%.

These results clearly paralleled the fluorescence microscopy observations. Intensity recorded with the MSPF showed that in the lamina the emission of the spongy tissue was 22% higher than the emission of the palisade at the significance threshold (p= 0,055). In the petiole, the emission intensity of the inner tissue was markedly lower than in the outer tissue ($p<10^{-4}$). It is interesting to observe that the emission intensity of the inner tissue corresponded to about

70% of the emission of the palisade. This is particularly noteworthy, because the Chl content in the inner part of the petiole was extremely lower than in the palisade tissue (Fig. 12 and Fig. 13)

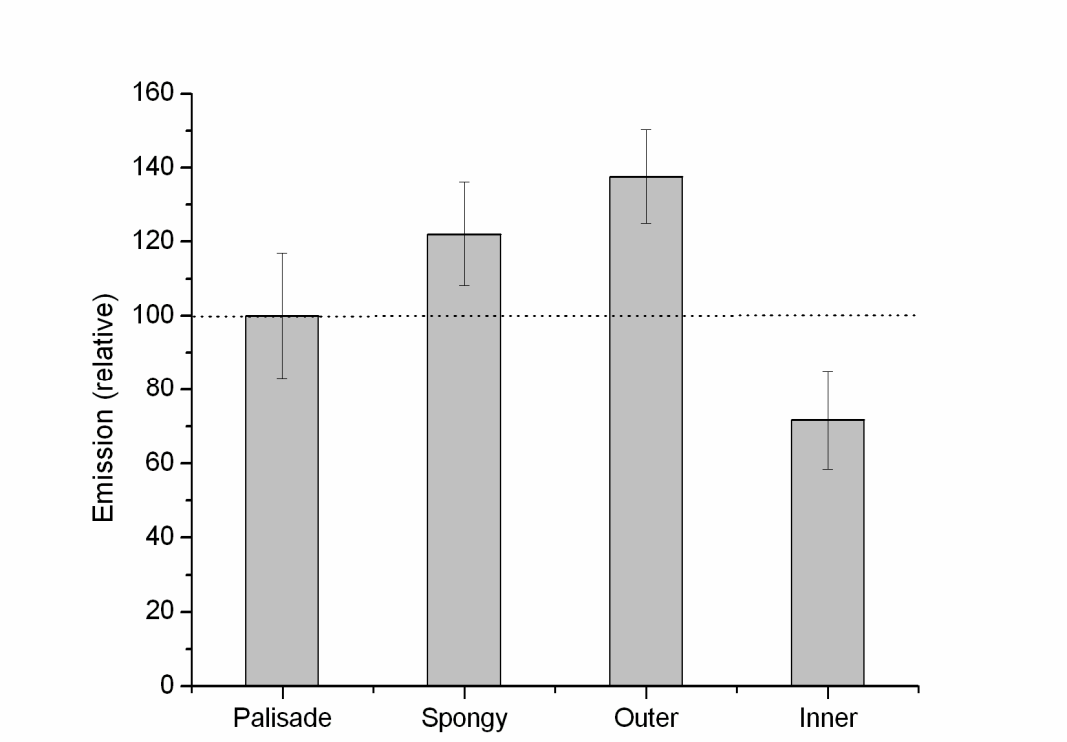

Fig. 21: Fluorescence emission intensity recorded at room temperature with the microspectrofluorimeter from different parts of *Arum italicum* leaf: lamina tissues (Palisade and Spongy) and petiole parts (Outer and Inner). Data correspond to the areas subtended under the fluorescence emission spectra in the range 650-750 nm, recorded from groups of 3-4 cells. Data are expressed as percentage of the palisade tissue ($n \geq 5$, bars are S.D.).

The microspectrofluorimetric data of *A. italicum* leaves are reported in Fig. 22.

Room temperature spectra typically present only one maximum, corresponding to the emission of the PSII. All the spectra recorded were normalised at this maximum. It was most evident that the inner tissue of the petiole had a markedly low emission in the region of the spectra after 700 nm (Fig. 22). This feature is also evident in Fig. 23, where the minus-palisade differences were calculated from normalised spectra. Different from the inner tissue, the spongy and the outer tissues showed minor differences in the same region. Finally, all the samples showed higher emission around 660 e 675 nm, corresponding to uncoupled Chls, and lower emission at 620-660 nm, corresponding to protoChls.

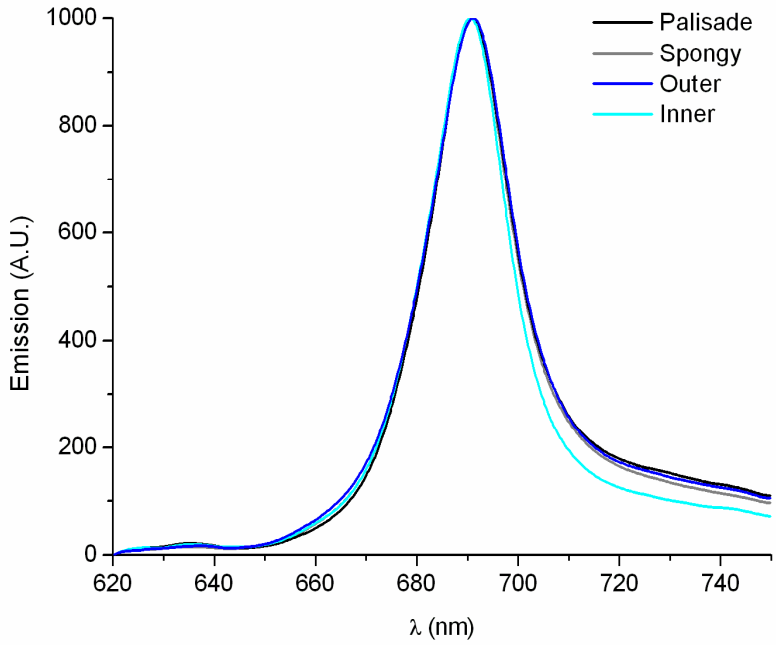

Fig. 22: Room temperature fluorescence emission spectra from different tissues of the leaf of *Arum italicum*. Spectra are normalised to their maximum.

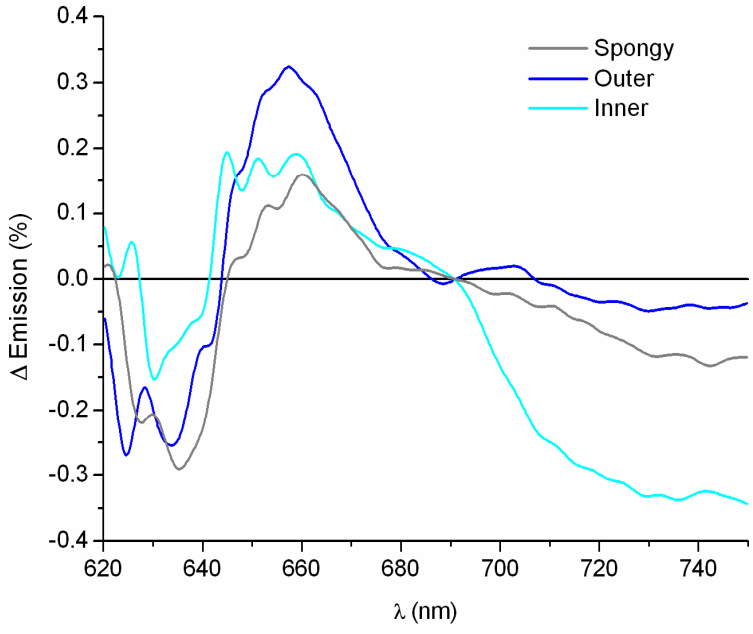

Fig. 23: Difference spectra calculated from the normalised room temperature fluorescence emission spectra reported in Fig. 22. Each line corresponds to “tissue-palisade”.

3.2. PLASTID DEVELOPMENT IN THE BERRY

The development of the berries of *Arum italicum* can be divided into two phases: maturation and ripening. The end point of maturation is the formation of a fully expanded green berry, which during ripening turns its colour into yellow and then to red. Several different developmental stages can be recognised:

- ivory berry - containing amyloplasts
- ivory-green berry - containing transition forms to chloroplasts
- green berry - containing chloroplasts
- green-yellow berry - containing transition forms to chromoplast
- yellow berry - with chromoplasts containing mainly membranes and globules
- orange and red berries - with fully developed chromoplasts

Each developmental step of the berry was separately analysed. Since the interest of this work was on the thylakoid system, the green berry was considered as a reference, because it is known to contain the most developed chloroplasts, whose ultrastructure is largely similar to that of the leaf lamina chloroplasts (Bonora *et al.* 2000).

3.2.1. Light and Fluorescence Microscopy Studies

The light and fluorescence microscopy images of the developing stages of *Arum italicum* berries are presented in Fig. 24.

In ivory berry almost no red Chl fluorescence could be detected. On the contrary, a brightly red fluorescence was observed in ivory-green berry, due to the chloroplast differentiation. It was evident that the Chl fluorescence was absent in the cell layer of the exocarp. In green berries a bright fluorescence was observed and individual chloroplasts inside the cells of the mesocarp were clearly visible and produced the green colouration when sections were examined with conventional light microscope. In green-yellow berries a strong decrease in fluorescence was evident. Moreover the cuticula was clearly distinguished on the epidermal cells due to a light blue fluorescence ascribable to phenolic compounds. In yellow berries the red plastid fluorescence had almost completely disappeared, remaining limited to some isolated areas. Finally, in orange berries an evident presence of carotenoids and the absence of red fluorescence were observed by light and fluorescence microscopy, respectively.

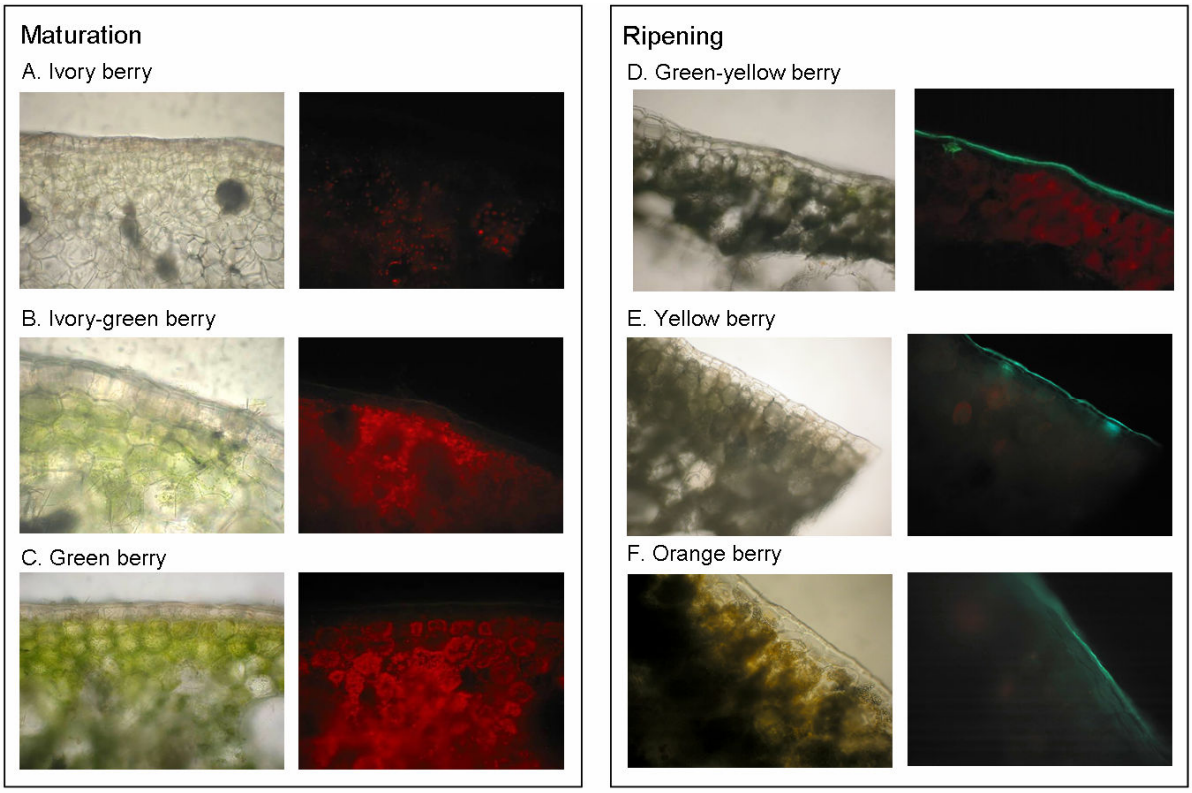

Fig. 24: Portions of cross sections of berries of *Arum italicum*. Light (left) and fluorescence (right) microscopy images are shown for each stage of ontogeny: ivory, ivory-green and green stages during the maturation process; green-yellow, yellow and orange stages during the ripening process.

3.2.2. Photosynthetic Pigments

Photosynthetic pigment concentrations and molar ratios in the berries of *Arum italicum* are reported in Fig. 25. Data reflected the different colour stages characterising the progressive development of the berry. In ivory berry only traces of Chl and Car were present due to the fact that the young infructescence is still enclosed in the enfolding spate and light, which drives Chl synthesis, is virtually absent. Chl accumulation increased during the maturation and reached the maximum level in the green berries. During the ripening process, Chls were degraded and were present only in traces in the yellow berry. Carotenoid content was increasing during the maturation. A moderate decrease occurred in the first steps of the ripening, in fact the carotenoid accumulation started only in the orange berry. As a consequence, the colour of the yellow stage was mainly due to the absence of Chls, rather than to a substantial increase in carotenoids.

The Chl *a*/*b* ratios calculated for the ivory-green, green, and green-yellow berries were not different. The synthesis and the degradation of Chl *a* and Chl *b* proceeded in equimolar

proportions during the transition from ivory-green to green berry and from green to green-yellow berry, respectively.

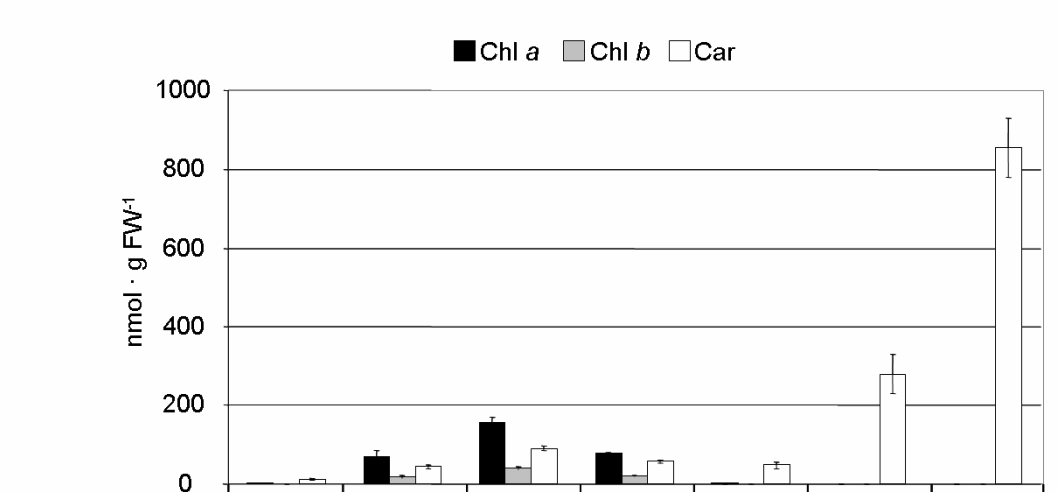

	Ivory	Ivory Green	Green	Green Yellow	Yellow	Orange	Red
Chl *a*/*b* ± SD	**6.82** 0.00	**3.92** 0.29	**3.87** 0.07	**3.76** 0.10	**3.11** 1.61	-	-
Chl (*a*+*b*) / Car ± SD	**0.13** 0.05	**2.06** 0.10	**2.16** 0.10	**1.69** 0.14	**0.05** 0.01	**0.00** 0.00	**0.00** 0.00

Fig. 25: Photosynthetic pigments and their molar ratios in the different stages of berry ontogeny of *Arum italicum*. Data are means of three independent experiments (bars are S.D.).

The Chl(*a*+*b*)/Car ratio paralleled the carotenoid accumulation and the loss of Chl during berry ontogeny. The ratio increased during the maturation, in accordance with the transition of amyloplast into chloroplast and then decreased during the ripening, in accordance with the disorganisation of the thylakoid system. The maxim value was reached in the green berry, with a Chl(*a*+*b*)/Car ratio of 2.16 ± 0.10.

3.2.3. Photosynthesis and Respiration Rates

Fig. 26 shows the CO_2 gas exchange data of *Arum italicum* berries. In all samples, the gas exchange per surface unit was calculated, whereas the gas exchange based on the total Chl content was calculated only for berries with a significant presence of Chl (ivory-green, green and green-yellow berries; Fig. 25).

An interesting result was that no positive net photosynthesis could be detected at any developmental stage of the berry (Fig. 26 a). Nevertheless, the ivory-green, green and green-yellow berries were capable of photosynthetic activity, but the gross photosynthesis was

compensated by the respiration. Recalculating the CO_2 exchange on a Chl basis did not reveal any further differences among the different developmental stages of the berries. Finally, a significant increase in the respiration rate was observed in the berries corresponding to the last developmental stages of the fruit (late ripening).

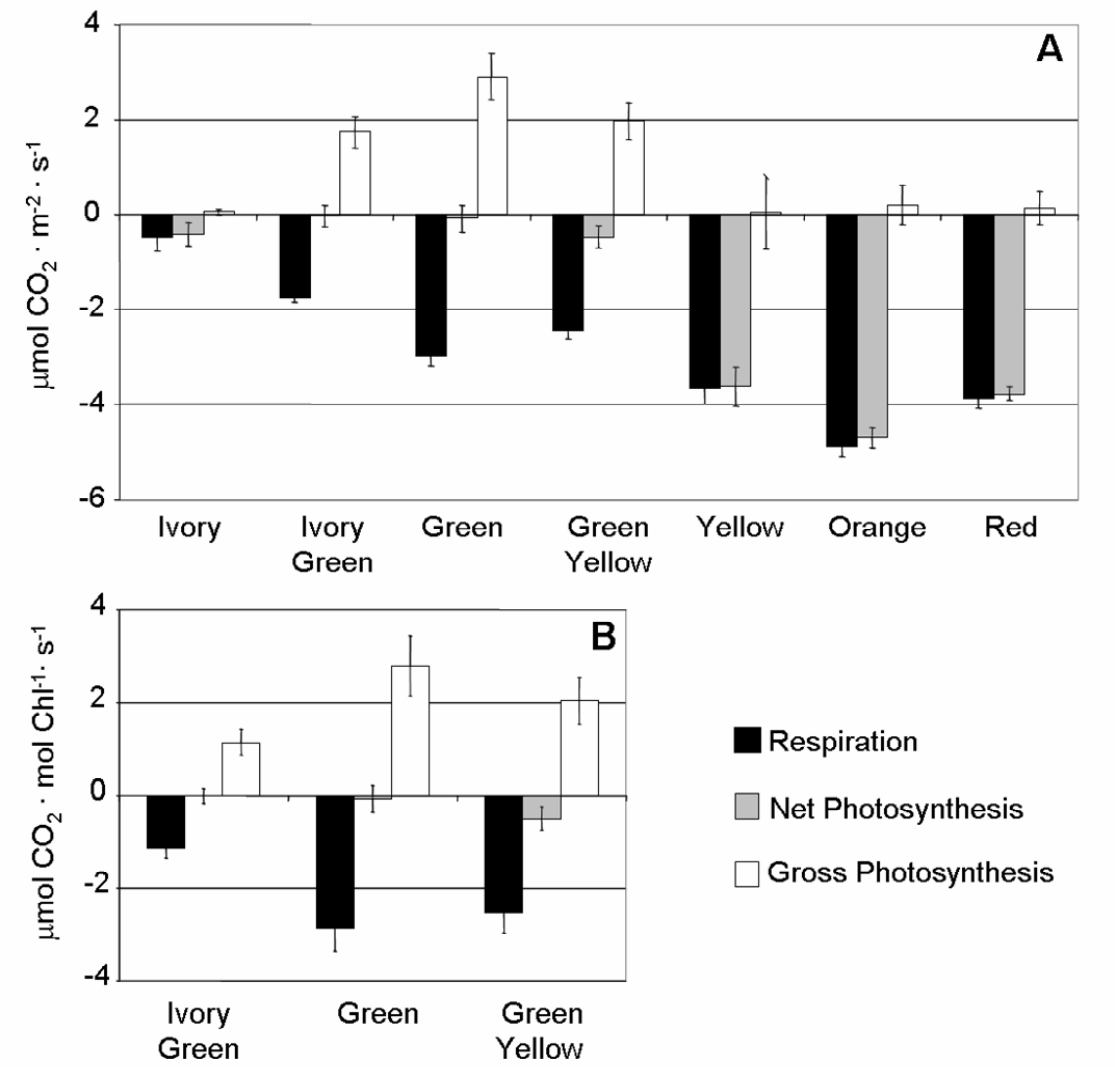

Fig. 26: CO_2 exchange in berries of *Arum italicum*, calculated per surface area (A) and on a Chl basis (B). Data are means of at least three independent experiments (bars are S.D.).

3.2.4. Thylakoid Protein Composition

The proteins present in the thylakoid membranes of *Arum italicum* berries were separated in a denaturing SDS-PAGE and stained with silver, as shown in Fig. 27. The protein patterns at different developmental stages of the berries were clearly different. In order to follow the development and the degradation of the photosynthetic apparatus, the samples were electroblotted on a PVDF membrane and analysed by means of different antibodies (Fig. 28). As the green berry harbours the most developed chloroplasts (Bonora *et al.* 2000), this stage

was considered as a reference for the comparisons of the protein contents between different developmental stages (Fig. 28 a).

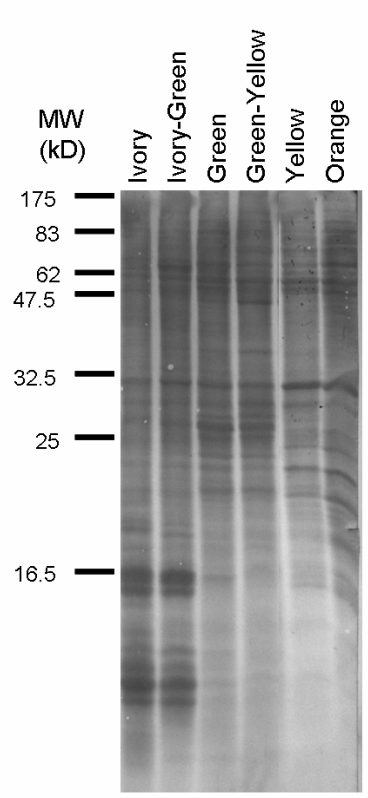

Fig. 27: Silver-stained SDS-PAGE of the thylakoid membrane proteins from different ontogeny stages of *Arum italicum* berries. On each lane, 75μg of proteins were loaded.

During maturation of the berries, from the ivory to the green berry, a progressive synthesis and accumulation of thylakoid proteins were observed. In the ivory berry the only proteins detected belonged to LHCII, at a concentration lower than 10% of that in the green berry. In the ivory-green berry the amount of LHCII strongly increased (50%) and traces of lhca4, Cyt *f* and D2 were also detected. Conversely, the D1 protein, which forms with the D2 the reaction centre of PSII, was not yet detected in this sample. This could be an artefact due to the loss of D1 during the preparation of the samples. The D1 and the CP47 were detected only in the green berry.

Ripening of the berries, being accompanied by a degradation of the chloroplast membranes and differentiation of chromoplasts (green-yellow berry) resulted in an abrupt decrease in the amounts of the D1, D2 and Cyt *f* proteins. In fact, the contents of these proteins were lower than 30% of that in the green berry. In the yellow berry, no D1, D2, CP47 or lhca4 proteins were detected, whereas traces of LHCII and Cyt *f* were still present. Traces of LHCII proteins were present even in the orange berry.

The antibodies raised against the D1 and D2 proteins were also reactive against the proteins bands at low molecular weight region (around 10 kD) present in ivory and ivory-green berries (data not shown).

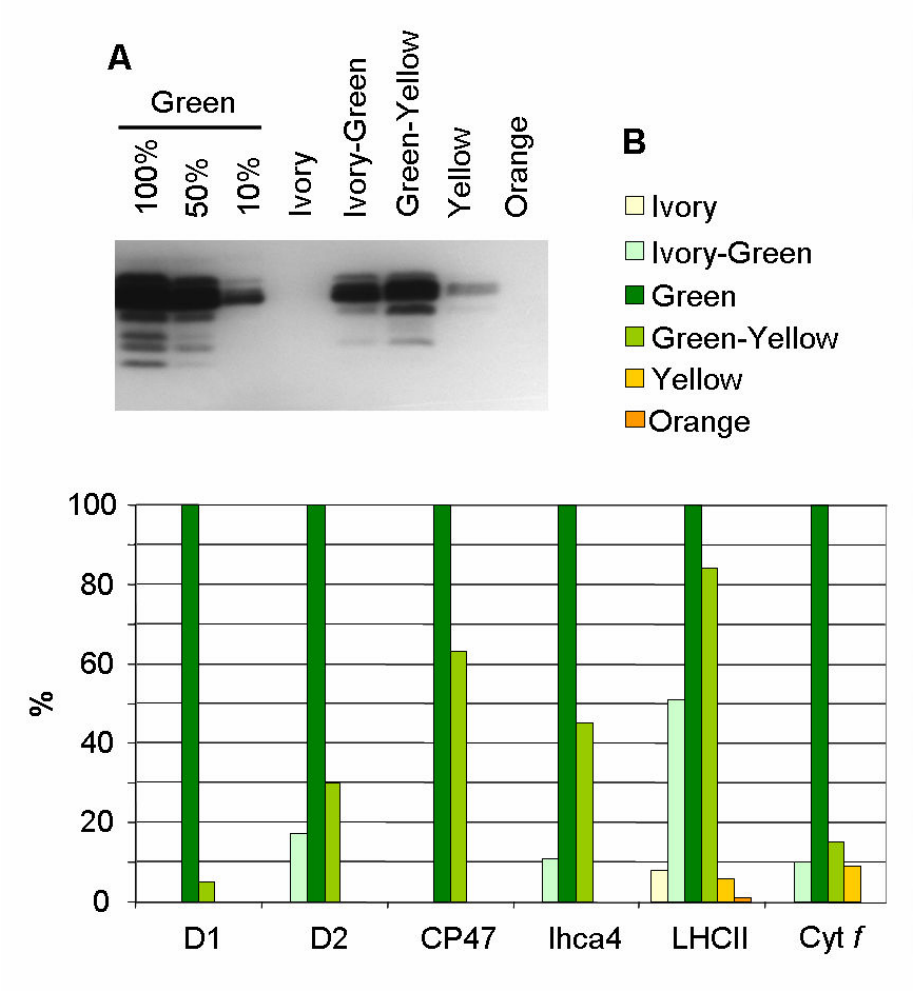

Fig. 28: Immunodetection of thylakoid proteins from berries of *Arum italicum* at different developmental stages. A) Immunoblot detection of LHCII proteins. For semi-quantitative comparisons, three different amounts of green-berry sample were loaded (as compared to 100 % loading for all other berries). B) Quantification of proteins after immunodetection. For each protein the amount in the green berry was considered as a reference, and set as 100% (Details on the antibodies are given in Materials and Methods).

3.2.5. Thylakoid Protein Complexes

Fig. 29 presents the 1-D and 2-D BN-SDS-PAGE gels made from the ivory-green, green and yellow-green berries of *Arum italicum*. This analysis was performed only on the stages of berry ontogeny that showed thylakoid proteins and chlorophylls in considerable amounts. In these samples, the presence of assembled thylakoid protein complexes was expected. The 2-D gels were electroblotted and proteins identified with specific antibodies.

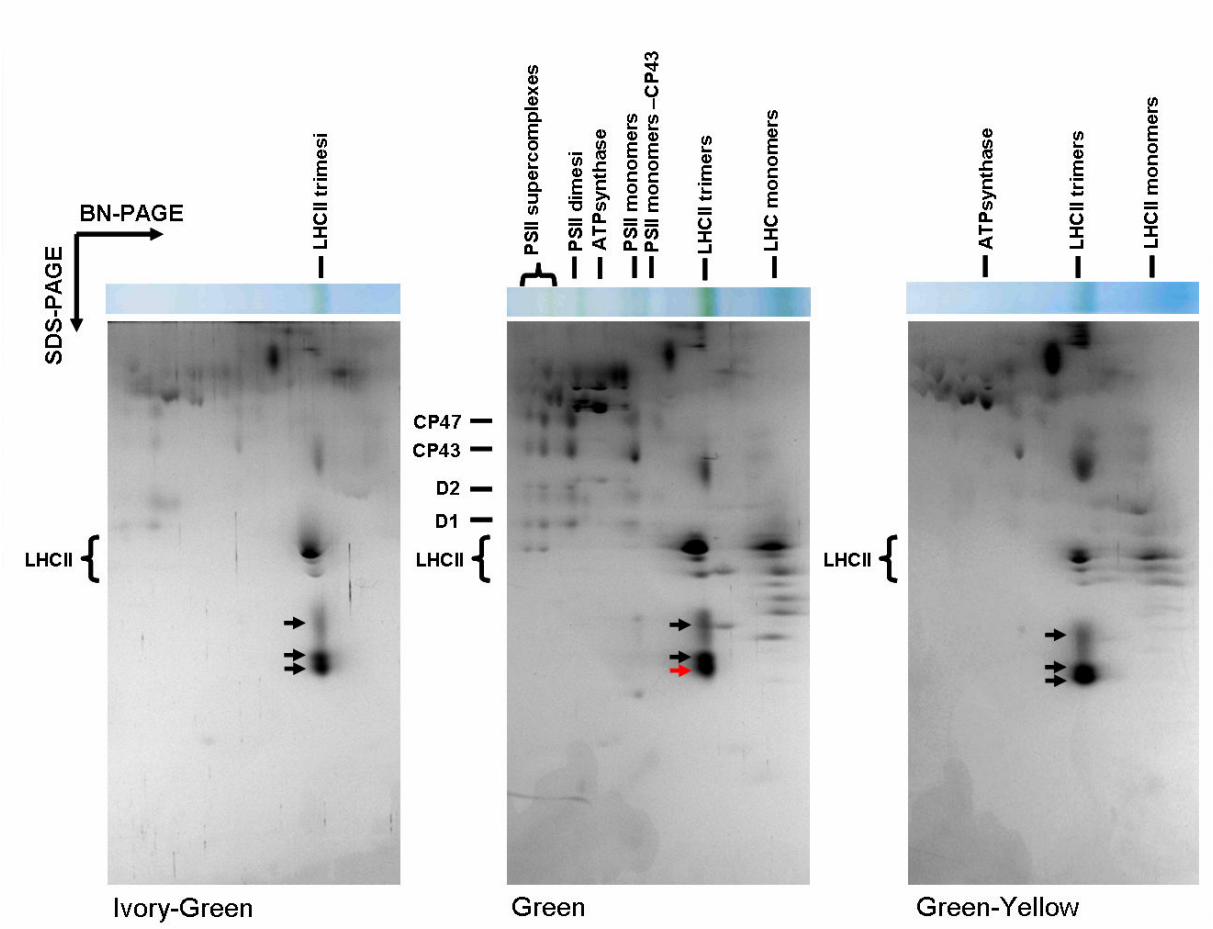

Fig. 29: 1D and 2D BN-SDS-PAGE gels of berries from *Arum italicum*. 1D gels and the protein complexes are presented on the top. Below are the second dimension SDS-PAGE gels stained with silver. The positions of the silver-stained spots corresponding to the D1, D2, CP47, and CP43 subunits of PSII and the LHCII proteins are indicated. Black arrows: unknown proteins. Red arrow: delta-TIP

In the 1-D gel of ivory-green berries, only two complexes of relatively low molecular mass were clearly visible: a green and a blue band, almost comigrating. The immunoblot analyses of the 2-D gel revealed that the green complex corresponded to trimers of LHCII. The second complex appeared to be composed of at least three different unknown proteins. Neither in the 1-D nor in the 2-D gel it was possible to recognise other proteins.

Several complexes were present in the 1-D gel of the green berry. The analyses of the 2-D gels revealed the presence of PSII-LHCII supercomplexes, clearly identified on the left side of the gel, of PSII core dimers and monomers, and LHC trimers and monomers, on the right side of the gel. The PSII core lacking CP43 was almost absent. Interestingly, in the silver-stained 2-D gel, the PSI, which is known to comigrate with the PSII dimers, was not visible.

Analysis of the green-yellow berry revealed a protein pattern similar to that of the ivory-green berry. In the 1-D BN gel only two complexes of low molecular mass were clearly visible. The green complex was recognised as trimers of LHCII. Differently from the ivory-green sample,

several monomers of LHCII were also present. Some complexes of high molecular mass possibly correspond to the ATPsyntase, but were not clearly identified.

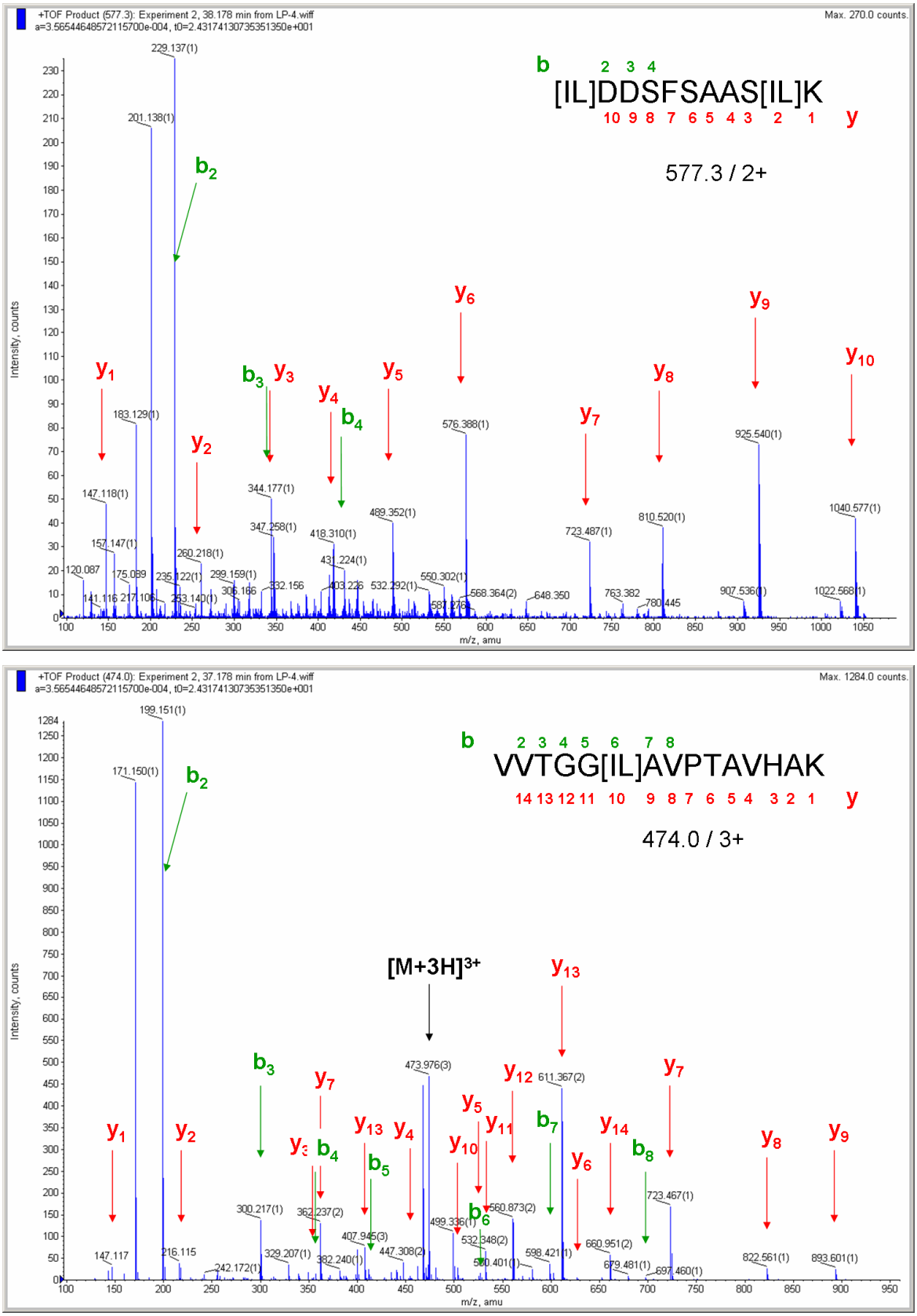

Fig. 30: ESI-MS/MS spectrum of the two peptide ions identified from the protein marked with the red arrows in Fig. 29.

Interestingly, in the 1-D BN gel of all samples, a protein complex with a molecular mass slightly lower than that of the LHCII trimers was evident. As shown in the 2-D gel, this complex was composed of at least 3 proteins, with apparent molecular masses lower than 30 kDa. In order to tentatively identify subunits of this protein complex, visible spots of membrane proteins were cut out of the 2-D gels and prepared for MS analyses. Although information of protein sequences of *A. italicum* is not present in database, two peptides were identified (Fig. 30). They both aligned with the sequence of a putative delta-TIP (accession number: AAG44945) from *Nicotiana glauca* (Fig. 31). The other proteins belonging to the same complex did not represent any known thylakoid protein complex, as deduced from several immunoblot experiments with antibodies raised against proteins of the known thylakoid protein complexes. This protein complex remains so far unknown, since also the mass spectrometric identifications of the proteins were unsuccessfull due to the fact that the genome of *A. italicum* is not available. Interestingly, this unknown protein complex increased in quantity in the thylakoid membranes during the development of the berries.

```
MPGIAFGRID DSFSVGSLKA YLAEFISTLL FVFAGVGSAI AYNKLTANAA
       RID DSFSAASLK

LDPAGLVAVA VCHGFALFVA VAVGANISGG HVNPAVTFGL ALGGQITLLT

GLFYIIAQLL GSIVACLLLK VVTGGLAVPT HNVAAGVGAL EGVVMEIIIT
                     K VVTGGLAVPT AVHAK

FALVYTVYAT AADPKKGSLG TIAPIAIGFI VGANILAAGP FSGGSMNPAR

SFGPAVASGD FTNNWIYWAG PLVGGGLAGL TYSNVFMQHE HAPLSSDF
```

Fig. 31: Protein sequence of putative delta-TIP from *Nicotiana glauca* and alignment with peptides identified in *Arum italicum* sample.

3.2.6. 77 K Fluorescence Emission Spectra

The 77 K fluorescence emission spectra of isolated thylakoids were recorded for ivory-green, green and green-yellow berries of *Arum italicum*.

In Fig. 32, the spectra are reported after normalisation at PSII emission peak (683-685 nm). Considering the green berry as a reference, both PSI and PSII peaks in the ivory-green and green-yellow berries were blue-shifted. In particular, the PSI peak was blue-shifted of about 3 nm (from 729 nm to 746 nm) and was characterised by an intensity lower than in the green berry. The blue-shift of the PSII peak was more evident in the green-yellow berry (from 685 to 683 nm) than in the ivory-green berry (from 685 to 684.5 nm). Fig. 33 reports the

differences of the normalised spectra with respect to the green berry. Both samples confirmed less intense emission at 733 nm and higher emission at 678.5 nm, particularly evident in the green-yellow berry.

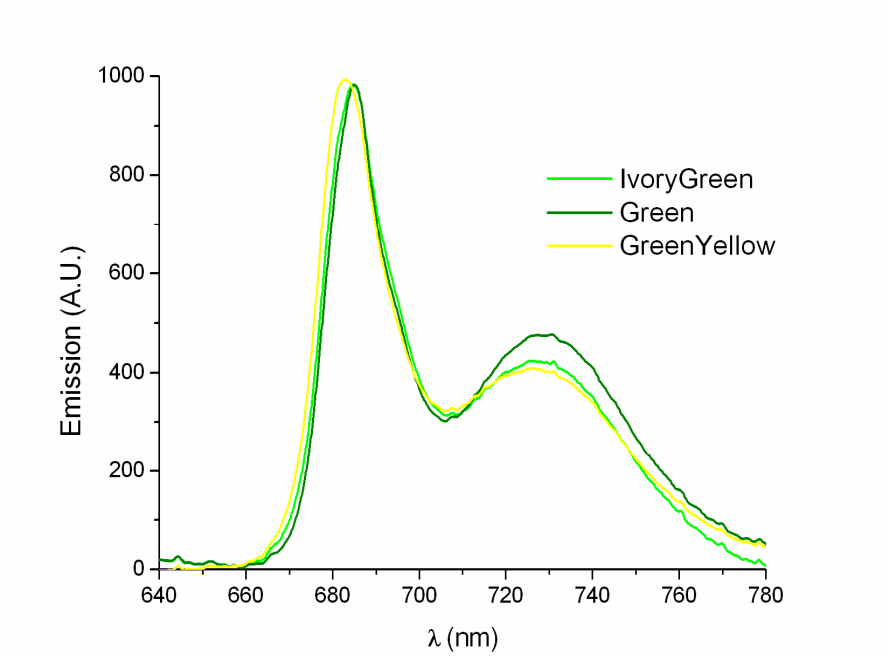

Fig. 32: 77 K fluorescence emission spectra from thylakoid samples of *Arum italicum* berries at three stages of ontogeny. Spectra are normalised to their maximum emission at 683-685 nm.

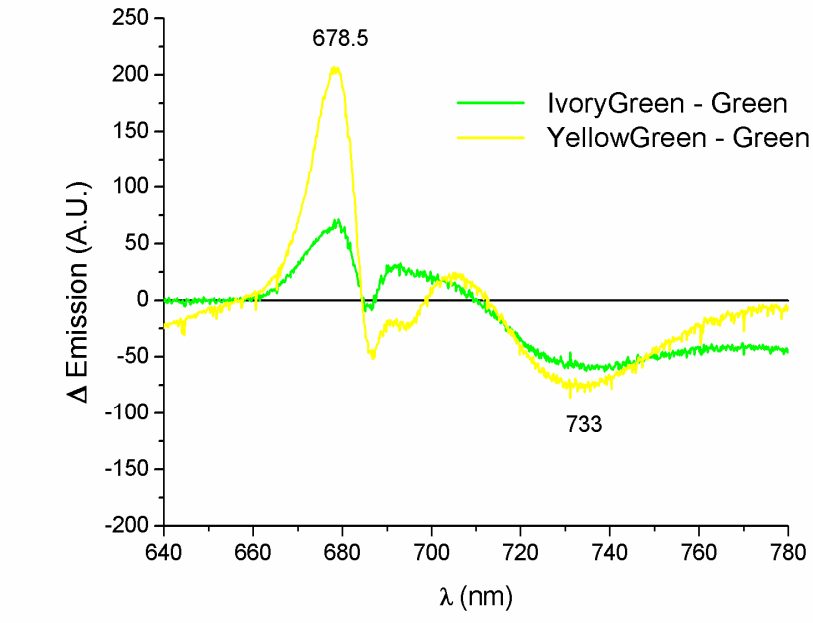

Fig. 33: Difference spectra calculated from the normalised 77 K fluorescence emission spectra reported in Fig. 32. Each line corresponds to “sample - green berry”.

3.2.7. Microspectrofluorimetric Analyses

In Fig. 34, the fluorescence emission intensity of berries of *Arum italicum* are reported. The emission levels were calculated from room temperature emission spectra (total area in the 650-750 nm range) and expressed as a percentage of the green berry emission, whose level was set as 100%.

The data clearly reflected the development and the degradation of the thylakoid system. In fact, emission increased progressively during the maturation, reached the maximum level in the green berry and than decreased during the ripening of the berries. At the orange stage the fluorescence was hardly detectable.

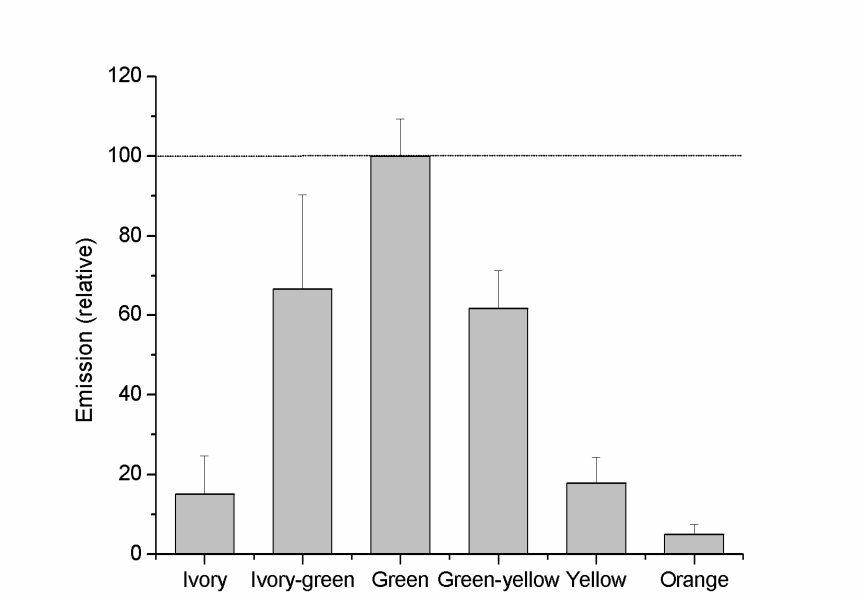

Fig. 34: Fluorescence emission intensity recorded at room temperature with the microspectrofluorimeter from different stages of berry ontogeny in *Arum italicum*. Data correspond to the areas subtended under the fluorescence emission spectra in the range 650-750 nm, recorded from groups of 3-4 cells. Data are expressed as percentage of the green berry ($n \geq 5$, bars are S.D.).

A preliminary analysis of the Chl emission region (660-750 nm) in different samples allowed to highlight small differences in normalised spectra so that they were not completely overlapping. This suggested that different components could contribute to the spectrum at different stages of ontogeny. A method to dissect fluorescence emission components in spectra is the Gaussian deconvolution, performed after a derivative analysis. For this purpose, spectra were analysed individually and the components listed in Tab. 1 were resolved, except in the late ripening stages, which almost or totally lacked Chl emissions (Fig. 35 and Fig. 36). In particular, the main fluorescence emission components were ascribable to the PSII core antennae CP43 and CP47 (two components in range between 683-697 nm). Minor emissions corresponded to the RCII (680 nm) and to uncoupled Chls (665-675 nn). One or two

emissions in the range between 700-710 nm were attributed to aggregated LHCII. Emissions over 715 nm are due to PSI and/or LHCI. In the samples analysed, the components of the spectra did not differ as concerns their position, but their intensity.

The spectra shown in Fig. 35 and Fig. 36 are representative of the resolved spectra for each stage of berry ontogeny. In particular, Fig. 35 presents the room temperature spectra recorded in berries during the maturation process, from ivory to green berry.

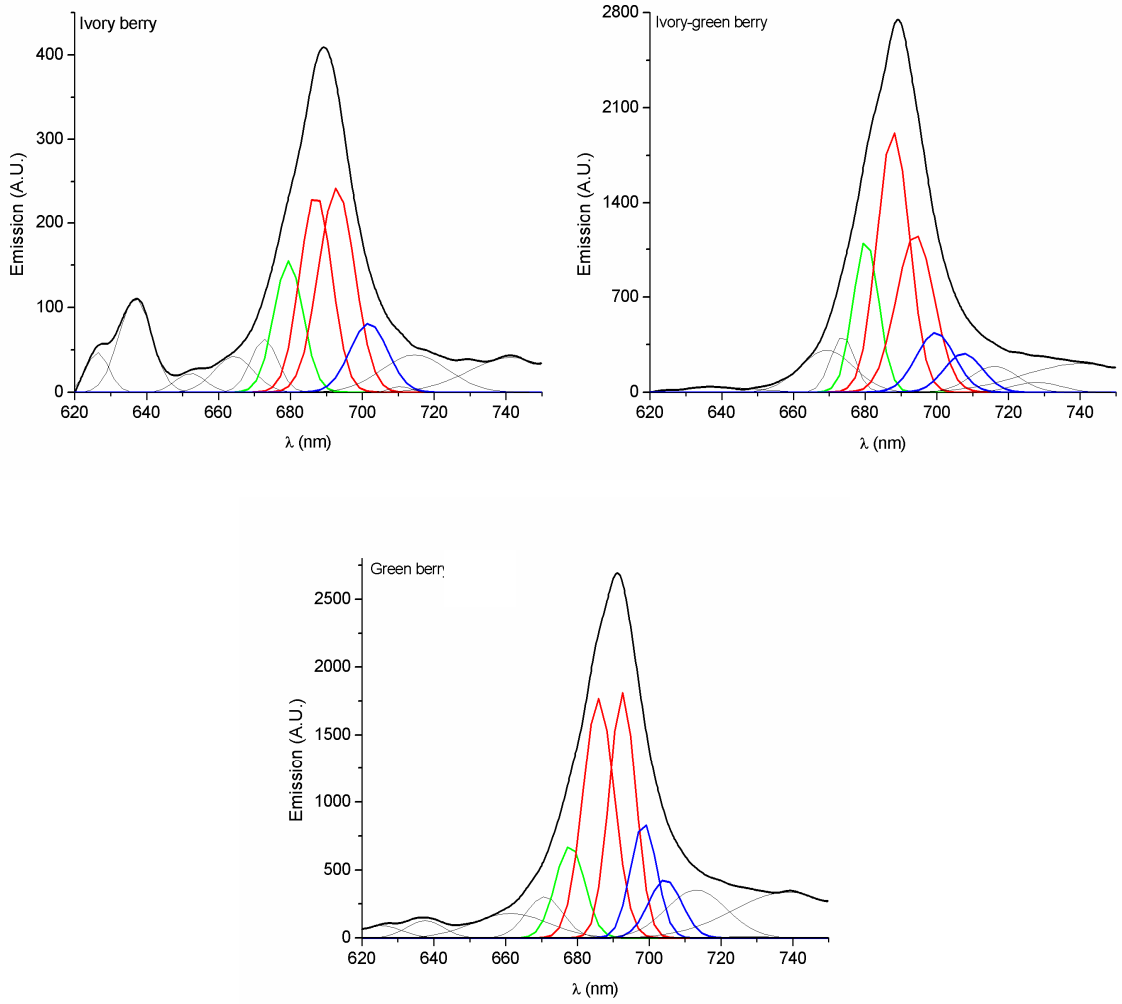

Fig. 35: Representative deconvoluted fluorescence emission spectra of *Arum italicum* berries during the maturation process (max. at 678-680 nm: RCII, green line; max. from 687–694 nm: CP43–47, red lines; max. from 700–710 nm: LHCII, blue lines).

In the ivory berry, a small protoChl peak at about 630 nm was observed. However, the main peak was observed at 689 nm and was ascribable to emissions of Chls associated with PSII components. The presence of these emissions seemed to be in contrast with pigment and protein quantification data (Fig. 25 and Fig. 28), which showed that the ivory berry is virtually free of Chls and PSII proteins. However, the pigment and protein quantifications

were performed on the whole berry, whereas microspectrofluorimetric analyses were circumscribed to small cell groups, selected by means of fluorescence microscopy observations. On the other hand, this technique gave consistent results with the microscopical surveys, which indicated the presence of Chl fluorescence in this sample (Fig. 24), though at a low level. With the progression of the maturation, the main events were the evident increase in Chl emission and a red shift of the maximum from 689 nm in the ivory berry to 690 nm in the ivory-green and to 691 nm in the green berry.

In Fig. 36, spectra recoded in the ripening berries are shown. Chl emission was detected until the yellow stage, in accordance with the microscopic examination. However, the maximum was blue shifted from 691 nm in the green berry, to 690 nm in the green yellow, to 689 nm in the yellow berry, while emission was progressively decreasing. Traces of Chls were detected even in the orange berry; in this stage a peak at around 636 nm attested to the presence of protoChl pigments, which remained the only emitting sources in the red berry.

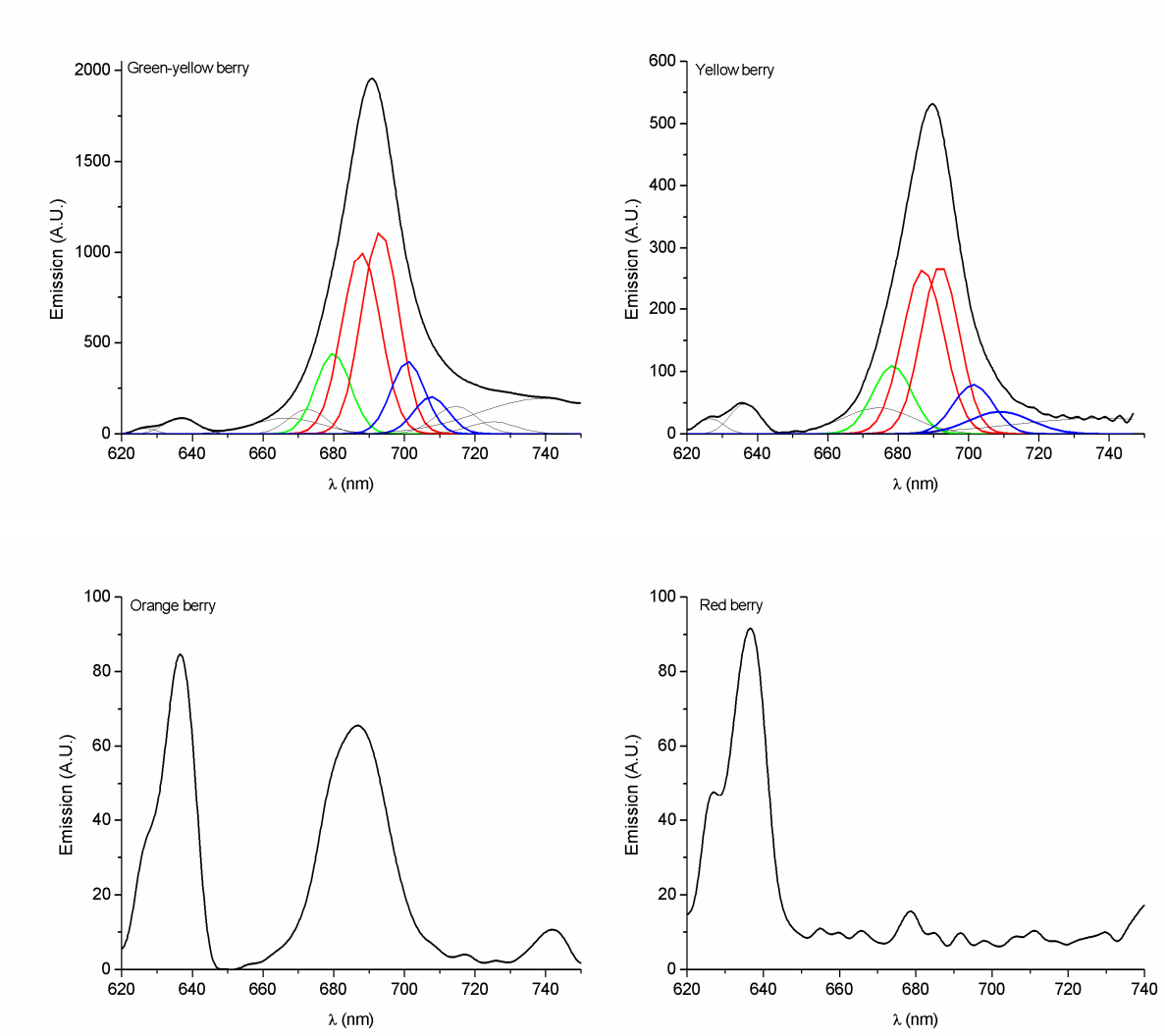

Fig. 36: Representative deconvoluted fluorescence emission spectra of *Arum italicum* berries during the ripening process (max. at 678-680 nm: RCII, green line; max. from 687–694 nm: CP43–47, red lines; max. from 700–710 nm: LHCII, blue lines).

In order to better understand the differences in intensity of the emission components resolved in room temperature emission spectra, the RCII/CP43–47 and LHCII/PSII ratios were calculated. As shown in Fig. 37, the relative fluorescence intensities underwent some modifications during the maturation and the ripening processes and both ratios varied.

During the early maturation the RCII/CP43–47 ratio was ca. 0.27. In the green berry the ratio decreased to the value of 0.21 ± 0.03, which was maintained also during the ripening, even at the yellow stage (Fig. 37 a).

The LHCII/PSII ratio showed an increasing trend during the maturation of the berry, indeed it was quite low in the ivory berry (0.13 ± 0.03.) and rose to 0.29 ± 0.03 in the green berry. During the ripening, the ratio fell down to ca. 0.20, without differences between green-yellow and yellow berries (Fig. 37 b).

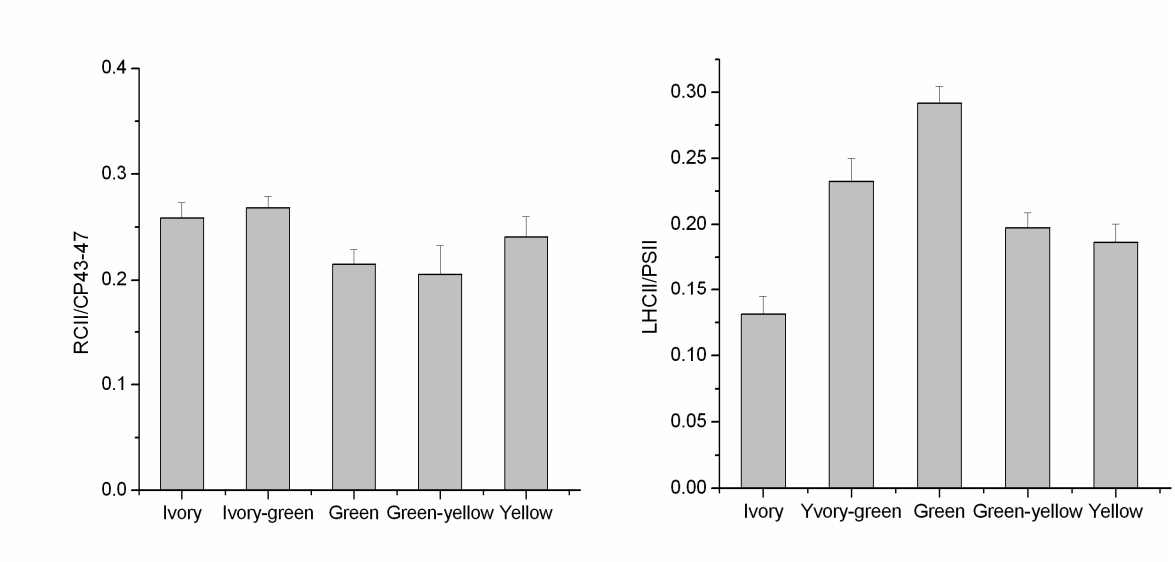

Fig. 37: RCII/CP43–47 and LHCII/PSII ratios during the ontogeny of *Arum italicum* berries. Data correspond to the areas subtended under the Gaussian curves reported in Fig. 35 and 36. PSII is the sum of RCII and CP43–47. (Data are mean of at least 5 replicates, bars are S.D.).

3.3. THE PALISADE TISSUE AND THE GREEN BERRY: COMPARISON

In the previous sections it has been shown that the thylakoid system in plastids of *Arum italicum* develops differently in the two organs: the leaf and the berry. It has also been shown that the palisade tissue contains the most functional thylakoid system in the leaf. Similarly, the green berry represents photosynthetically the most active stage in berry development. Consequently, it is of interest to compare the photosynthetic activity and the thylakoid

composition in those two samples, which harbour chloroplasts apparently very similar in ultrastructure (Bonora *et al.* 2000).

The data presented in this section consist mainly of results already shown above but are re-elaborated here in the perspective of a direct comparison between the two green tissues.

3.3.1. Photosynthetic Pigments

Fig. 38 summarises the pigment data obtained by analysing the palisade tissue and the green berry of *Arum italicum*.

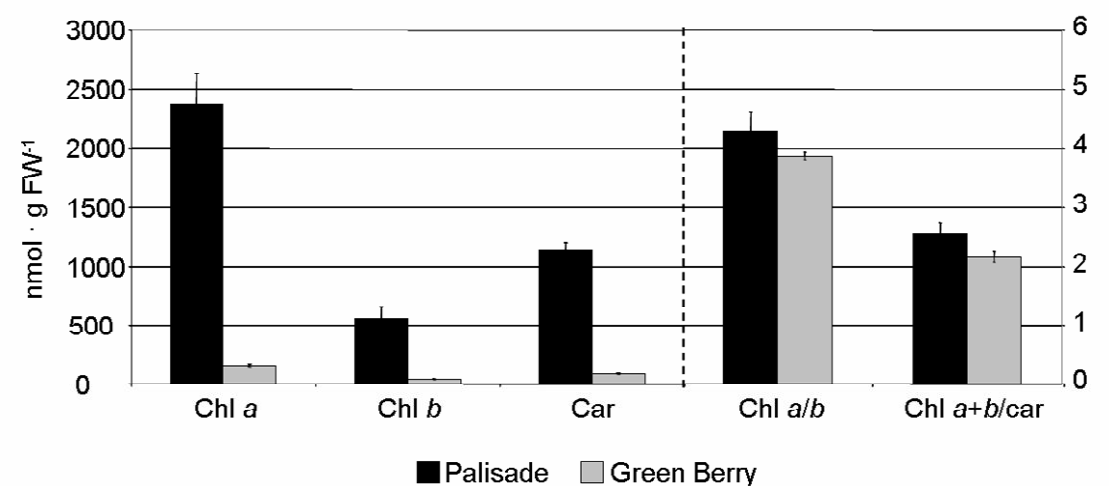

Fig. 38: Photosynthetic pigments (left scale) and their molar ratios (right scale) in palisade tissue and green berry of *Arum italicum*. Data are means of at least three independent experiments (bars are S.D.).

It was evident that the pigment concentration per fresh weight was markedly lower in the green berry than in the palisade tissue, corresponding to about 7%.

However, the two samples showed very similar Chl*a*/Chl*b* ratios. On the contrary, it was noteworthy that the Chl(*a*+*b*)/Car ratio of the green berry (2.16 ±0.10) was lower than that of the palisade tissue (2.56 ± 0.19). Interestingly, the value of Chl(*a*+*b*)/Car ratio observed in the green berry was the highest value during berry ontogeny. This is also consistent with the work by Bonora et al (2000), which demonstrated that 5-10% of chloroplasts in green berries already showed the presence of early carotene crystalloids, representing the first signs of transition into chromoplast.

3.3.2. Photosynthesis and Respiration Rates

Fig. 39 shows the CO_2 gas exchange of the green berry and leaf lamina of *Arum italicum*, calculated per surface area and on a Chl basis.

The respiration of the berry was markedly more intense than the respiration of the lamina. It is also noteworthy that the net photosynthesis rate of the green berry was around zero, the gross photosynthesis compensating the respiration rate. The gross photosynthesis of the green berry was statistically lower than the value recorded in the lamina, corresponding to about 30%.

The differences observed in CO_2 gas exchange were not only due to the different pigment concentration in the two green tissues, as evidenced when expressing the values on a Chl basis (Fig. 39 b).

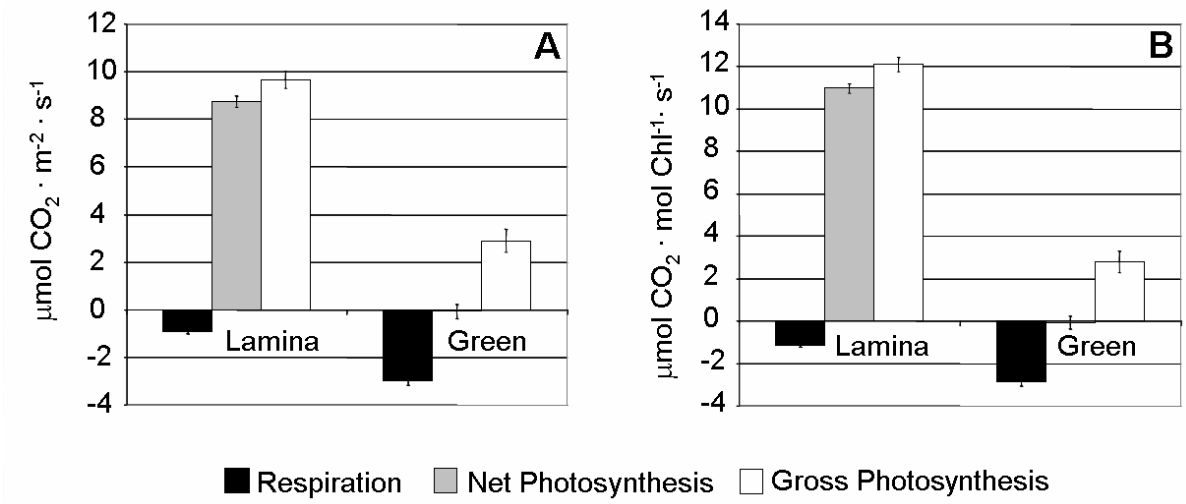

Fig. 39: CO_2 exchange in leaf lamina and green berry of *Arum italicum*, calculated per surface area (A) and on a Chl basis (B). Data are means of at least three independent experiments (bars are S.D.).

3.3.3. Thylakoid Protein Composition

Fig. 40 presents the silver-stained gels obtained after SDS-PAGE of the total thylakoid protein samples from the palisade tissue and the green berry. The protein patterns clearly showed several differences in the composition and amounts of thylakoid proteins. By means of specific antibodies, the amounts of several thylakoid proteins were compared between the palisade and the green berry tissues, by loading the gels based on the total protein content (Fig. 40 b).

In green berry, the D2 protein of the reaction centre of PSII, the Cyt F and the subunit lhca4 of LHCI were present at levels around 20-30% of that in the palisade tissue. Conversely, the

most abundant proteins in the green berry belonged to LHCII, corresponding to about 50% of that in the palisade tissue. Surprisingly, the PSI was hardly detectable in green berry (<10%), in spite of the abundance of the PSI antenna LHCI.

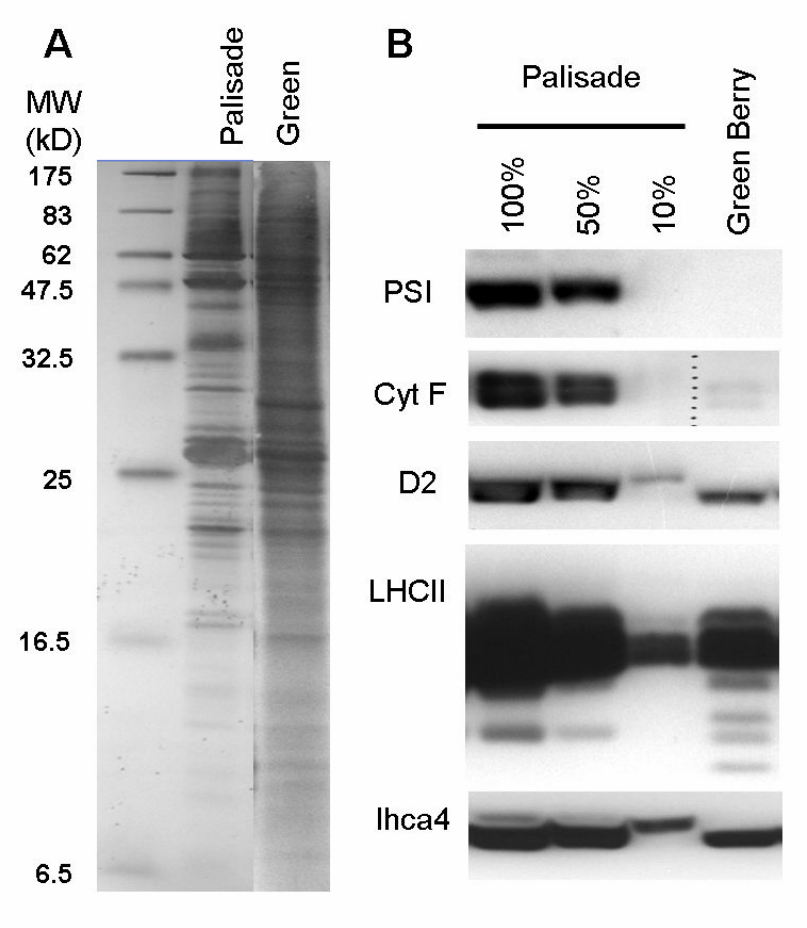

Fig. 40: SDS-PAGE and immunodetection of thylakoid proteins of the palisade tissue (Palisade) and green berry (Green) of *Arum italicum.* A) SDS-PAGE. Proteins equivalent to 75μg were loaded on each well. B) Immunoblot detection of thylakoid proteins. For semi-quantitative comparison of the protein amounts, three dilutions (100 %, 50 % and 10 %) of the palisade sample were loaded. (Details on the antibodies are given in Materials and Methods).

3.3.4. Thylakoid Protein Complexes

In Fig. 41, the 1D and 2D BN-SDS-PAGE gels of the palisade tissue and green berry are compared.

The silver-stained 2-D gels failed in revealing the presence of the PSI complex in the green berry. On the other hand, PSII was present in both tissues and appeared to be correctly assembled, showing supercomplexes with LHCII, core dimers and monomers and traces of core monomers lacking CP43. In both samples, the LHCII trimers and monomers were clearly

detected. Finally, some non-identified complexes were more abundant in the green berry than in the palisade tissue.

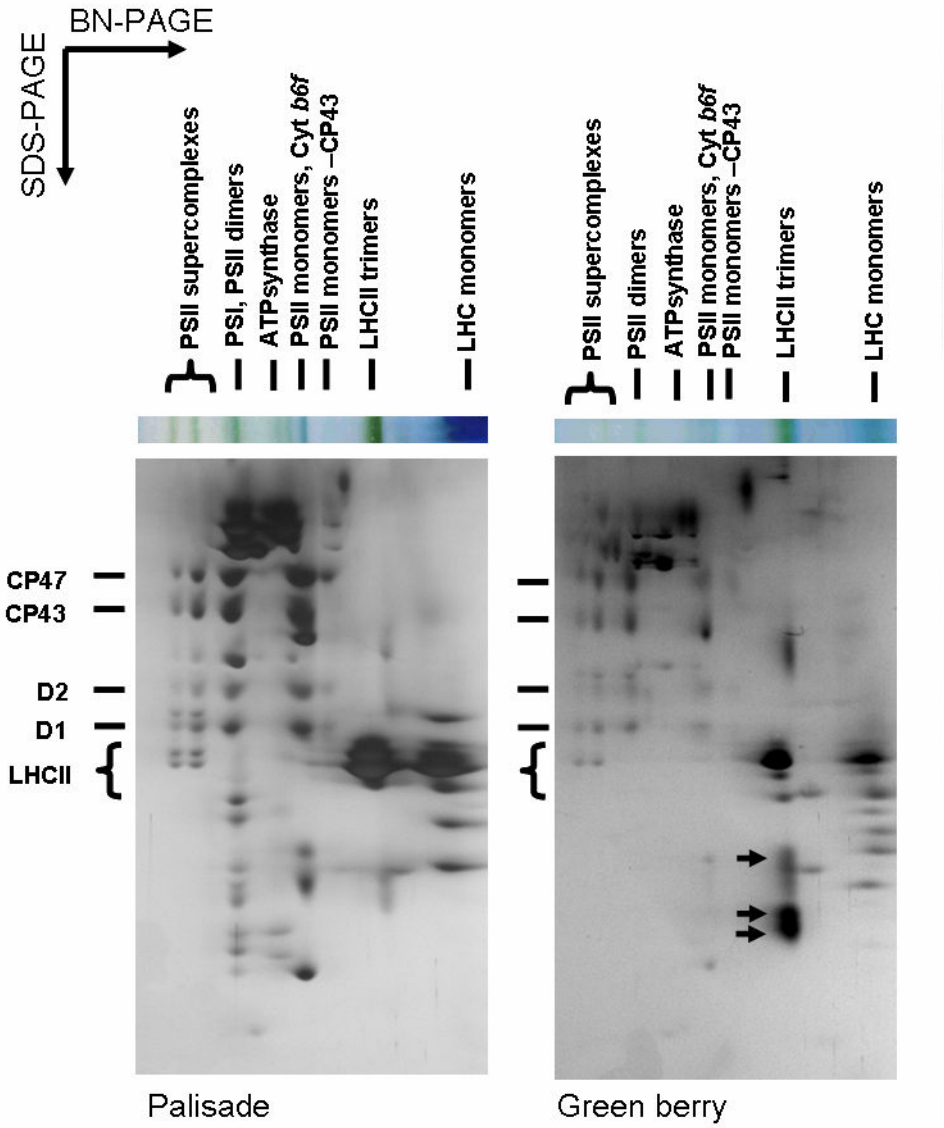

Fig. 41: 1D and 2D BN-SDS-PAGE of palisade tissue (left) and green berry (right) of *Arum italicum*. 1D BN-gels are shown on the top and the location of different thylakoid protein complexes is indicated. In the second dimension SDS-gel (below) the positions of the silver-stained spots corresponding to the D1, D2, CP47, and CP43 subunits of PSII and the LHCII proteins are indicated. Arrows: unknown proteins.

3.3.5. 77 K Fluorescence Emission Spectra

The 77 K fluorescence emission spectra of the palisade and the green berry tissues are shown in Fig. 42. The spectra are normalised to the maximum peak, which in both the palisade and the green berry corresponded to PSII (685 nm). The PSI peak was interestingly present in both samples, though less intense in the green berry than in the palisade tissue. No shifts in

the PSI and PSII peak positions were observed. The difference spectra confirmed the lower emission of the green berry at 731 nm and highlighted a relatively less marked loss in emission at 692 nm (Fig. 43).

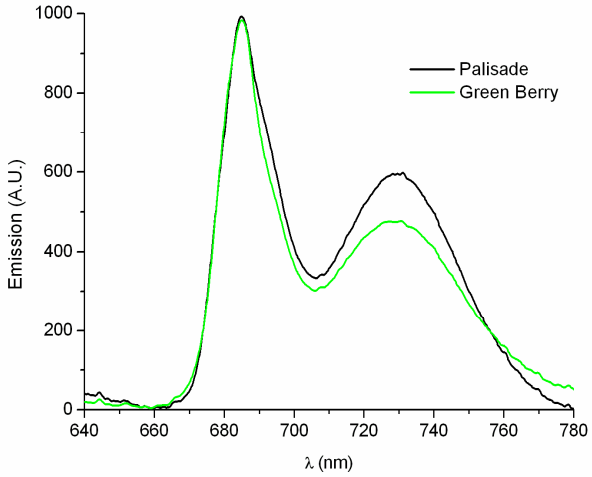

Fig. 42: 77 K fluorescence emission spectra from thylakoid samples of the palisade tissue and the green berry of *Arum italicum*. Spectra are normalised to the maximum emission at 685 nm.

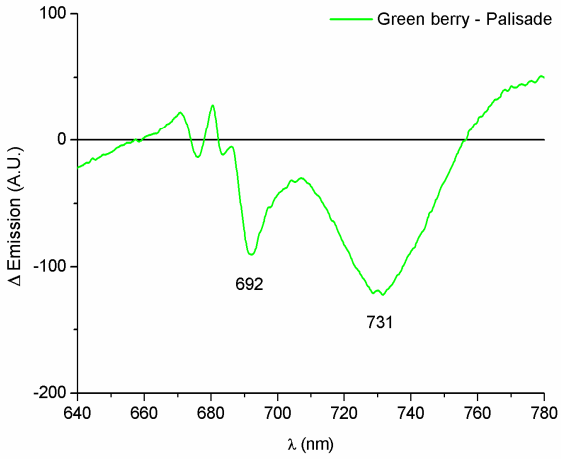

Fig. 43: Difference spectrum calculated from the normalised 77 K fluorescence emission spectra reported in Fig. 42.

3.3.6. Microspectrofluorimetric Analyses

Despite the lower Chl content, the fluorescence emission in the green berry was markedly higher than in the palisade tissue (+69% ca.). In Fig. 44 two representative spectra are shown after Gaussian deconvolution. The spectral region of Chl (660-750 nm) showed essentially the same emission components. However, there were interesting differences in the relative intensity of components ascribable to PSII. In fact, the RCII/CP43–47 ratio resulted slightly

but significantly lower in the green berry than in the palisade tissue. What was more markedly different, was the LHCII/PSII ratio, which in the green berry increased by ca. 45% with respect to the palisade tissue.

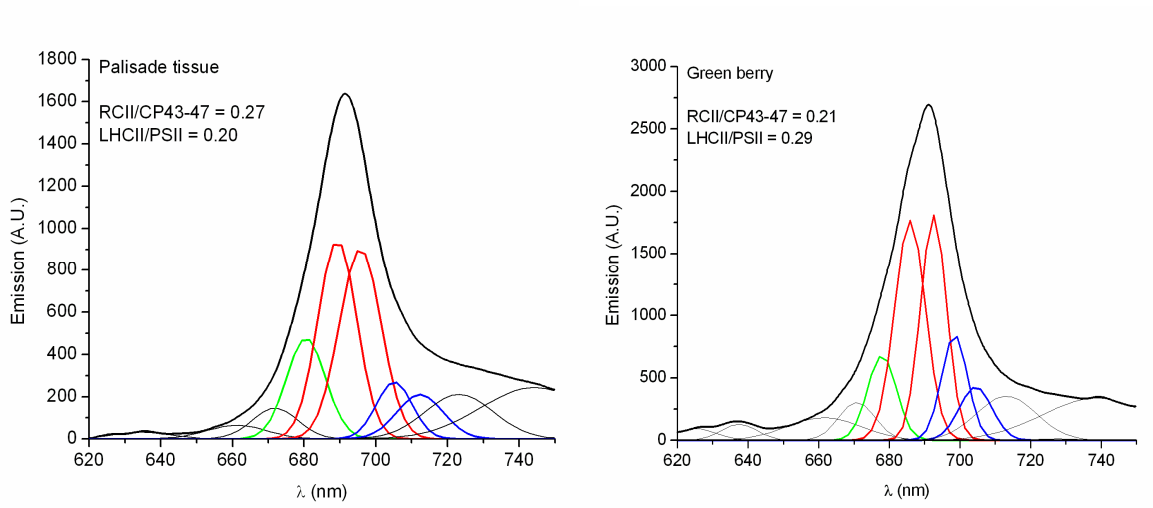

Fig. 44: Representative deconvoluted fluorescence emission spectra of palisade tissue (left) and green berry (right) (max. at 678-680 nm: RCII, green line; max. from 687–694 nm: CP43–47, red line; max. from 700–710 nm: LHCII, blue line). PSII is the sum of RCII and CP43–47. RCII/CP43–47 and LHCII/PSII ratios are means of 5 different replicates (SD ≤ 0.04).

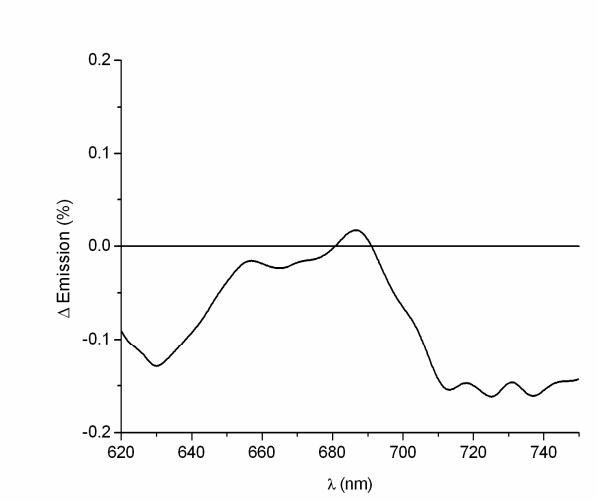

Fig. 45: Green berry minus palisade difference spectrum calculated from the normalised room temperature fluorescence emission spectra reported in Fig. 44.

As concern the PSI spectral region (720-750 nm) it seemed that the green berry yielded a lower emission. This was confirmed with a difference spectrum, which showed a considerable loss in emission at long wavelength (Fig. 45).

4. DISCUSSION

4.1. CHLOROPLAST DIMORPHISM IN THE WINTER LEAF

In this study, the comparison of the different lamina tissues reveals interesting similarities and differences between the palisade and the spongy parenchyma. These two tissues have the same photosynthetic pigment concentration per fresh weight, but a significantly different Chl *a*/*b* molar ratio, the palisade tissue showing a higher ratio than the spongy tissue. This is a characteristic feature when a sun-shade dimorphism is observed in leaves (Anderson, 1986). Moreover, the fluorescence emission from the spongy tissue is higher than the emission from the palisade tissue, despite the same pigment concentration, providing further support for physiological diversity of the two tissues. In 1998, Pancaldi and co-workers excluded the existence of a sun-shade dimorphism in palisade and spongy tissues of *Arum italicum*. Their conclusion was based on the presence of the same Chl *a*/*b* molar ratio in both tissues and the absence of ultrastructural differences in the chloroplasts. This discrepancy with the conclusion by Pancaldi and co-workers (1998) cannot be due to the use of different plants, because both studies have been performed on the same *A. italicum* population, stably growing in the area of Po plains (Italy). Moreover, the reproduction of this plant is mainly vegetative, thus substantially leading to natural populations which are genetically uniform. However, it should be considered that the first study was carried out more than 10 years ago, in February 1996, on plants developed during a season characterised by foggy weather. Consequently, it can be proposed that a sun-shade dimorphism in the leaf lamina can possibly be induced by the different environmental conditions occurred during the last winters. A higher mean irradiance likely promoted the development of dimorphic characteristics in the chloroplasts of the lamina tissues. Indeed, the plants described by (Pancaldi *et al.* 1998) were adapted to intermediate shade, as evidenced by their low Chl *a*/*b* ratio (2.7-2.9), whereas the plants analysed in this study showed sun adaptation, with Chl *a*/*b* ratio ranging from 3.3 to 4.3. Conversely, thylakoid proteins do not present an evident dimorphism between palisade and spongy parenchyma; in fact, the relative amounts of individual proteins are almost the same in the two tissues. Moreover, they both present similar protein assembly patterns, when analysed by means of BN-SDS-PAGE. However, the presence in monocots of less stable PSII supercomplexes is shown by several authors (Ciambella *et al.* 2005) and this feature might

reduce the potential of BN-PAGE analysis in highlighting differences that mainly affect the PSII-LHCII assembly state, such as the sun-shade dimorphism.

Among the characteristic features of *Arum* leaf, Pancaldi and co-workers (1998) highlighted a distinct plastid dimorphism between the outer and the inner parts of the petiole. While the outer chlorenchyma chloroplasts are similar to those of the lamina, the inner aerenchyma contains chloroplasts with an extreme shade ultrastructure, and a pigment composition which is anomalous and inadequate for completely differentiated plastids. In this thesis, more data were collected to characterise the petiole chloroplasts. The photosynthetic pigment concentration per fresh weight in the petiole is clearly lower than that in the lamina (Fig. 13). However, the outer petiole has a fluorescence emission yield similar to that of the spongy tissue and the inner petiole even reaches 70% of the emission of the palisade in spite of a 90% lower pigment concentration (Fig. 12 and Fig. 21). However, the room temperature fluorescence emission spectra recorded from different parts of *A. italicum* leaf do not shown marked variations (Fig. 22). Therefore, these great discrepancies between the pigment concentration and fluorescence emission could be due to an altered thermal dissipation rather than an altered PSII functionality. The most evident variation is the lower emission from the inner tissue in the spectral region above 700 nm. These wavelengths are characteristic of PSI emission components, which are known to contribute at extremely low levels in the room temperature measurements. In order to clarify the PSI emission features, the 77 K fluorimetry was employed. Both inner and outer parts of the petiole show lower emission at 713-719 nm, the wavelengths ascribable to PSI core, and at 690-692 nm, ascribable to PSII core. Moreover, both tissues have the 678-677 nm emission higher than that in the palisade, most probably indicating that the major part of LHCII is not associated with PSII. All these features are more prominent in the inner part of the petiole than in the outer part. The anomalous spectrofluorimetric characteristics seen in the petiole, in particular in the inner part, suggest important alterations in the protein composition, as could be highlighted by electrophoretical analysis of thylakoid proteins. Not only the concentration of proteins belonging to photosynthetic complexes is generally lower in the petiole, but their relative amounts markedly differ from those in the palisade tissue. In fact, in the outer petiole only few proteins belonging to PSII and PSI core can be detected, while the LHCII proteins are particularly abundant. Moreover, the PSII-LHCII supercomplexes are clearly less abundant than in the palisade and spongy tissues, as shown by BN-PAGE (Fig. 17). The inner part of the petiole shows features even more anomalous than the outer part. In fact, the SDS-PAGE and

immunoblot data show a strong excess of LHCII over the other protein components analysed, and moreover the BN-PAGE protein pattern shows the absence of PSII supercomplexes, and PSII core monomers and dimers are hardly detectable. The presence in extremely low amounts of assembled complexes can explain the high fluorescence emission observed by means of room temperature microspectrofluorimetry. These findings are in accordance with the previous report: by means of pigment analyses and cytochemical reactions, Pancaldi and co-workers (1998) suggested the presence of a great extent of LHC, in the outer part of the petiole compared to the lamina, in spite of the maintenance of a ultrastructure similar to that in the palisade chloroplasts. The authors also suggested that a correct assembly of PSs, particularly of PSII, is strongly impaired in the inner part of the petiole.

In conclusion, it appears that the higher irradiance levels characterising the last winters induce dimorphism in the lamina, but do not induce significant modifications in the petiole parts. Consequently, the maintenance of a strong dimorphism between the inner and the outer part of the petiole, in spite of the environmental change, suggests that the dimorphism in the petiole is not a condition induced by low light exposure, but is rather an intrinsic characteristic of the chloroplasts of the inner part of the petiole. Finally, the CO_2 exchange rates measured from the entire lamina and petiole are worthy of attention. The data presented in this thesis show that the gross photosynthesis of the petiole corresponds only to 20-30% of that of the lamina, when measured in saturating light conditions. In fact, the irradiance value during the measurement was 1500 ± 200 μmol photons m^{-2} s^{-1}, as determined by the PAR sensor incorporated in the infrared gas analyser system employed. Collectively, the contribution of the petiole to the photosynthesis of the leaf appears not to be particularly conspicuous. Conversely, the CO_2 exchange data presented by Pancaldi and co-workers (1998) were measured with irradiance of only 300 to 800 μmol photons m^{-2} s^{-1}, in the brightest winter days of February 1996. In those conditions, the petiole was capable of a significant contribution to the overall photosynthesis of the plant, enhancing the light capture and utilisation. The contribution of the petiole to the overall photosynthetic performance of *A. italicum* leaves becomes nearly insignificant when the leaf has developed in an environment rich in irradiance.

4.2. THYLAKOID DEVELOPMENT AND DEGRADATION IN THE BERRY

The maturation is the first part of fruit ontogeny, which consists of carpel modifications and ends when the maximum organ expansion has been reached. During the maturation of *Arum italicum* berries, their colour changes from ivory to ivory-green till deep green, reflecting the differentiation of the amyloplasts, present in the ivory berry, to the chloroplasts, characterizing the green berry. Simultaneously, the respiration rate of the berry increases and the photosynthetic activity is progressively developed. In fact, the CO_2 gas exchange data shows that ivory berries are photosynthetically inactive or nearly inactive, whereas the ivory-green berry has a net photosynthetic rate exactly compensating the respiration rate (Fig. 26). The same feature is maintained in the green berry.

The transition from amyloplast to chloroplast involves the degradation of the starch grains accumulated in the ivory berry as well as the development of the thylakoid system (Bonora *et al.* 2000). Consequently, the photosynthetic pigment and protein concentrations are progressively increasing, both reaching their maximum level in the green berry (Fig. 25 and Fig. 28). The accumulation of pigments proceeds without differences for Chl *a* and Chl *b*, as shown by the constant Chl *a*/*b* molar ratio. The first proteins to be synthesised belong to LHCII, and are already detected in the ivory berry. Ultrastructural observations of these plastids carried out by Bonora and co-workers (2000) demonstrated the presence in the ivory berry of few, long, and usually concentrically ordered thylakoids, which can possibly harbour the LHCII. Moreover, they showed a conspicuous presence of lutein (36% of total carotenoids), which supports a precocious synthesis of LHCII proteins. The assembly of photosynthetic complexes seems to start with the formation of LHCII trimers, which are the only complexes clearly identified in BN gels of ivory-green berry, whereas the presence of properly assembled PSII reaction centres is detected only later. In ivory and ivory-green berry, wide bands at low molecular mass region (ca. 10 kDa) are reactive with antibodies raised against D1 and D2. The presence of these fragments can indicate that the synthesis of D1 and D2 proteins probably occurs also in early maturation, but they are either degraded rapidly or their synthesis is not complete. On the other hand, microspectrofluorimetric data show the presence of fluorescence emission components ascribable to Chls associated with PSII proteins (Fig. 35) even in the ivory berry. This result probably reflects the spot-like distribution of assembled thylakoids, highlighted for the sensitivity of the method. This is in agreement with the microscopy observations, where only small areas with bright red fluorescence are observed in berry cross sections (Fig. 24). Moreover, the decrease in

RC/CP43-47 ratio during the last phase of the maturation suggests that better energy transfer to PSII reaction centre is achieved in the green berry, following the assembly of PSII. Surprisingly, the PSI complex is not detected by means of specific antibodies. However, 77 K fluorescence emission spectra clearly show an emission peak corresponding to PSI (730 nm).

The ripening is the second part of fruit ontogeny and involves several modifications in the chemical composition of the organ. The chloroplast of *A. italicum* differentiates into a chromoplast. In the red fully ripened berry, the content of carotenoids reaches the maximum level, the respiration starts to decline, the berry increases its softness and is ready for the dispersion of seeds.

The CO_2 exchange data collected during ripening of the berries deserve some attention. As a net increase in respiration levels is observed in late ripening, it is highly conceivable that *A. italicum* berry is a climateric fruit. Conversely, the photosynthetic activity declines during the ripening. The green-yellow stage is still photosynthetically active, however, the net photosynthesis does not exactly compensate respiration anymore, and the yellow berry is already photosynthetically inactive or nearly inactive. The decline in photosynthetic activity occurs in parallel with a decline in photosynthetic pigment and protein concentrations. However, the Chl *a*/*b* molar ratio remains unaffected, indicating that the degradation also takes place in a coordinated way. Interestingly, the yellow colour is due to the absence of Chls, which have been degraded before the synthesis of the carotenoids characterising the fully ripe berry. The direct colour transition from green to red, which characterises i.e. the ripening of tomato fruit, is due to a massive accumulation of carotenoids and the simultaneous degradation of Chls (Telef *et al.* 2006). Conversely, in *A. italicum* these two processes are clearly not simultaneous, so that it is possible to observe a further colour stage (i.e. the yellow one). In spite of the low concentration of pigments, the microspectrofluorimetic analyses still highlighted the presence of properly assembled Chl-protein complexes in the green-yellow berry. Nevertheless, a significantly lower amount of thylakoid proteins is already observed at this stage. The degradation of proteins affects mainly the reaction centres, that in the green-yellow berry are already less abundant, as shown by Fig. 28 and Fig. 29. Conversely, the only complexes clearly identified with BN-PAGE are the LHCII trimers and monomers. Moreover, traces of LHCII are surprisingly detected even in the orange stage. In such chromoplasts Bonora et al (2000) observed a few wavy thylakoid membrane remnants where the LHCII proteins could still be localised. Emission ascribable to assembled PSII is not detectable at this stage of the ripening.

Other protein complexes are persistent during the early ripening e.g. the ATP synthase. Some other protein complexes seem to become even more abundant i.e. the complex corresponding to the putative deltaTIP identified in the green berry. However, it is highly possible that this complex is an impurity of the thylakoid membrane preparation.

4.3. COMPARATIVE PHOTOSYNTHETIC FEATURES IN PALISADE TISSUE AND GREEN BERRY

The main function of colouration in ripening fruits is considered to be the attraction of disperser animals, even if "green-ripe" fruits tend to be dispersed only by rather few mammals (i.e. bats) so that the green colour has a minor importance in this concern (Aschan *et al.* 2003). The green berry of *Arum italicum* does not represent the ripe fruit, so that the development of a chloroplast with vexillary role can be excluded. Consequently, in this plant the achievement of a photosynthetic activity in the fruit remains a concrete alternative to the vexillary function.

Higher plants can potentially utilize almost all vegetative and reproductive structures to perform photosynthetic CO_2 assimilation (Aschan *et al.* 2003 and references therein). In green fruits of several plants, the photosynthetic rate per unit area is generally reduced as compared to the leaves of the same plant, because of the different chloroplast density in the photosynthetic tissues of the two organs. On the other hand, when calculated on a Chl basis, the photosynthetic rates in fruits and leaves are quite comparable (Aschan *et al.* 2003). This is not the case with *A. italicum*, where the gross photosynthetic rate in the berry corresponds to only about 25% of that of the lamina. This raises a question about the actual role of chloroplasts in a stage of the berry ontogeny. The growing seeds are sink organs dependent on the import of assimilates. However, *A. italicum* leaves are already absent during the late maturation. Moreover, when *A. italicum* leaves are cut out before flowering, the presence of underground reserves is sufficient to sustain the development of new flowers and new berries. Consequently, the seed development is dependent upon the assimilates stored in the underground tuber, at least during the early maturation and late ripening (ontogeny stages lacking active chloroplasts in the plant). The most evident feature observed in photosynthetic activity of the green berry is that the respiration rate is exactly compensated. This suggests that the berry photosynthesis actually contributes to the carbon economy of *A. italicum* plants by refixing internally respired CO_2, which is demonstrated to be a widespread activity in several green fruits and reproductive green structures (Aschan *et al.* 2003).

When compared with the palisade tissue chloroplasts, the green berry chloroplasts appear to be similar in ultrastructure (Bonora *et al.* 2000). However, several anomalies affect the protein and pigment composition and the spectrofluorimetric features of the green berry chloroplasts: a large excess of LHCII proteins (Fig. 40), a hardly detectable presence of PSI (Fig. 41 vs. Fig. 42), a fluorescence emission higher than that in the palisade tissue (Fig. 44), and finally an anomalous composition in carotenoids (Bonora *et al.* 2000).

The exceptionally low concentrations of PSI complexes in relation to the PSII complexes makes it difficult to explain how these chloroplasts obtain the reducing power for carbon fixation (Shen *et al.* 1993). How this can be performed remains an open question, which needs further studies.

The extremely high abundance of apparently free LHCII proteins rises several problems. First of all, the large excess of LHCII proteins detected does not increase the stacking degree of the thylakoid membranes in the green berry (Bonora *et al.* 2000). The relatively high LHCII/PSII fluorescence ratio most probably reflects this disproportion between LHCII and reaction centres, causing an unbalance in energy transfer. Moreover, the pigment composition is also anomalous in the green berry: the Chl *a*/*b* ratio is unaffected despite the high presence of LHCII (Fig. 38) and the carotenoids of the xantophyll cycle are undetectable (Bonora *et al.* 2000), partially explaining the high fluorescence emission observed. Actually, energy dissipation by disconnected LHCII is not fully lacking: mechanisms other than the xantophyll cycle can contribute to quench fluorescence emission, in particular the presence of lutein molecules. Lutein, which is abundant in green berries, is indeed known to dissipate excess excitation along with xantophyll cycle pigments (Matsubara *et al.* 2005). A hypothetical role of LHCII in the chloroplasts of *A. italicum* berry is the involvement of these proteins in chromoplast development. The LHCII related proteins ELIPs (early-light inducible proteins) have been shown to be expressed in all stages of tomato fruit ripening, suggesting that they may play a newly recognised role in the development of chromoplast, mainly during the transition form maturation to ripening (Bruno *et al.* 2004). Upon development from green to yellow berries in *A. italicum*, the concentration of carotenoids is nearly unchanged, suggesting that these pigments may, at least partially, be relocated from LHCII to carotenoid-bearing structures, before the massive synthesis takes place in the orange berry (Bonora *et al.* 2000). Therefore, abundant LHCII could contribute to carotenoid accumulation.

AKNOWLEDGMENTS

I would like to thank my supervisor, Prof. Simonetta Pancaldi,
for accepting me as her PhD student and for always believing in me.
Without her none of this would have been possible!
I would like to thank my second supervisor, Prof. Eva-Mari Aro,
who welcomed me so warmly and allowed me to work in her lab at Turku University.

A special thanks to Lorenzo,
for the invaluable help during research and writing
and not less important, for being always so open to dialogue,
even when we have had different opinions.
Many other colleagues were of much help.
I would like to thank Costanza, Ulla-Maija, Sari, Natalia and Yagut
for being always so patient with me and so ready to teach and help.
I also would like to thank all the colleagues and students I have met during the last three years. They collaborated with me, helping, suggesting, discussing and even being critical.

I thank my whole family, my parents Paolo and Valeria, my sister Anna,
and, not less important, aunt Giuli, uncle Pietro and my cousin Federico.
They have always tried to support me and always accepted my choices,
even when these went against their wishes.
Among all the people that have been close to me,
I would like to thank Federica and, last but not least, Davide.

Finally, I wish to thank Prof. Maria Palmira Fasulo, who first taught botany to me, stimulating the desire to learn more and more about plants.

Kiitos, Grazie

Laura

REFERENCE LIST

Albre J, Quilichini A, Gibernau M. 2003. Pollination ecology of *Arum italicum* (Araceae). *Botanical Journal of the Linnean Society* **141,** 205-214.

Alfonso M, Montoya G, Cases R, Rodriguez R, Picorel R. 1994. Core Antenna Complexes, CP43 and CP47, of Higher-Plant Photosystem-II - Spectral Properties, Pigment Stoichiometry, and Amino-Acid-Composition. *Biochemistry* **33,** 10494-10500.

Anderson JM. 1986. Photoregulation of the Composition, Function, and Structure of Thylakoid Membranes. *Annual Review of Plant Physiology and Plant Molecular Biology* **37,** 93-136.

Andersson B, Anderson JM. 1980. Lateral Heterogeneity in the Distribution of Chlorophyll-Protein Complexes of the Thylakoid Membranes of Spinach-Chloroplasts. *Biochimica et Biophysica Acta* **593,** 427-440.

Arvidsson PO, Sundby C. 1999. A model for the topology of the chloroplast thylakoid membrane. *Australian Journal of Plant Physiology* **26,** 687-694.

Aschan G, Pfanz H. 2003. Non-foliar photosynthesis - a strategy of additional carbon acquisition. *Flora* **198,** 81-97.

Baldisserotto C, Ferroni L, Andreoli C, Fasulo MP, Bonora A, Pancaldi S. 2005a. Dark-acclimation of the chloroplast in *Koliella antarctica* exposed to a simulated austral night condition. *Arctic Antarctic and Alpine Research* **37,** 146-156.

Baldisserotto C, Ferroni L, Anfuso E, Pagnoni A, Fasulo MP, Pancaldi S. 2007. Responses of *Trapa natans* L. floating laminae to high concentrations of manganese. *Protoplasma* **231,** 65-82.

Baldisserotto C, Ferroni L, Medici V, Pagnoni A, Pellizzari M, Fasulo MP, Fagioli F, Bonora A, Pancaldi S. 2004. Specific intra-tissue responses to manganese in the floating lamina of *Trapa natans* L. *Plant Bioogy* **6,** 578-589.

Baldisserotto C, Ferroni L, Moro I, Fasulo MP, Pancaldi S. 2005b. Modulations of the thylakoid system in snow xanthophycean alga cultured in the dark for two months: comparison between microspectrofluorimetric responses and morphological aspects. *Protoplasma* **226,** 125-135.

Barabe D, Lacroix C, Gibernau M. 2003. Development of the flower and inflorescence of *Arum italicum* (Araceae). *Canadian Journal of Botany-Revue Canadienne de Botanique* **81,** 622-632.

Block MA, Douce R, Joyard J, Rolland N. 2007. Chloroplast envelope membranes: a dynamic interface between plastids and the cytosol. *Photosynthesis Research* **92,** 225-244.

Boddi B, Franck F. 1997. Room temperature fluorescence spectra of protochlorophyllide and chlorophyllide forms in etiolated bean leaves. *Journal of Photochemistry and Photobiology B-Biology* **41,** 73-82.

Bonora A, Pancaldi S, Gualandri R, Fasulo MP. 2000. Carotenoid and ultrastructure variations in plastids of *Arum italicum* Miller fruit during maturation and ripening. *Journal of Experimental Botany* **51,** 873-884.

Brangeon J, Mustardy L. 1979. Ontogenetic Assembly of Intra-Chloroplastic Lamellae Viewed in 3-Dimension. *Biologie Cellulaire* **36,** 71

Camara B, Hugueney P, Bouvier F, Kuntz M, Moneger R. 1995. Biochemistry and molecular biology of chromoplast development. *International Review of Cytology* **163,** 175-247

Cavalier-Smith T. 1999. Principles of protein and lipid targeting in secondary symbiogenesis: euglenoid, dinoflagellate, and sporozoan plastid origins and the eukaryote family tree. *Journal of Eukaryotic Microbiology* **46,** 347-366.

Chow WS, Kim EH, Horton P, Anderson JM. 2005. Granal stacking of thylakoid membranes in higher plant chloroplasts: the physicochemical forces at work and the functional consequences that ensue. *Photochemical & Photobiological Sciences* **4,** 1081-1090.

Ciambella C, Roepstorff P, Aro EM, Zolla L. 2005. A proteomic approach for investigation of photosynthetic apparatus in plants. *Proteomics* **5,** 746-757.

Danielsson R, Suorsa M, Paakkarinen V, Albertsson PA, Styring S, Aro EM, Mamedov F. 2006. Dimeric and monomeric organization of photosystem II - Distribution of five distinct complexes in the different domains of the thylakoid membrane. *Journal of Biological Chemistry* **281,** 14241-14249.

Deruere J, Romer S, Dharlingue A, Backhaus RA, Kuntz M, Camara B. 1994. Fibril Assembly and Carotenoid Overaccumulation in Chromoplasts - A Model for Supramolecular Lipoprotein Structures. *Plant Cell* **6,** 119-133.

Douce R, Joyard J. 1990. Biochemistry and Function of the Plastid Envelope. *Annual Review of Cell Biology* **6,** 173-216.

Faurobert M, Mihr C, Bertin N, Pawlowski T, Negroni L, Sommerer N, Causse M. 2007. Major proteome variations associated with cherry tomato pericarp development and ripening. *Plant Physiology* **143,** 1327-1346.

Ferroni L, Baldisserotto C, Fasulo MP, Pagnoni A, Pancaldi S. 2004. Adaptive modifications of the photosynthetic apparatus in *Euglena gracilis* Klebs exposed to manganese excess. *Protoplasma* **224,** 167-177.

Ferroni L, Baldisserotto C, Zennaro V, Soldani C, Fasulo MP, Pancaldi S. 2007. Acclimation to darkness in the marine chlorophyte *Koliella antarctica* cultured under low salinity: hypotheses on its origin in the polar environment. *European Journal of Phycology* **42,** 91-104.

Giovannoni J. 2001. Molecular biology of fruit maturation and ripening. *Annual Review of Plant Physiology and Plant Molecular Biology* **52,** 725-749.

Giovannoni JJ. 2004. Genetic regulation of fruit development and ripening. *Plant Cell* **16,** S170-S180.

Groot ML, Frese RN, de Weerd FL, Bromek K, Pettersson A, Peterman EJG, van Stokkum IHM, van Grondelle R, Dekker JP. 1999. Spectroscopic properties of the CP43 core antenna protein of photosystem II. *Biophysical Journal* **77,** 3328-3340.

Gutensohn M, Fan E, Frielingsdorf S, Hanner P, Hou B, Hust B, Klosgen RB. 2006. Toc, Tic, Tat et al.: structure and function of protein transport machineries in chloroplasts. *Journal of Plant Physiology* **163,** 333-347.

Horner HT, Healy RA, Ren G, Fritz D, Klyne A, Seames C, Thornburg RW. 2007. Amyloplast to chromoplast conversion in developing ornamental tobacco floral nectaries provides sugar for nectar and antioxidants for protection. *American Journal of Botany* **94,** 12-24.

Ignatov NV, Litvin FF. 1998. A comparative study of the terminal stages of chlorophyll biosynthesis before and after heavy water (D_2O) introduction into greening plant leaves. *Photosynthesis Research* **56,** 83-93.

Ignatov NV, Litvin FF. 1994. Photoinduced Formation of Pheophytin/Chlorophyll-Containing Complexes During the Greening of Plant-Leaves. *Photosynthesis Research* **42,** 27-35.

Kanervo E, Suorsa M, Aro EM. 2005. Functional flexibility and acclimation of the thylakoid membrane. *Photochemical & Photobiological Sciences* **4,** 1072-1080.

Keranen M, Aro EM, Tyystjarvi E. 1999. Excitation-emission map as a tool in studies of photosynthetic pigment-protein complexes. *Photosynthetica* **37,** 225-237.

Kessler F, Schnell DJ. 2006. The function and diversity of plastid protein import pathways: A multilane GTPase highway into plastids. *Traffic* **7,** 248-257.

Krause GH, Weis E. 1991. Chlorophyll Fluorescence and Photosynthesis - the Basics. *Annual Review of Plant Physiology and Plant Molecular Biology* **42,** 313-349.

Laemmli UK. 1970. Cleavage of structural proteins during the assembly of the head of bacteriophage T4. *Nature* **227,** 680-685.

Larkum A, Lockhart P, Howe C. 2007. The origin of plastids: A shopping bag model. *Photosynthesis Research* **91,** 272.

Ljubicic JM, Wrischer M, Ljubesic N. 1998. Formation of the photosynthetic apparatus in plastids during greening of potato microtubers. *Plant Physiology and Biochemistry* **36,** 747-752.

Lopez-Juez E. 2007. Plastid biogenesis, between light and shadows. *Journal of Experimental Botany* **58,** 11-26.

Lopez-Juez E, Pyke KA. 2005. Plastids unleashed: their development and their integration in plant development. *International Journal of Developmental Biology* **49,** 557-577.

Marano MR, Carrillo N. 1992. Constitutive Transcription and Stable RNA Accumulation in Plastids During the Conversion of Chloroplasts to Chromoplasts in Ripening Tomato Fruits. *Plant Physiology* **100,** 1103-1113.

Marano MR, Serra EC, Orellano EG, Carrillo N. 1993b. The Path of Chromoplast Development in Fruits and Flowers. *Plant Science* **94,** 1-17.

Martin W, Kowallik KV. 1999. Annotated English translation of Mereschkowsky's 1905 paper "Über Natur und Ursprung der Chromatophoren im Pflanzenreiche". *European Journal of Phycology* **34,** 287-295.

Matsubara S, Naumann M, Martin R, Nichol C, Rascher U, Morosinotto T, Bassi R, Osmond B. 2005. Slowly reversible de-epoxidation of lutein-epoxide in deep shade leaves of a tropical tree legume may 'lock-in' lutein-based photoprotection during acclimation to strong light. *Journal of Experimental Botany* **56,** 461-468.

Melkozernov AN, Blankenship RE. 2005. Structural and functional organization of the peripheral light-harvesting system in Photosystem I. *Photosynthesis Research* **85,** 33-50.

Mendez M, Diaz A. 2001. Flowering dynamics in *Arum italicum* (Araceae): Relative role of inflorescence traits, flowering synchrony, and pollination context on fruit initiation. *American Journal of Botany* **88,** 1774-1780.

Menke W. 1966. The molecular structure of photosynthetic lamellar systems. *Brookhaven.Symp.Biol.* **19,** 328-340.

Miyazawa Y, Kato H, Muranaka T, Yoshida S. 2002. Amyloplast formation in cultured tobacco BY-2 cells requires a high cytokinin content. *Plant and Cell Physiology* **43,** 1534-1541.

Miyazawa Y, Sakai A, Miyagishima S, Takano H, Kawano S, Kuroiwa T. 1999. Auxin and cytokinin have opposite effects on amyloplast development and the expression of starch synthesis genes in cultured Bright Yellow-2 tobacco cells. *Plant Physiology* **121,** 461-469.

Moreira D, Philippe H. 2001. Sure facts and open questions about the origin and evolution of photosynthetic plastids. *Research in Microbiology* **152,** 771-780.

Mullineaux CW. 2005. Function and evolution of grana. *Trends in Plant Science* **10,** 521-525.

Mustardy L, Garab G. 2003. Granum revisited. A three-dimensional model - where things fall into place. *Trends in Plant Science* **8,** 117-122.

Nelson N, Ben-Shem A. 2004. The complex architecture of oxygenic photosynthesis. *Nature Reviews Molecular Cell Biology* **5,** 971-982.

Nelson N, Yocum CF. 2006. Structure and function of photosystems I and II. *Annual Review of Plant Biology* **57,** 521-565.

Nozaki H. 2005. A new scenario of plastid evolution: plastid primary endosymbiosis before the divergence of the "Plantae," emended. *Journal of Plant Research* **118,** 247-255.

Pancaldi S, Baldisserotto C, Ferroni L, Bonora A, Fasulo MP. 2002. Room temperature microspectrofluorimetry as a useful tool for studying the assembly of the PSII chlorophyll-protein complexes in single living cells of etiolated *Euglena gracilis* Klebs during the greening process. *Journal of Experimental Botany.* **53,** 1753-1763.

Pancaldi S, Bonora A, Gualandri R, Gerdol R, Manservigi R, Fasulo MP. 1998. Intra-tissue characteristics of chloroplasts in the lamina and petiole of mature winter leaf of *Arum italicum* Miller. *Botanica Acta* **111,** 261-272.

Paolillo DJ, Jr. 1970. The three-dimensional arrangement of intergranal lamellae in chloroplasts. *Journal of Cell Science* **6,** 243-255.

Paolillo DJ, Garvin DF, Parthasarathy MV. 2004. The chromoplasts of Or mutants of cauliflower (Brassica oleracea L. var. botrytis). *Protoplasma* **224,** 245-253.

Piechulla B, Glick RE, Bahl H, Melis A, Gruissem W. 1987. Changes in Photosynthetic Capacity and Photosynthetic Protein Pattern During Tomato Fruit Ripening. *Plant Physiology* **84,** 911-917.

Porra RJ, Thompson WA, Kriedemann PE. 1989. Determination of Accurate Extinction Coefficients and Simultaneous-Equations for Assaying Chlorophyll-*a* and Chlorophyll-*b* Extracted with 4 Different Solvents - Verification of the Concentration of Chlorophyll Standards by Atomic-Absorption Spectroscopy. *Biochimica et Biophysica Acta* **975,** 384-394.

Prychid CJ, Rudall PJ. 1999. Calcium oxalate crystals in monocotyledons: A review of their structure and systematics. *Annals of Botany* **84,** 725-739.

Ris H, Plaut W. 1962. Ultrastructure of DNA-containing areas in the chloroplast of Chlamydomonas. *Journal of Cell Biology* **13,** 383-391.

Rodriguez-Ezpeleta N, Philippe H. 2006. Plastid origin: Replaying the tape. *Current Biology* **16,** R53-R56.

Rokka A, Suorsa M, Saleem A, Battchikova N, Aro EM. 2005. Synthesis and assembly of thylakoid protein complexes: multiple assembly steps of photosystem II. *Biochemical Journal* **388,** 159-168.

Saglik S, Alpinar K, Imre S. 2002. Fatty acid composition of *Dracunculus vulgaris* Schott (Araceae) seed oil from Turkey. *Journal of Pharmacy and Pharmaceutical Sciences* **5,** 231-233.

Sakai A, Miyazawa Y, Saito C, Nagata N, Takano H, Hirano HY, Kuroiwa T. 1999. Amyloplast formation in cultured tobacco cells. III - Determination of the timing of gene expression necessary for starch accumulation. *Plant Cell Reports* **18,** 589-594.

Santabarbara S, Neverov KV, Garlaschi FM, Zucchelli G, Jennings RC. 2001. Involvement of uncoupled antenna chlorophylls in photoinhibition in thylakoids. *Febs Letters* **491,** 109-113.

Scheller HV, Jensen PE, Haldrup A, Lunde C, Knoetzel J. 2001. Role of subunits in eukaryotic Photosystem I. *Biochimica et Biophysica Acta-Bioenergetics* **1507,** 41-60.

Shen GZ, Boussiba S, Vermaas WFJ. 1993. Synechocystis Sp Pcc-6803 Strains Lacking Photosystem-I and Phycobilisome Function. *Plant Cell* **5,** 1853-1863.

Shimoni E, Rav-Hon O, Ohad I, Brumfeld V, Reich Z. 2005. Three-dimensional organization of higher-plant chloroplast thylakoid membranes revealed by electron tomography. *Plant Cell* **17,** 2580-2586.

Siffel P, Braunova Z. 1999. Release and aggregation of the light-harvesting complex in intact leaves subjected to strong CO (2) deficit. *Photosynthesis Research* **61,** 217-226.

Simkin AJ, Gaffe J, Alcaraz JP, Carde JP, Bramley PM, Fraser PD, Kuntz M. 2007. Fibrillin influence on plastid ultrastructure and pigment content in tomato fruit. *Phytochemistry* **68,** 1545-1556.

Staehelin LA. 2003. Chloroplast structure: from chlorophyll granules to supra-molecular architecture of thylakoid membranes. *Photosynthesis Research* **76,** 185-196.

Sugiura M. 1992. The Chloroplast Genome. *Plant Molecular Biology* **19,** 149-168.

Telef N, Stammitti-Bert L, Mortain-Bertrand A, Maucourt M, Carde JP, Rolin D, Gallusci P. 2006. Sucrose deficiency delays lycopene accumulation in tomato fruit pericarp discs. *Plant Molecular Biology* **62,** 453-469.

Theissen U, Martin W. 2006. The difference between organelles and endosymbionts. *Current Biology* **16,** R1016-R1017.

Thomson WW, Whatley JM. 1980. Development of Non-Green Plastids. *Annual Review of Plant Physiology and Plant Molecular Biology* **31,** 375-394.

Timmis JN, Ayliffe MA, Huang CY, Martin W. 2004. Endosymbiotic gene transfer: Organelle genomes forge eukaryotic chromosomes. *Nature Reviews Genetics* **5,** 123-U16.

Vasquez-Caicedo AL, Heller A, Neidhart S, Carle R. 2006. Chromoplast morphology and beta-carotene accumulation during postharvest ripening of mango cv. 'Tommy Atkins'. *Journal of Agricultural and Food Chemistry* **54,** 5769-5776.

Vassiliev IR, Kolber Z, Wyman KD, Mauzerall D, Shukla VK, Falkowski PG. 1995. Effects of Iron Limitation on Photosystem-II Composition and Light Utilization in *Dunaliella tertiolecta*. *Plant Physiology* **109,** 963-972.

Vishnevetsky M, Ovadis M, Vainstein A. 1999. Carotenoid sequestration in plants: the role of carotenoid-associated proteins. *Trends in Plant Science* **4,** 232-235.

Vothknecht UC, Westhoff P. 2001. Biogenesis and origin of thylakoid membranes. *Biochimica et Biophysica Acta-Molecular Cell Research* **1541,** 91-101.

Wan JX, Blakeley SD, Dennis DT, Ko K. 1996. Transit peptides play a major role in the preferential import of proteins into leucoplasts and chloroplasts. *Journal of Biological Chemistry* **271,** 31227-31233.

Wellburn AR. 1994. The Spectral Determination of Chlorophyll-*a* and Chlorophhyll-*b*, As Well As Total Carotenoids, Using Various Solvents with Spectrophotometers of Different Resolution. *Journal of Plant Physiology* **144,** 307-313.

Wise RR, Hoober JK. 2007. The Structure and Function of Plastids. *Advances in Photosynthesis and Respiration* **23,** 1-575